UNIVERSITÀ DEGLI STUDI DI TRIESTE

XXVII CICLO DEL DOTTORATO DI RICERCA IN INGEGNERIA DELL'INFORMAZIONE

PERSONALIZED SETUP OF HIGH FREQUENCY PERCUSSIVE VENTILATOR BY ESTIMATION OF RESPIRATORY SYSTEM VISCOELASTIC PARAMETERS

Settore scientifico-disciplinare: ING-INF/06

DOTTORANDO
MILOŠ AJČEVIĆ

COORDINATORE
CHIAR.MO PROF. ROBERTO VESCOVO

SUPERVISORE DI TESI
CHIAR.MO PROF. AGOSTINO ACCARDO

ANNO ACCADEMICO 2013 / 2014

Abstract

High Frequency Percussive Ventilation (HFPV) is a non-conventional ventilatory modality which has proven highly effective in patients with severe gas exchange impairment. However, at the present time, HFPV ventilator provides only airway pressure measurement. The airway pressure measurements and gas exchange analysis are currently the only parameters that guide the physician during the HFPV ventilator setup and treatment monitoring. The evaluation of respiratory system resistance and compliance parameters in patients undergoing mechanical ventilation is used for lung dysfunctions detection, ventilation setup and treatment effect evaluation. Furthermore, the pressure measured by ventilator represents the sum of the endotracheal tube pressure drop and the tracheal pressure. From the clinical point of view, it is very important to take into account the real amount of pressure dissipated by endotracheal tube to avoid lung injury. HFPV is pressure controlled logic ventilation, thus hypoventilation and hyperventilation cases are possible because of tidal volume variations in function of pulmonary and endotracheal tube impedance.

This thesis offers a new approach for HFPV ventilator setup in accordance with protective ventilatory strategy and optimization of alveolar recruitment using estimation of the respiratory mechanics parameters and endotracheal pressure drop. Respiratory system resistance and compliance parameters were estimated, firstly in vitro and successively in patients undergoing HFPV, applying least squares regression on Dorkin high frequency model starting from measured respiratory signals. The Blasius model was identified as the most adequate to estimate pressure drop across the endotracheal tube during HFPV. Beside measurement device was developed in order to measure respiratory parameters in patients undergoing HFPV.

The possibility to tailor HFPV ventilator setup, using respiratory signals measurement and estimation of respiratory system resistance, compliance and endotracheal tube pressure drop, provided by this thesis, opens a new prospective to this particular ventilatory strategy, improving its beneficial effects and minimizing ventilator-induced lung damage.

Sommario

La ventilazione percussiva ad alta frequenza (HFPV, High Frequency Percussive Ventilation) è stata impiegata con successo in diverse malattie polmonari che determinano la compromissione dello scambio gassoso. Attualmente, l'unico parametro fornito dal ventilatore è la misura della pressione erogata dal ventilatore mentre la misurazione della pressione e l'analisi degli scambi gassosi sono in questo momento gli unici parametri che guidano il medico durante l'impostazione del ventilatore e durante il monitoraggio del trattamento HFPV. La valutazione della resistenza e della compliance del sistema respiratorio nei pazienti sottoposti a ventilazione meccanica può essere utilizzata per il rilevamento delle disfunzioni polmonari, per le impostazioni del ventilatore e per la valutazione dell'effetto del trattamento. Tuttavia, la presenza del tubo endotracheale determina un'impedenza aggiuntiva, che va a sommarsi a quella del sistema respiratorio, e che modifica la pressione misurata dal ventilatore. Dal punto da vista clinico è importante conoscere il valore reale della caduta di pressione dovuta al tubo endotracheale per evitare un sovra- o sotto- trattamento. Essendo l'HFPV una ventilazione a pressione controllata, sono possibili casi di ipoventilazione e iperventilazione a causa di variazioni del volume corrente in funzione dell'impedenza del sistema respiratorio e del tubo endotracheale.

Questa tesi propone un approccio personalizzato per l'impostazione del ventilatore HFPV in conformità con la strategia ventilatoria protettiva e per ottimizzare il reclutamento alveolare utilizzando la stima dei parametri della meccanica respiratoria e della caduta di pressione dovuta al tubo endotracheale. La resistenza e la compliance del sistema respiratorio sono state stimate, prima in vitro e successivamente in pazienti sottoposti all'HFPV, applicando il metodo dei minimi quadrati sul modello ad alta frequenza di Dorkin a partire dai segnali respiratori misurati. Il modello di Blasius è stato identificato come il più adeguato per stimare la caduta di pressione attraverso il tubo endotracheale durante la HFPV. Al fine di misurare i parametri respiratori nei pazienti sottoposti ad HFPV è stato sviluppato un dispositivo di misura al letto del paziente.

La possibilità di personalizzare l'impostazione del ventilatore HFPV, utilizzando la misura di segnali respiratori e la stima della resistenza, della compliance e della caduta di

pressione dovuta al tubo endotracheale, apre una nuova prospettiva per questa particolare strategia ventilatoria, migliorando i suoi effetti benefici e riducendo al minimo danni iatrogeni.

Contents

Introduction

Artificial ventilation and intubation are lifesaving therapies frequently used in patients with acute respiratory failure. High frequency percussive ventilation (HFPV) is an advanced ventilatory strategy which has proven highly effective in case of severe gas exchange impairment. HFPV associates the beneficial aspects of conventional mechanical ventilation with those of high-frequency ventilation. This particular high frequency ventilation modality delivers a series of high-frequency sub-tidal volumes, by pulsatile flow, in combination with low-frequency breathing cycles. Consequently HFPV improves gas exchange encompassing two complementary ventilatory mechanisms: convective and diffusive, corresponding to high frequency oscillations and pressure controlled conventional ventilation, respectively.

HFPV ventilator VDR-4® (Percussionaire Corporation, USA) provides convective and diffusive cardiopulmonary support to most critical patients, from neonates through pediatrics to adult patients. At the present time, HFPV ventilator monitoring unit provides only airway pressure measurement and corresponding peak and mean airway pressures. Thus these pressure measurements and gas exchange analysis are only parameters that guide the physician during the treatment setup and monitoring. On the other side pressure, flow and volume delivered by HFPV depend on viscoelastic parameters of the respiratory system. HFPV is not an intuitive ventilatory modality and the absence of valuable information during the treatment, as delivered tidal volume, respiratory system resistance and compliance, produces disaffection among the physicians.

Assessment of respiratory system viscoelastic parameters and tidal volume delivery play an important role in the management of severe hypoxemic patients undergoing artificial ventilation. The evaluation of respiratory resistance and compliance parameters is very important in order to detect and understand lung dysfunctions, decide therapeutic measures, evaluate effect of the treatment, improve patient–ventilator interaction and prevent ventilator induced complications.

Furthermore, the airway pressure measured by HFPV ventilator represents the sum of the endotracheal tube pressure drop and the tracheal pressure dissipated to inflate lung.

The estimation of pressure drop across endotracheal tube may be very useful to the clinician to avoid lung injury or alveolar de-recruitment.

The clinical efficacy of an artificial ventilator is directly related to the physician's overall medical knowledge and ability to effectively setup ventilation treatment. Avoiding the baro and volu-trauma is the cornerstone of the protective ventilation strategy. At the same time from a clinical point of view, alveolar de-recruitment must be avoided, so recruitment maneuvers are frequently necessary to keep the lung open. Presently it is not possible to evaluate the delivered tidal volume, respiratory mechanics parameters, endotracheal pressure drop and the alveolar recruitment effect in patients undergoing HFPV treatment.

The aim of this doctoral thesis was to personalize HFPV ventilator setup in accordance with protective ventilatory strategy and optimization of alveolar recruitment by providing tools for estimation of the main respiratory parameters and endotracheal pressure drop.

The first chapter describes respiratory system, gas exchange and artificial ventilation principles and techniques.

HFPV technique and ventilator description, effects of respiratory system impedance on pressure, flow and volume delivered by HFPV and the main clinical applications of HFPV systems are reported in the second chapter.

In the third chapter an appropriate method for estimation of respiratory system viscoelastic resistive and compliance parameters was identified.

An adequate model for estimation of endotracheal tube pressure drop over time was proposed and identified in Chapter 4.

Respiratory parameters measurement in patients undergoing HFPV and the results of ventilator setup based on such measurements and estimations are reported in Chapter 5.

A proper acquisition system for bedside measurement of pressure, flow and volume during this particular ventilation strategy was designed and developed in this work. The study was performed in collaboration between Department of Engineering and Architecture of University of Trieste and Department of Perioperative Medicine, Intensive Care and Emergency of Cattinara Hospital of University of Trieste.

Chapter 1 – Respiratory system and Artificial Ventilation

1.1 Respiratory system

The primary function of the respiratory system is to ensure the gas exchange of oxygen and carbon dioxide between the environment air and the blood, thus providing the necessary supply of oxygen to the body and removing the carbon dioxide. The respiratory system, which allows gases to transfer by convective and diffusive processes between the atmospheric air and blood, is constituted by two functionally different anatomical parts:

- The airways, where the air and gases contained in it are conveyed inside or outside the body, during the processes of inspiration and expiration, respectively;
- The lungs, where gas exchange occurs with the blood at the level of alveoli.

The oxygen rich air enters in the respiratory system through the mouth and the nose and passes through the larynx and the trachea which splits into two smaller tubes called the bronchi. Subsequently the each primary bronchus divides generating the bronchial tubes, which lead directly into the lungs where they divide into many smaller tubes which connect to tiny sacs surrounded by capillaries, called alveoli. The breathed in oxygen passes into the alveoli and then diffuses through the capillaries into the arterial blood. At the same time, the carbon dioxide rich blood from the veins releases its carbon dioxide into the alveoli, which is breathe out through the same path.

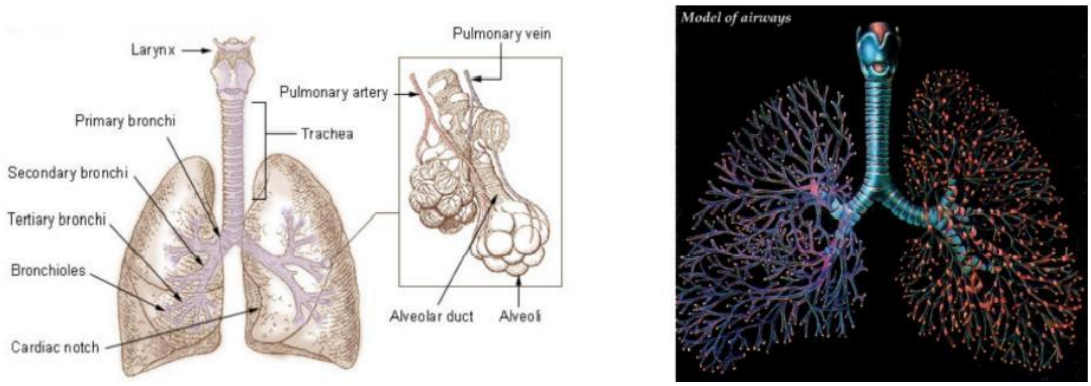

Figure 1.1 Respiratory system tracheobronchial tree.

In spontaneous breathing, the lungs can expand and retract by the action of the respiratory muscles (diaphragm, intercostal muscles and abs), even if, during a quiet breathing, inspiration is almost entirely due to the lowering of the diaphragm while exhalation is a consequence of the elastic return, once the diaphragm is released. The mechanisms that allow a patient to be ventilated with artificial ventilator are different from those of spontaneous breathing.

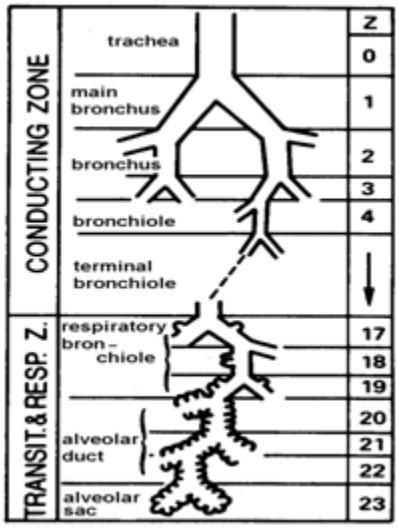

Figure 1.2 Weibel model of the tracheobronchial tree [1]

The respiratory system lung from morphological point of view can be seen as a tree structure (tracheobronchial tree) that starts from the trachea and divides progressively until reaching the alveolar sacs. An ideal morphological model of the tracheobronchial - bronchial was proposed by Weibel [1]. The Weibel model consists of 24 identified generations (Figure 1.2). The first seventeen (i.e. trachea and the sixteen subsequent ramifications) are forming the conduction zone, while the last seven generations constitute the respiratory area, site of gas exchange with the cardiocirculatory system. Movement of gases in the respiratory airways occurs mainly by convection to the fifteenth generation, while beyond the fifteenth generation, gas diffusion is relatively more important.

1.2 Respiratory mechanics functional models

In the study of respiratory mechanics is essentially the search for a simple but useful mechanical behavior model of respiratory system [2]. Although the respiratory mechanics is not the only process involved in breathing, it is however a fundamental aspect

of respiratory function, widely studied in physiology and carefully evaluated in the clinic to determine the pathophysiologic conditions of patients. Given the complexity of the system, respiratory mechanics studies draw considerable advantages from the use of simple models to describe the main functional characteristics of the respiratory system. Respiratory mechanics models describe the mechanical behaviour of the respiratory system exposed to pressure, flow and volume variations over the course of inspiration and expiration. The relation among them is described by the equation of motion for the respiratory system, derived from force-balance equation. The pressure applied on proximal airways is balanced with opposing pressures arising from several factors which include elastic forces within the lung and chest wall, viscous forces due to flow of gas along the airways and lung and chest wall tissues, and inertial forces. The elastic, viscous and inertial properties of respiratory system can be described by compliance (C), resistance (R) and inertance (I) parameters, respectively.

In respiratory physiology, lung compliance (C) describes the willingness of the lungs to distend, and elastance (E) the willingness to return to the resting position [3]. Compliance is defined by the following equation:

$$C = \frac{V}{P_V} \text{ [L cmH}_2\text{O}^{-1}\text{]}$$

where V is change in volume, and P_V is change in pressure. The inverse of compliance is elastance (E= 1/C). The static pressure-volume relationship is nonlinear, presenting lower static compliance at the extremes of lung volume [4].

The respiratory system resistance represent viscous resistance offered to the airflow:

$$R = \frac{P_R}{\dot{V}} \text{ [cmH}_2\text{O L}^{-1}\text{ s]}$$

where $\dot{V}$ is airflow and P_R is pressure drop to friction. In airways and lungs, both laminar and turbulent flows are present. In case of turbulent flow pressure-flow relationship is nonlinear. Resistance may be present in the conducting airways or endotracheal tube, in the lung tissue, and in the tissues of the chest wall. The expiratory resistance is usually higher than inspiratory resistance because of the smaller more distensible airways are more open during inspiration. [4].

The respiratory system inertance describes pressure changes during volume acceleration:

$$I = \frac{P_I}{\ddot{V}} \ [\text{cmH}_2\text{O L}^{-1} \text{ s}^2]$$

where $\ddot{V}$ is volume acceleration and P_I pressure variation during volume acceleration. Inertance has traditionally been excluded from the low frequency models.

The systems of different physical nature that are governed by the same equations (more precisely, by equations having the same formal structure) can be observed in a similar way, according to a criterion introduced by Maxwell in the nineteenth century, which is now useful to use in the most varied fields of physics and its applications. Thus the mechanical systems can be represented as electrical networks. In particular the analogy between the behaviour of an electrical oscillator - RLC circuit and a mechanical oscillator. The respiratory system presents properties of resistance, compliance, and inertance analogous to the electrical properties of resistance, capacitance, and inductance [5].

Despite the respiratory system complexity, the breathing dynamics have been satisfactory represented, for the clinical purposes, by a single-compartment linear model consisting of a rigid tube and a compliant balloon [6-8] (Figure 1.3).

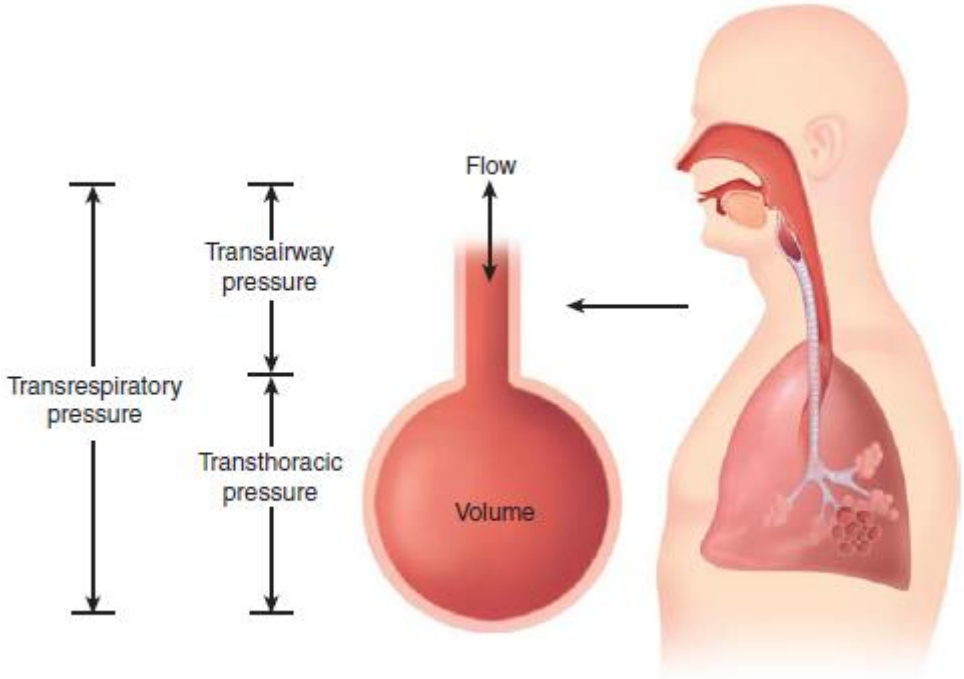

Figure 1.3 Respiratory system modelled as a rigid tube and a compliant balloon single, corresponding to airflow resistance and compliance, respectively [2].

This model, described by following equation motion, consists of a single resistance (representing the endotracheal tube and the airways) and a compliance (representing the lungs and chest wall) [2]:

$$P(t) = \frac{1}{C} \cdot V(t) + R \cdot \dot{V}(t)$$

where P(t) the pressure applied to the respiratory system, V(t) is the pulmonary volume and $\dot{V}(t)$ is the airflow. This first-order model can be applied both during spontaneous ventilation and during constant flow passive ventilation. The electrical analog model is reported in Figure 1.4.

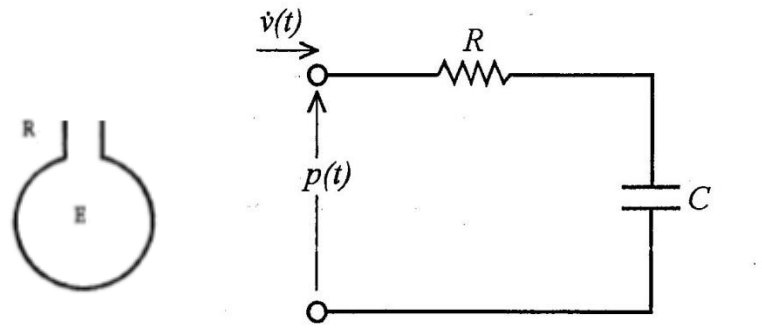

Figure 1.4 First-order single compartment linear model [5].

The more complex two-compartment viscoelastic Otis [9], Mead [10] and Mount [11] models provide a more accurate description of the mechanical behavior of the respiratory system. The Otis model (Figure 1.5) describes pulmonary inhomogeneities and parallel gas redistribution between two lungs [9].

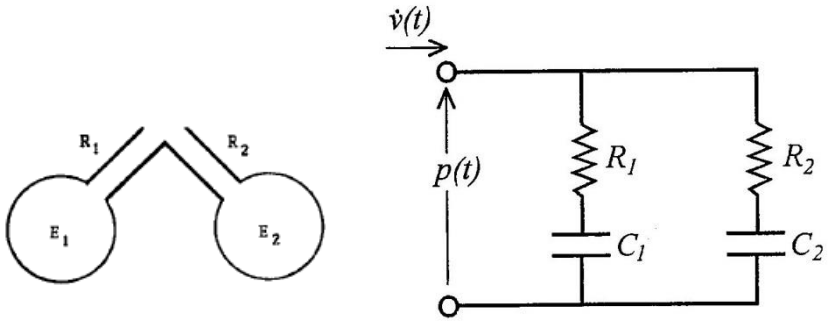

Figure 1.5 Otis model [5].

The Mead model (Figure 1.6) describes homogeneous lungs with central airway compliance and subsequent series gas redistribution [10]. In this model respiratory

mechanics is described by central resistance (R_1) in a series with parallel coupled central compliance (E_1) and a series with compliance (E_2) and resistance (R_2).

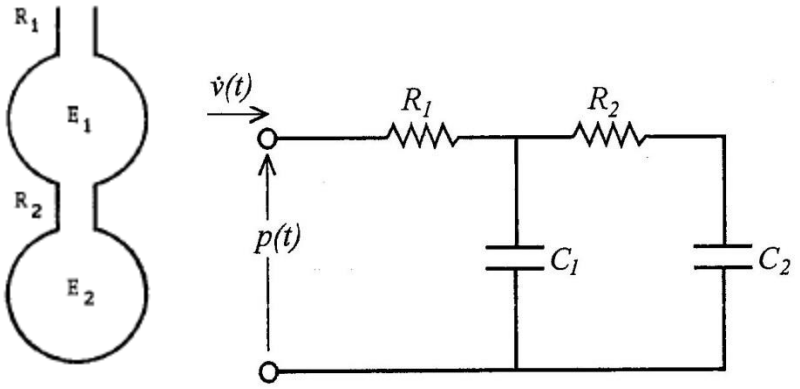

Figure 1.6 Mead model for homogeneous lung with serial gas redistribution [5].

The Mount model (Figure 1.7) later further developed by Bates describes a homogeneous lung without any gas redistribution. In this model, stress relaxation originates from lung tissue and/or surfactant viscoelastic properties [11] [12].

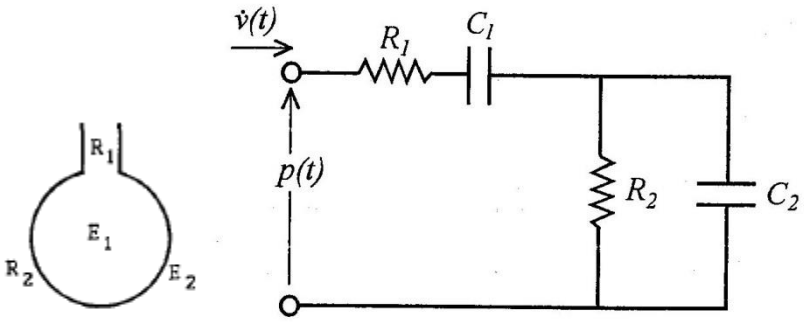

Figure 1.7 Mount model for homogeneous lung with tissue and/or surfactant component [5].

The previously described models are not valid at higher respiratory frequencies. In particular at frequencies between 4 to 32 Hz, the respiratory mechanics may be described by simple one-compartment second-order linear model [13] (Figure 1.8).

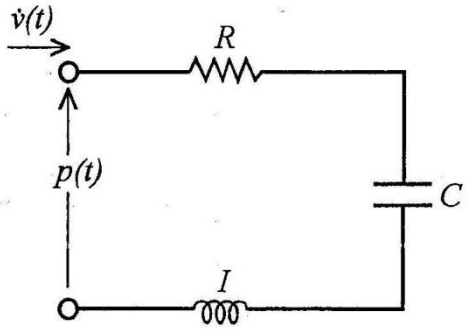

Figure 1.8 One-compartment second-order linear model [5].

The Dorkin model can be represented by a series combination of a resistance, a compliance and an inertance. The equation of motion which describes this model:

$$P(t) = \frac{1}{C} \cdot V(t) + R \cdot \dot{V}(t) + I \cdot \ddot{V}(t)$$

is characterized by additional inertance term [I·V̈(t)], where I is the respiratory system inertance and V̈(t) is volume acceleration.

However, for the higher frequencies till 200 Hz, it is more suitable to use more sophisticated models than the simple three element model as that showed in Figure 1.9.

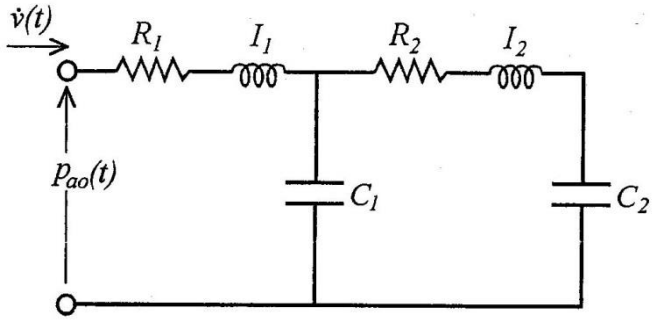

Figure 1.9 Six elements, high frequency linear model [5].

1.3 Artificial ventilation

In intensive care units and operating theaters artificial ventilation devices are regularly used to keep alive patients with acute respiratory failure or patients undergoing surgery. Usually the artificial respiration takes place through a mechanical ventilator that allows the input of oxygen-rich air according to precise clinical protocols. The patient is

usually intubated and connected to the ventilator through a system of cylindrical ducts. The mechanical ventilation can be defined as a method which mechanically assists or replaces spontaneous breathing. There are two main types of mechanical ventilation: positive and negative pressure ventilation, characterized by the air is insufflated into the trachea and air drawn into the lungs, respectively. Particular attention in bioengineering is generally paid to positive pressure ventilation. The ventilators operating at positive pressures generate inspiratory flow by applying higher pressure than the atmospheric to the respiratory system. The applied pressure drives the air inside the alveoli, causing the expansion of the lungs.

1.3.1 Conventional ventilation

The conventional ventilation is characterized by low pressure breathing cycles generated by positive pressures applied on respiratory system. There are different modalities of conventional mechanical ventilation delivery according to the breathing control logic (i.e. based on the variable which controls the interrupt of air insufflation). The two main types of conventional ventilation are based on pressure or volume control.

Volume Controlled ventilation (VC) modality is characterized by a tidal volume V_T (i.e. volume delivered during inspiration), which is programmed and delivered by the ventilator in each respiratory act. This is the mode used most often at the beginning of ventilation support to a patient. The physician determines the respiratory rate and the tidal volume according to the patient needs. The pressure value needed to achieve the predetermined tidal volume varies between the respiratory acts and is determined by resistance and compliance of the respiratory circuit and patient respiratory system. For the predetermined V_T ventilator will continue to insufflate air up to achieving that value. When the V_T is reached, the ventilator stops the insufflation and opens the expiratory valve to allow air to outflow (exhalation). The airflow is generally constant (square wave) during inspiration, while the pressure in the airways increases progressively until the end of the inspiratory time (Figure 1.10). This type of ventilation ensures the delivery of set tidal volume even at the cost of achieving very high airway pressures: in this way can cause barotrauma injuries that can put to immediate risk the patient's life. In fact, when the

airway pressure reaches the predetermined safety limit insufflation ceases and the valve that allows the exhalation opens allowing the intrathoracic pressure to descend. The case maximum pressure reaching is the only situation in which volume controlled ventilation not guarantees the programmed V_T.

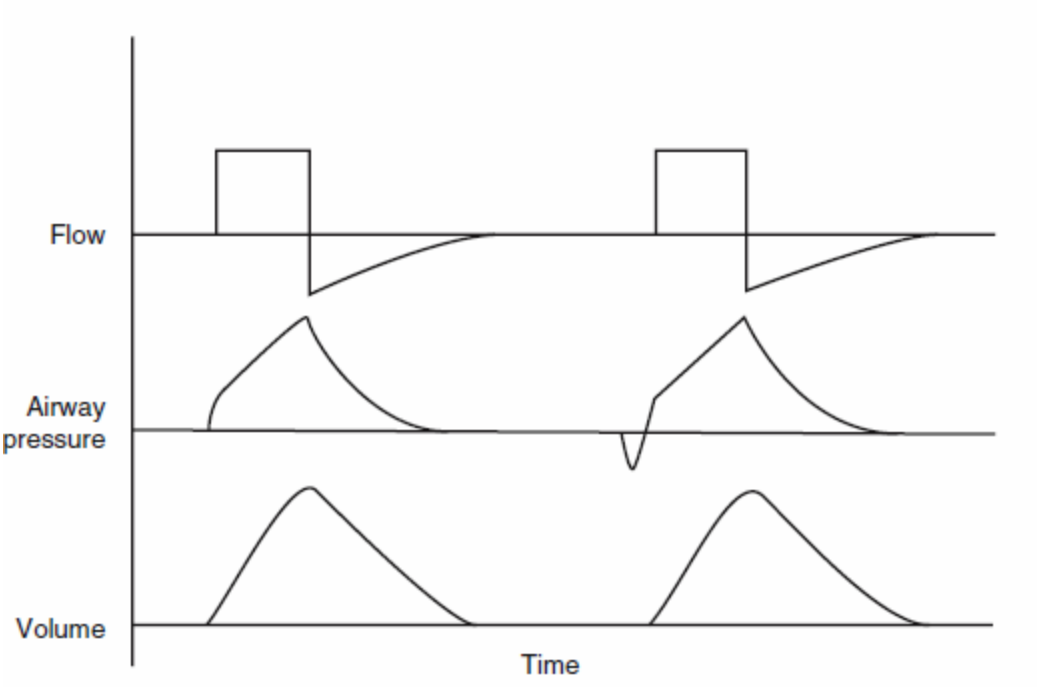

Figure 1.10 Volume-controlled (VC) ventilation: flow, airway pressure and volume tracings.

Pressure Controlled ventilation (PC) mode is characterized by a predetermined peak inspiratory pressure (PIP - Peak inspiratory pressure), which is programmed on the ventilator. The ventilator insufflates air up to the value of set pressure. In correspondence with this limit, the ventilator will stop insufflation and open the valve to allow air to escape (exhalation). During this mode, cases of hypoventilation and hyperventilation are possible because of tidal volume variations in function of pulmonary impedance.

The pressure remains constant during the entire inhalation, in the same time the flow rate rise up to the maximum value and then decreases progressively with the filling of the lungs. The ventilator ensures that the airway pressure does not exceed the set value. This should reduce the risks of barotrauma, and achieve a better oxygenation thanks to the fact that the inspiratory flow is decelerated. It should be underlined that the ventilator in this modality does not guarantee the delivered V_T. In fact, if the airway resistance increase (bronchospasm, obstruction of the tube) and/or if the compliance is reduced (worsening

ARDS), at constant airway pressure pressurizing the tidal volume will be reduced, and in the absence of increased respiratory rate will lead to hypoventilation. On the contrary, the reduction of resistances (endotracheal tube replaced with a tracheotomy) and/or the increased compliance (resolution a pulmonary edema) will lead to an increase of V_T. This type of ventilation is more appropriate for patients well adapted to the ventilator and can be very useful in management of ventilation situations when the ventilation circuit is not well airtight (uncuffed endotracheal tubes in patients etc.).

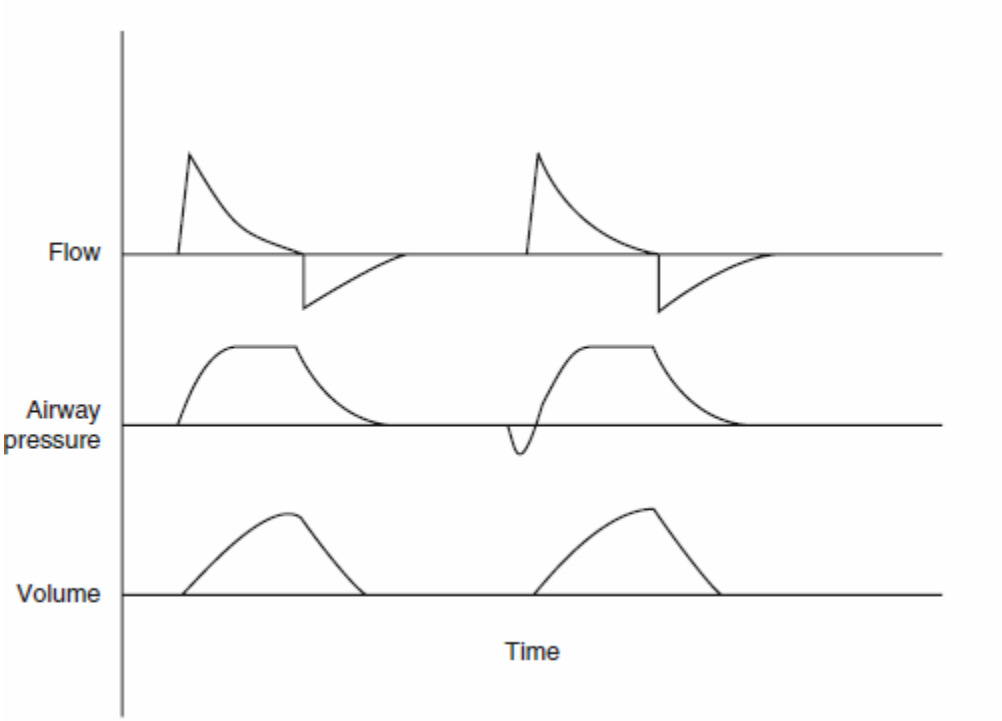

Figure 1.11 Pressure –controlled (PC) ventilation: flow, airway pressure and volume tracings.

In several ventilator models the characteristics of both volume and pressure controlled modes were combined in an effort to better meet the needs of the patient. This hybrid modality, named Pressure regulated Volume Controlled (PRVC) ventilation, can be defined as pressure-limited, volume-targeted, time-cycled breaths ventilation. The pressure controlled flow pattern (due to constant pressure application) is delivered to achieve a target tidal volume that is set by the clinician. Thus the peak inspiratory pressure provided by the ventilator changes from breath-to-breath, and corresponds to set tidal volume value (Figure 1.12).

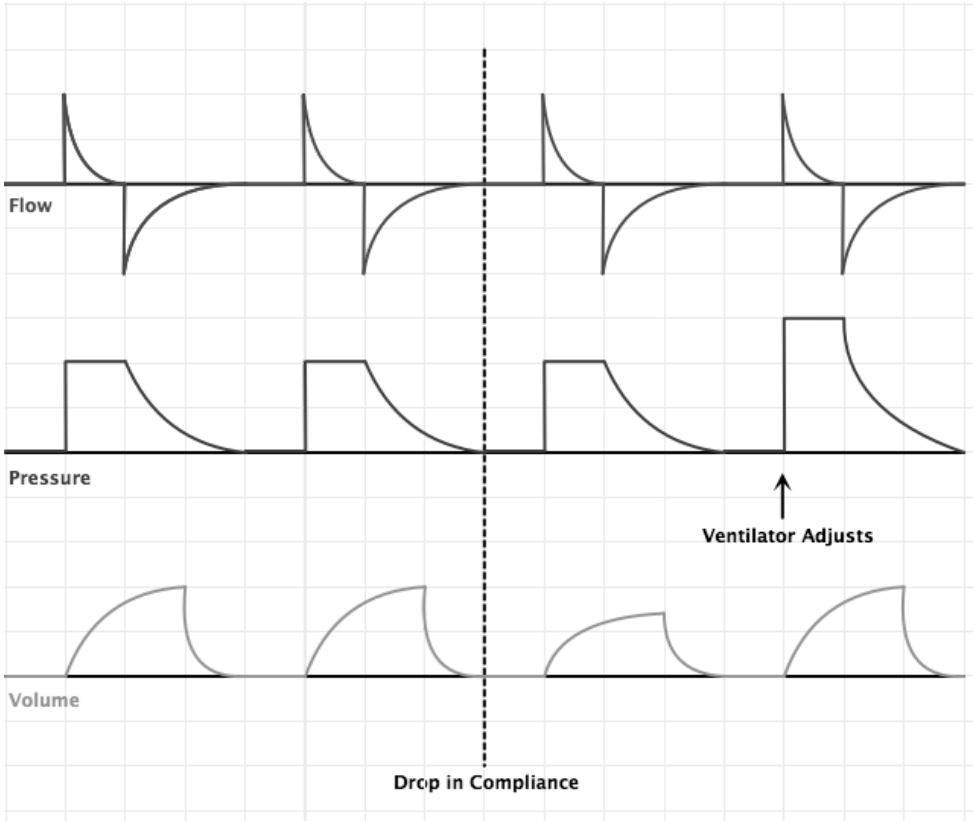

Figure 1.12 Pressure regulated Volume Controlled ventilation (PRVC): flow, airway pressure and volume tracings. Ventilator adjusts the pressure needed to deliver preset tidal volume after compliance variation.

1.3.2 High frequency ventilation

High frequency ventilation (HFV) is a non-conventional modality of mechanical ventilation characterized by respiratory rates greater than 150 cycles per minute and very small tidal volumes which are less than the combined mechanical and anatomical dead space volume, presenting low peak pressures when compared to conventional mechanical ventilation [14] [15]. This ventilation strategy was introduced in clinical practice in the early 1970s, following the experiences by Oberg and Sjostrand [16]. High frequency ventilation is designed as a lung protective ventilation in order to reduce ventilator-associated lung injury, especially in the context of ARDS and acute lung injury [14]. Another important beneficial feature of high-frequency ventilation is the improvement in gas exchange and different mechanisms explains gas transport under HFV [17-20]:

- Direct bulk flow can promote gas exchange by traditional mechanisms of convective on bulk flow;
- Taylorian dispersion can produce a mixing of fresh and residual gas in the centre of the airway, increasing the amount of gas exchange that would occur from simple bulk flow;
- Pendelluft effect resulting from variation in regional resistance and compliance causes some regions to fill and empty more rapidly than others, yielding a net gas flow between them;
- Asymmetric velocity profiles, or coaxial flow, directs gas in the centre of the airway lumen further into the lung while gas on the margin (close to the wall) moves out toward the mouth;
- Cardiogenic mixing secondary to mechanical agitation from the contracting heart adds to gas mixing, especially in the peripheral lung units in close proximity to the heart;
- Molecular diffusion may play an important role in mixing gas in the smallest bronchioles and alveoli.

High frequency ventilation may be used alone, or in combination with conventional mechanical ventilation. There are different high frequency ventilation techniques, characterized by the delivery system and the expiratory phase modality [14] [15]:

High Frequency Oscilatory Ventilation (HFOV) is characterized by high frequencies oscillatory flow (210 - 900 cycles per minute) with both inhalation and exhalation maintained by active pressures. In this HFV technique the pressure oscillates around the constant baseline pressure, equal in this case to mean airway pressure and to positive end-expiratory pressure (PEEP). The gas is insufflated into the lung during inspiration, and then drawn out during expiration. The tidal volumes are very low, and usually lower than the dead space of the lung. This technique is used in adult and especially in neonates patients reduce lung injury, or to prevent further lung injury [21].

High Frequency Jet Ventilation (HFJV) uses an endotracheal tube adaptor in place for the standard one. A high pressure jet flow, of brief duration (about 0.02 seconds) and

high respiratory rate (4-11 Hz), goes through the adaptor into the patient airways. Low tidal volumes ≤ 1 mL/Kg are delivered during HFJV and the expiratory phase is passive. In order to achieve optimal exhalation this ventilators utilize different I:E ratios from 1:1.1 to 1:12. In addition, conventional mechanical breaths are sometimes used to aid in reinflating the lung. The ventilator induced lung injury during this HFV modality is reduced by 20%.

HFFI High Frequency Flow Interruption (HFFI) is very similar to HFJV but it differs in delivery mechanism. HFFI gas delivery is usually based on rotating bar with a small opening placed in the path of a high pressure gas. During the rotation of the bar the opening lines-up with the gas flow, and a brief pulse of gas enters in the airway. The maximum pulse frequency is 15 Hz.

High Frequency Positive Pressure Ventilation (HFPPV) is technique which employs a conventional ventilator at the upper frequency range of the device in order to deliver HFV. HFPPV modality, rarely used any more in clinical practice, delivers a conventional breath. The delivered tidal volumes are usually higher respect to other HFV modalities.

High Frequency Percussive Ventilation (HFPV) is based on high frequency pulsatile flow combined HFV with time cycled pressure controlled ventilation, and will be described in detail in the Chapter 2.

Chapter 2 – High Frequency Percussive Ventilation

High Frequency Percussive Ventilation (HFPV) is an advanced ventilatory strategy which administrates small sub-tidal volumes, or percussions, at higher than conventional frequencies. High frequency ventilation was introduced in the clinical practice in the early seventies while HFPV mode was developed and introduced by F. M. Bird in the early 1980's and initially used for the treatment of burn patients with acute respiratory failure due to smoke inhalation [22].

HFPV associates the beneficial aspects of conventional mechanical ventilation with those of high-frequency ventilation [23]. This particular high frequency oscillation ventilation modality delivers a series of high-frequency sub-tidal volumes, by pulsatile flow (200-900 cycles/min), in combination with low-frequency breathing cycles (10-15 cycles/min). Consequently HFPV encompasses two complementary ventilatory mechanisms convective and diffusive, corresponding to high frequency oscillations and pressure controlled conventional ventilation, respectively. HFPV acts as a rhythmic cyclic ventilation with physically servoed flow regulation, which produces a controlled staking tidal volume by pulsatile flow [23]. HFPV pressure, flow and volume characteristic tracings during a single respiratory cycle are depicted in Figure 2.1. During inspiratory phase lung volumes are progressively increased in controlled stepwise fashion by repetitively diminishing sub-tidal volume deliveries. Depending on the respiratory system elastance an oscillatory plateau can be reached and maintained during inspiration. The ranking part of the volume curve is principally responsible for the convection of the gas delivery. The plateau phase favors the diffusion of the gases, so allowing better gas exchange and favoring secretions removal [24]. The expiratory phase is completely passive. HFPV, like other HFV techniques, offers an advantage over conventional ventilation by providing an adequate oxygenation at lower airway pressure and tidal volume, therefore reducing the risk of barotrauma and volutrauma in acute lung injury and acute respiratory distress syndrome patients.

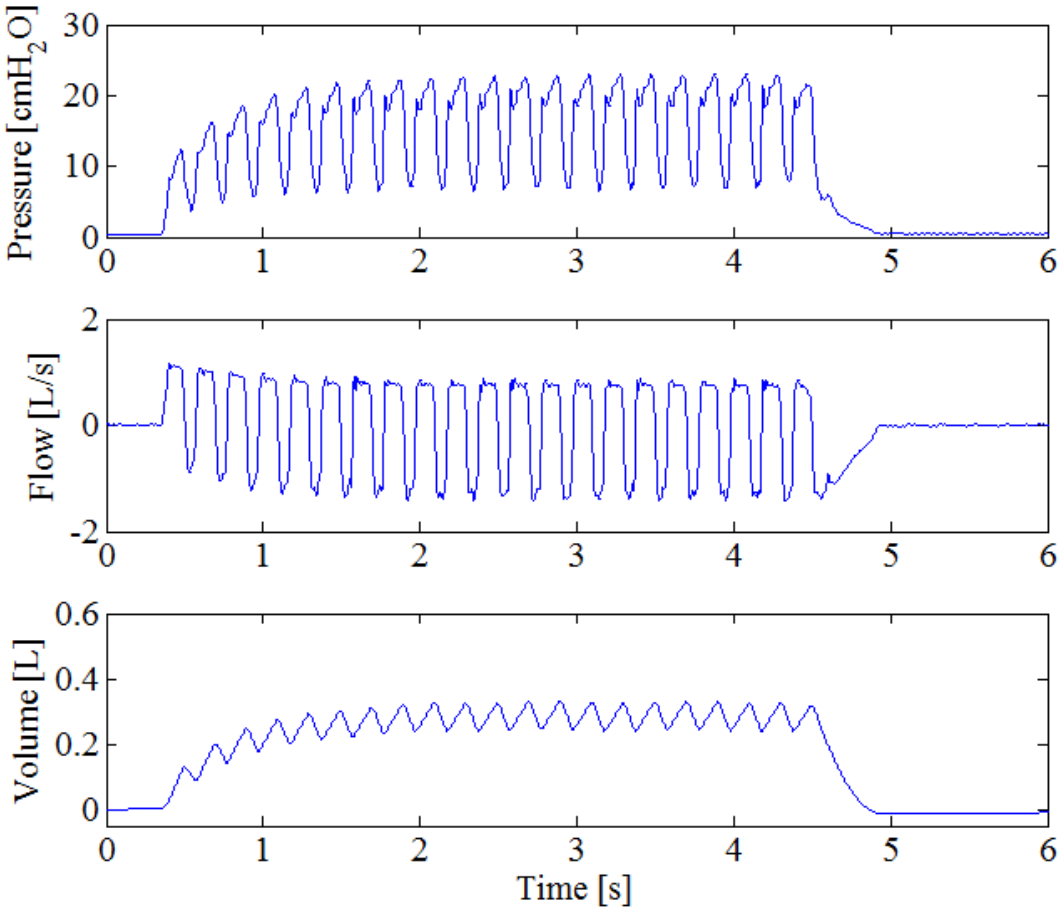

Figure 2.1 Pressure, flow and volume tracings during a single respiratory cycle of High frequency percussive ventilation.

2.1 HFPV ventilator

The only ventilator that delivers HFPV is the Volumetric Diffusive Respirator VDR-4® (Percussionaire Corporation , Sandpoint, Idaho, USA). This ventilator provides diffusive\convective cardiopulmonary support to most critical patients, from neonates through pediatrics to adult patients [25]. The VDR-4® ventilator generates high frequency pulsatile flow using a pneumatically powered, pressure limited, time cycled flow interrupter together with phasitron device, flow amplifier which represents the interface between the patient and the ventilator [22] [25] [26].

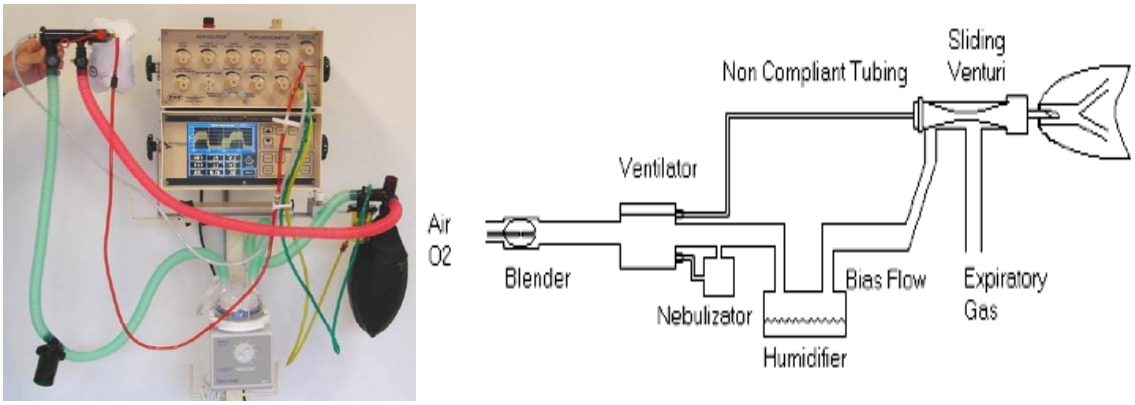

Figure 2.2 HFPV system (right) and its schematic diagram [22] (left).

Figure 2.2 represents a schematic diagram of HFPV system, which consists of a ventilator, high and low pressure inspiratory circuits, phasitron, nebulization system, volume reservoir and expiratory circuit. The ventilator is fed by oxygen and air sources, and the high pressure inspiratory circuit originates from it. The high pressure circuit consists of non-compliant tubing which connects high pressure pneumatic generator to the high pressure inspiratory port of phasitron. The low pressure circuit connects ventilator, volume reservoir and ambient air to low pressure inspiratory port of phasitron through nebulizator and humidifier downstream from one another. The phasitron is also connected through exhalation port to the expiratory circuit and equipped with the side-port, located nearby the endotracheal tube connection, for the real-time measurement of the pressure delivered to the patient. The nebulization system (Figure 2.3) is connected to a volume reservoir and linked to an accessory line which delivers a high-pressure flow synchronized pulse flow delivered to the phasitron [22]. This system allows administration of bronchodilators, mucolytics, and pulmonary vasodilators [27], and together with the humidification system provides to the inspiratory circuit a gaseous mixture heated with 100% humidity.

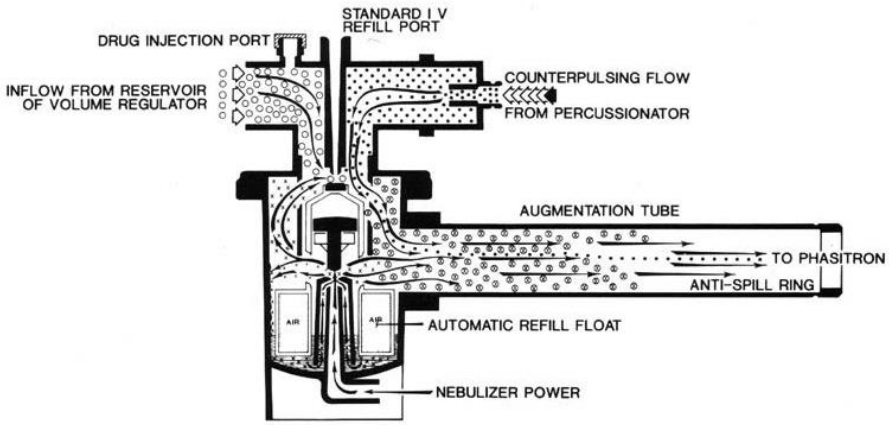

Figure 2.3 Nebulization system: Drug injection port (system for the delivery of drugs); Standard IV refill port (accessory line); Inflow from reservoir of regulators (connection to the reservoir); Counterpulsing flow from Percussionator (flow from the ventilator); Augmentation tube (low-pressure inspiratory flow); Automatic refill float (drugs containing reservoir); Nebulizer Power (accessory line) [22].

The phasitron represents the heart of the HFPV system and it's based on the Venturi principle. The device is composed of a hollow cylinder in which the high frequency airflow provided by high pressure circuit causes a spring-controlled sliding venturi body to move back and forth (Figure 2.4). During the inspiration, phasitron draws gas from low pressure circuit in addition to the jet flow provided by high pressure circuit. According to the Venturi principle, low pressure circuit contributes to the total pulsatile flow delivered to patient with a value inversely proportional to the pressure reached at the level of the airways (Figure 2.5).

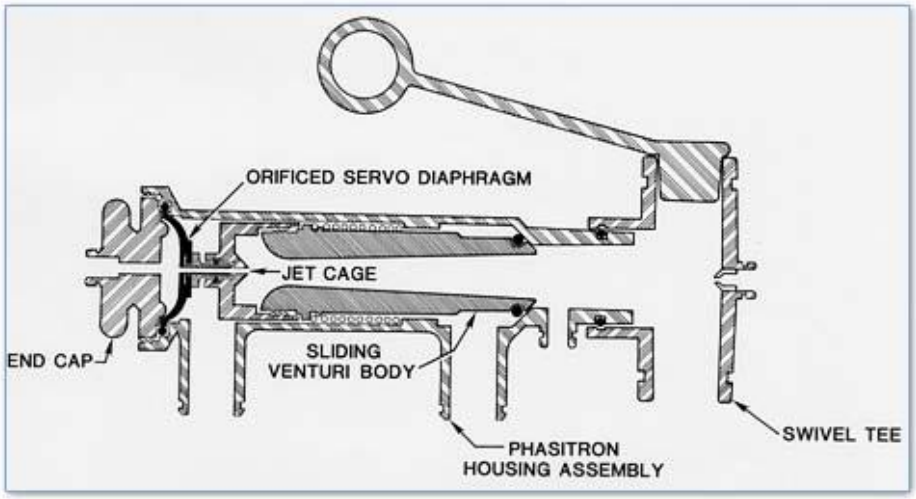

Figure 2.4 Cross section of Phasitron device [28].

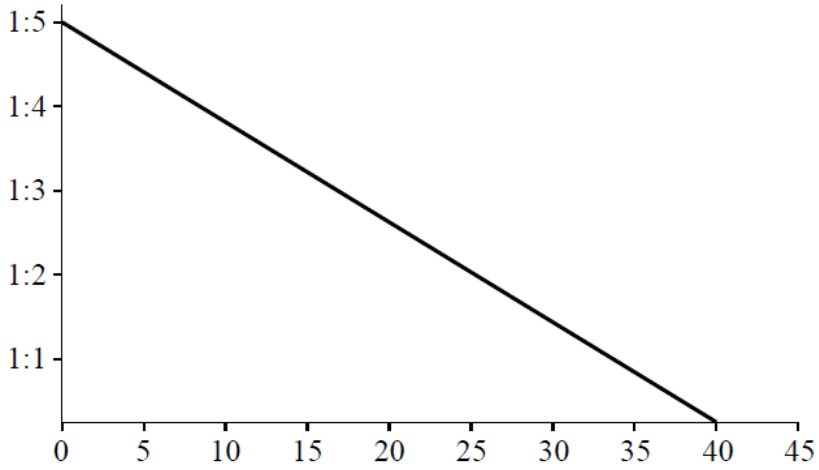

Figure 2.5 Relationship between the proportions of air coming from the high pressure and low-pressure systems (ordinate) and the airways pressure (abscissa). The increase of the latter corresponds to a reduction of the proportions of air coming from the high and low-pressure circuits. Once the set value is reached (40 cmH_2O), the plateau pressure is maintained mainly by the pulsatile system, which draws poorly by low-pressure circuit [28].

The flow introduced into the phasitron from the low pressure inspiratory circuit, which is at atmospheric pressure, is about five times greater than the jet flow that comes from high pressure circuit, in the absence of mechanical load in the output circuit [28]. However, during the inspiration the lungs are filled with air, resulting in a pressure increase at the phasitron output. This pressure reduces the flow speed and consequently decreases the air that is drown in from the low pressure circuit. The ratio between jet flow and low pressure circuit flow, from 1:5 goes to a 1:1 ratio when the high pressures are reached. When the desired pressure level is approaching, the airflow supplied to the patient is almost exclusively coming from the high-pressure circuit. Thus the inspiratory flow delivery to the patient is controlled by a pressure feedback. HFPV delivery system and respiratory circuits can be applied both in neonatal and pediatric as in adult patients [22]. During inspiratory phase the sliding piston will slide forward and the Phasitron closing exhalation port, while during expiratory phase the piston is not pressurized and slides back and the passive exhalation occurs through the exhalation port. The phasitron is also equipped with an inspiratory and an expiratory safety valve, which allow to maintain the predetermined pressure. The respiratory circuit remains constantly open to the air, thus the risk of barotrauma and volutrauma is limited.

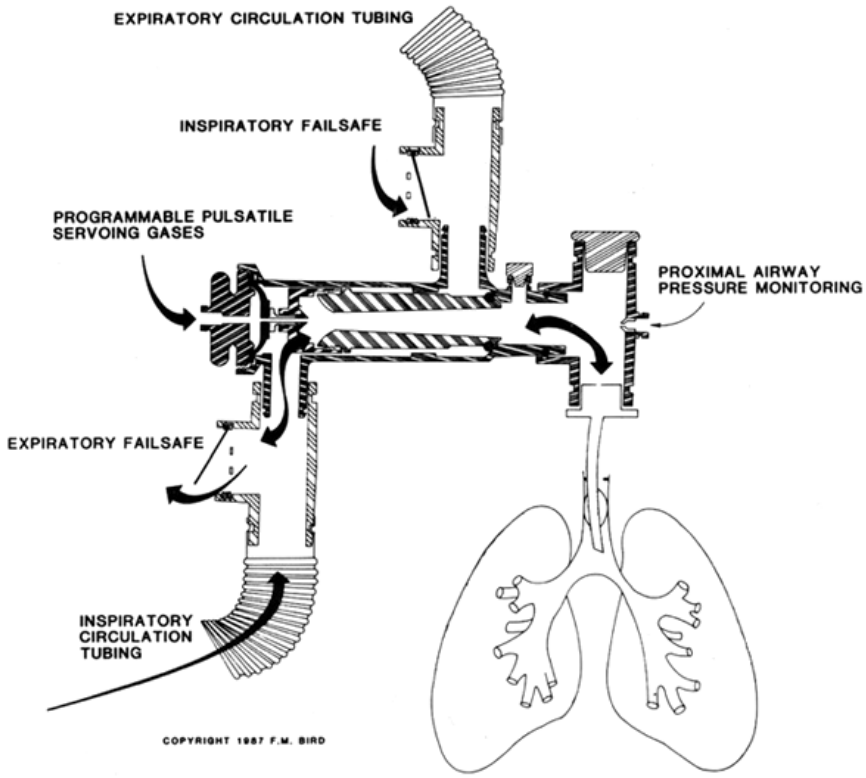

Figure 2.6 HFPV circuit. Programmable pulsatile servoing gases: inspiratory high-pressure circuit; Inspiratory circulation tubing: low-pressure inspiratory circuit, Inspiratory/Expiratory failsafe: inspiratory/expiratory safety valves; Proximal airway pressure monitoring: system for monitoring airway pressure [22].

The VDR-4® ventilator allows different ventilatory parameters to be adjusted by acting on diverse control dials (Figure 2.7). First of all it is possible to adjust the pulsatile flowrate of high pressure circuit, which together with additional flow from low pressure circuit generates the desired working pressure (P_{work}), i.e peak airway pressure depending on the respiratory system impedance. The convective rate and inspiratory to expiratory ratio (I:E) can be set by modifying inspiratory (I) and expiratory (E) times. By adjusting the inspiratory and expiratory times, it is possible to determine a breath rate and mean airway pressure (Paw_{mean}) equal to the conventional mechanical ventilation. Moreover, the pulse inspiratory (i) and expiratory (e) period of a single mini burst can be also adjusted. The percussive pulse frequency (*f*) can be set by the operator in a variable range between 200 and 900 cycles/min. The pulse frequency is a highly important factor in the management of hypoxia. The convective phenomenon is prevalent at low percussion frequencies (200-400 cycles/min), resulting in an increased CO_2 wash-out, while the

diffusive phenomenon is more significant at high percussion frequencies (600-900 cycles/min) [22].

Figure 2.7 VDR-4® HFPV ventilator and Monitron® pressure wave form analyzer [28].

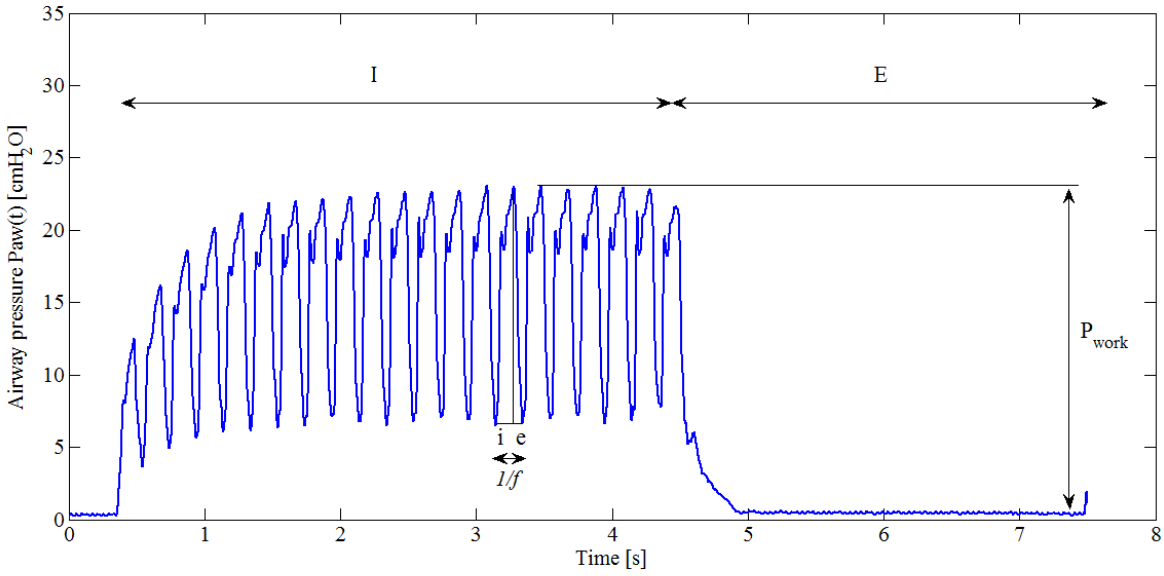

2.8 HFPV pressure curve during a single respiratory cycle and settable features

The positive end-expiratory pressure (PEEP) can be also adjusted and can have constant or oscillating flow pattern (Oscillatory PEEP). During the inspiratory phase the additional convective contribution can be provided through the convective pressure rise (Figure 2.9). Through the air-oxygen blender dial it is possible to set the fraction of inspired oxygen FiO_2. Thus, by acting on these ventilatory parameters it is possible to set the desired HFPV ventilation pattern.

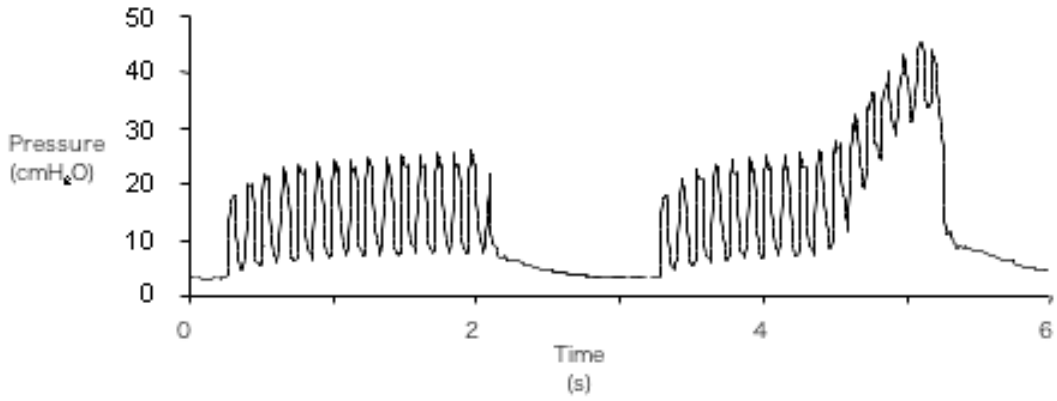

Figure 2.10 Pressure curves during HFPV. The tele-inspiratory phase of the second act has a pressure increase caused by a supplementary flow set by the operator. This option allows, for the same inspiratory time (I), an increase in the volume delivered due to convection [22].

The ventilation monitoring unit Monitron® provided together with the HFPV VDR-4® ventilator is exclusively based on airway pressure signal recordings. The airway pressure is recorded at the patient output of phasitron and is displayed on monitoring device together with parameters extracted from pressure signal (Figure 2.11). The device provide information about I:E and i:e ratio, low frequency breath rate (i.e convective rate), inspiration and expiration time, percussive frequency, peak and mean airway pressure, as also positive end expiratory pressure. These parameter readings are used by physician or therapist during the ventilation setup and later on during ventilation monitoring.

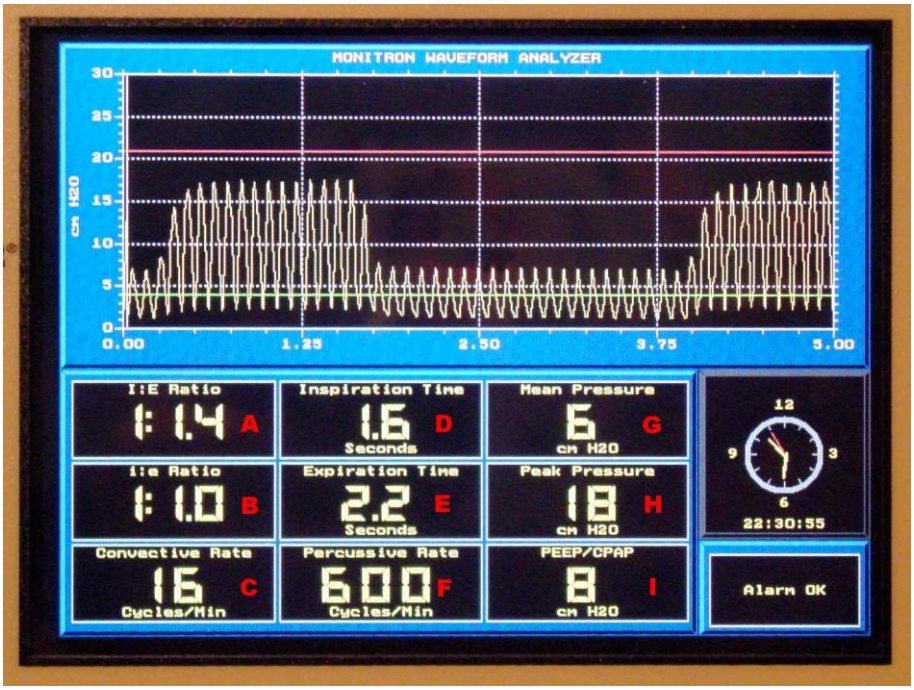

Figure 2.11 Display of HFPV monitoring unit Monitron® [28].

2.2 Impact of mechanical load on pressure flow and volume delivery during HFPV

HFPV delivery system together with phasitron modulates flow administration, therefore it is important to evaluate how the generated pressure, flow and volume change in face of different lung loads. Lucangelo et al studied the effects of mechanical load on pressure, flow and volume delivered by high-frequency percussive ventilation using a single-compartment lung simulator with varying elastic and resistive loads [15][29].

Respiratory signals in the output of ventilator were recorded maintaining the selected ventilatory settings of the HFPV device, while resistance (R) and elastance (E) values were modified. The percussive frequency was 500 cycles/min, the mini-burst i/e ratio was 1:2.75, while the convective ventilation rate amounted to 10 cycles/min, and the I/E ratio equalled 1:1.25. The expiratory phase was passive. The pulsatile flowrate dial was kept constant during the experiment. The initial setting was: E = 20 cmH_2O/L, R = 0 $cmH_2O/L/s$. Ventilator delivery was evaluated in 15 different combinations of three elastic (E = 20, 50, 100 cmH_2O/L), and five resistive loads (R = 0, 5, 20, 50, 200 $cmH_2O/L/s$).

In the Figure 2.12 are depicted flow, volume, and pressure (Paw) tracings during a single respiratory cycle under four different lung loads.

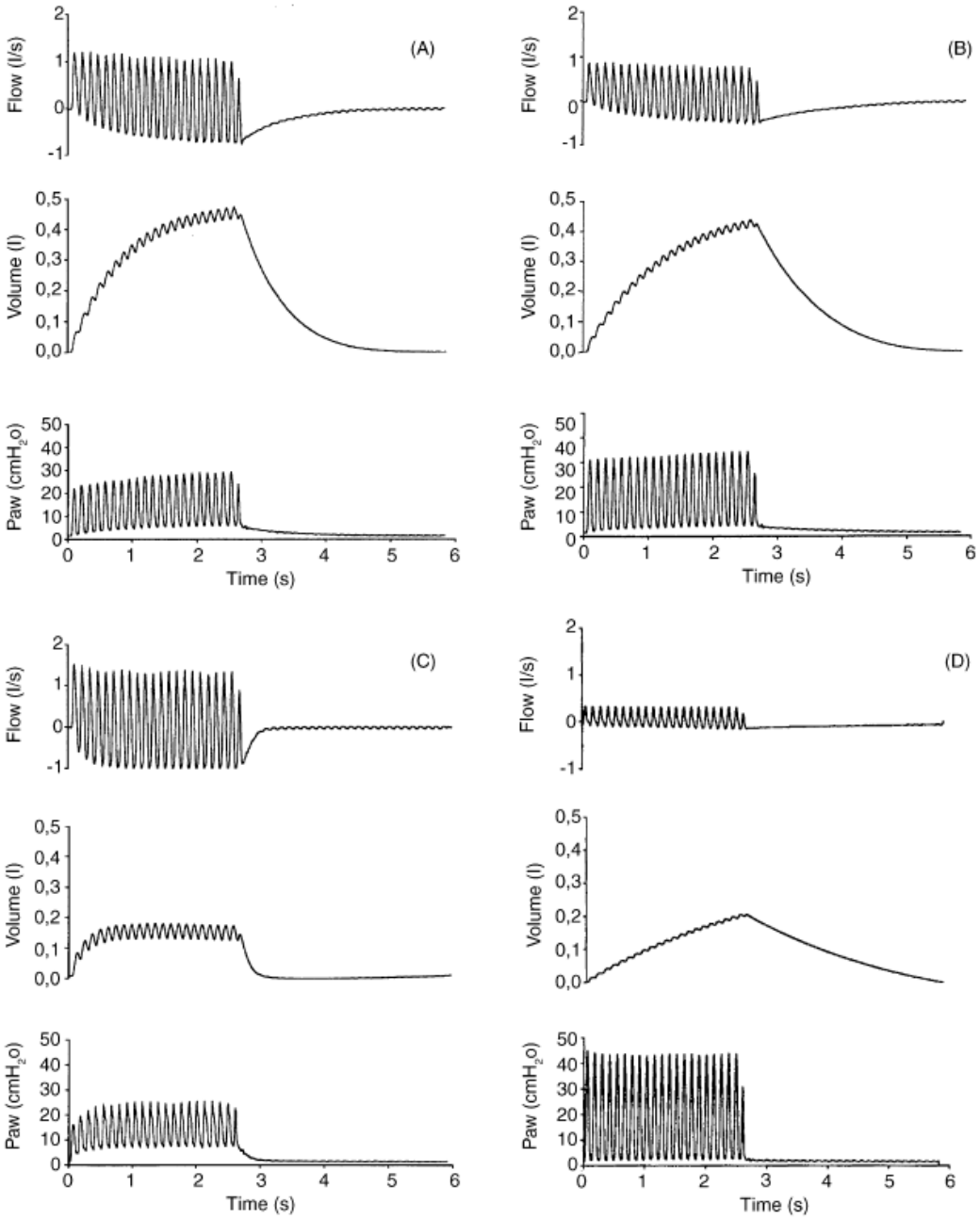

Figure 2.12. Flow, volume, and airway (Paw) pressures tracings during a single respiratory cycle under four different simulated lung loads. Panels A–D the values of E and R are, respectively: 20 cmH_2O/l and 0 cmH_2O/l/s, 20 cmH_2O/l and 20 cmH_2O/l/s, 100 cmH_2O/l and 0 cmH_2O/l/s, and 100 cmH_2O/l and 200 cmH_2O/l/s [15].

Maintaining the same elastance value, resistance increase resulted in flow reduction (Figure 2.12 A-B). This is due to the fact that higher airway resistance produces higher airway pressures and flow decreases as a consequence of phasitron pressure feedback. This phenomenon is even more noticeable comparing pressure e flow considering extreme resistance values (Figure 2.12 C-D). In all cases during initial part of inspiration the positive peak flow was definitely higher than the negative (Figure 2.12). Thus in this phase the quantity of air introduced into the system is greater than the volume washed out of it. The tidal volume rises till it reaches a plateau at the end of inspiration phase, in which the absolute values of the positive and the negative peak flows are very similar, and the net flow approaches zero (Figure 2.13).

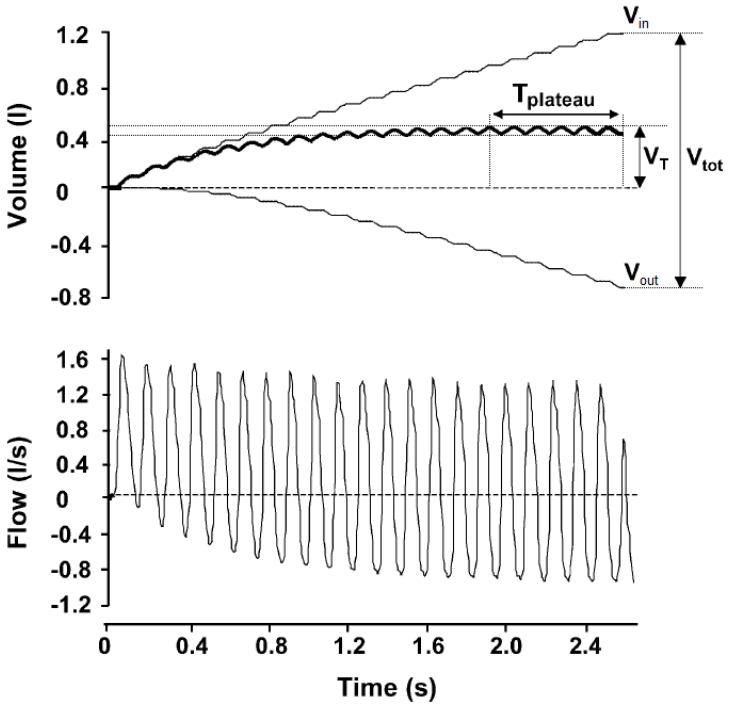

Figure 2.13 Volume and flow traces during a single inspiration. Cumulative input-volume (Vin), cumulative output-volume (Vout), total cumulative volume Vtot and plateau period Tplateau are also depicted in the top panel. Figure modified from [29].

These flow oscillations during the plateau phase may be useful for gas exchange, but they do not increase the inspired volume, so the final tidal volume value V_T is reached in this phase. In the case of low resistance and high elastance the plateau phase in the

volume curve was reached much earlier during inspiration and had greater duration of the plateau (Figure 2.12 C).

In figure 2.14 are depicted iso-elastance volume tracings in the presence of different resistance loads. The end-inspiratory plateau was reached only in the first two low resistance conditions V_T did not change significantly between R=0, 5, 20 $cmH_2O/L/s$.

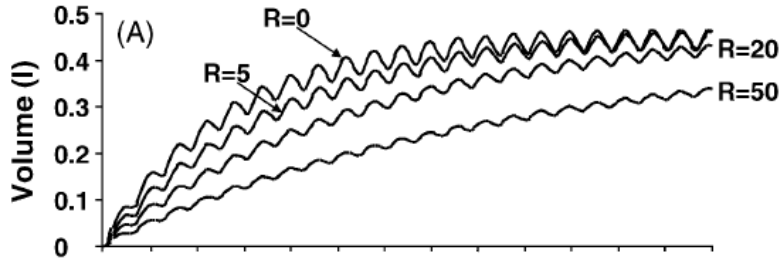

Figure 2.14. Iso-elastance (*E*=20 cmH_2O/L) volume curves in the presence of different resistance loads. From top to bottom *R* = 0, 5, 20, and 50 cmH_2O/L s [29].

In Figure 2.15 are shown iso-resistance (R = 0 $cmH_2O/L/s$) volume curves in the presence of different resistance loads. Tidal volume decreases and plateau phase was reached earlier for higher E values.

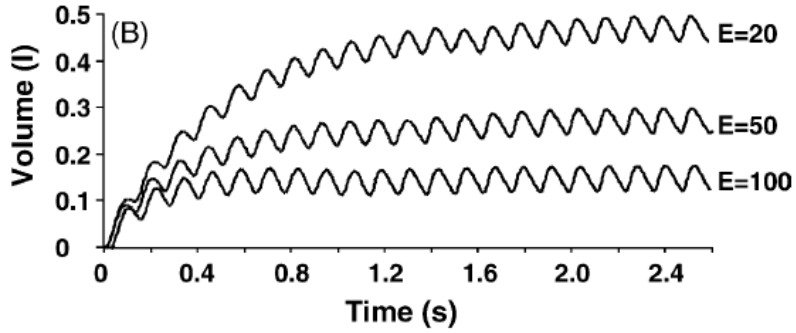

Figure 2.15. Iso-resistance (R = 0 cmH_2O) volume curves in the presence of different elastic loads. From top to bottom E = 20, 50 and 100 cmH_2O/L [29].

The values of the mean and peak airway pressure, inspiratory positive and negative peak flows and tidal volume in all evaluated respiratory impedance combinations are summarized in Table 2.1.

R $cmH_2O\ L^{-1}\ s$	E $cmH_2O\ L^{-1}$	Paw_m cmH_2O	Paw_{peak} cmH_2O	V_{Ppeak} $L\ s^{-1}$	V_{Npeak} $L\ s^{-1}$	V_T mL
0	20	6.91	26.68	1.59	-1.03	465
0	50	7.09	26.55	1.54	-1.03	269
0	100	7.17	26.54	1.54	-1.03	163
5	20	7.57	29.22	1.21	-0.78	470
5	50	7.63	29.82	1.23	-0.79	258
5	100	7.75	28.90	1.22	-0.83	141
20	20	8.23	34.36	0.87	-0.53	437
20	50	8.26	34.75	0.88	-0.56	215
20	100	8.32	34.49	0.88	-0.59	120
50	20	8.60	39.06	0.56	-0.32	257
50	50	8.87	39.72	0.57	-0.37	162
50	100	8.83	39.75	0.57	-0.41	96
200	20	9.27	44.84	0.33	-0.16	205
200	50	9.34	45.43	0.34	-0.19	164
200	100	9.43	45.43	0.34	-0.23	115

Table 2.1 Pressure, flow and volume values for different combination of resistive and elastic loads. Pawm and Pawpeak are mean and peak airway pressures, respectively. V_{Ppeak} and V_{Npeak} are inspiratory positive and negative peak flows are the maximum and minimum values of flow during inspiration. V_T is tidal volume, the maximum volume value during inspiration [15].

Peak and mean airway pressures, positive and negative peak flows, as also delivered tidal depend on resistive load variations, while elastance load variations influence only tidal volume (Table 2.1). Peak airway pressure and mean airway pressure increase when resistance increases, the elastance variation resulted in an insignificant variation of Paw_{peak} and Paw_m (Figures 2.16, 2.17, respectively). For the same elastance values a curvilinear relationship between Paw_{peak} and R was detected.

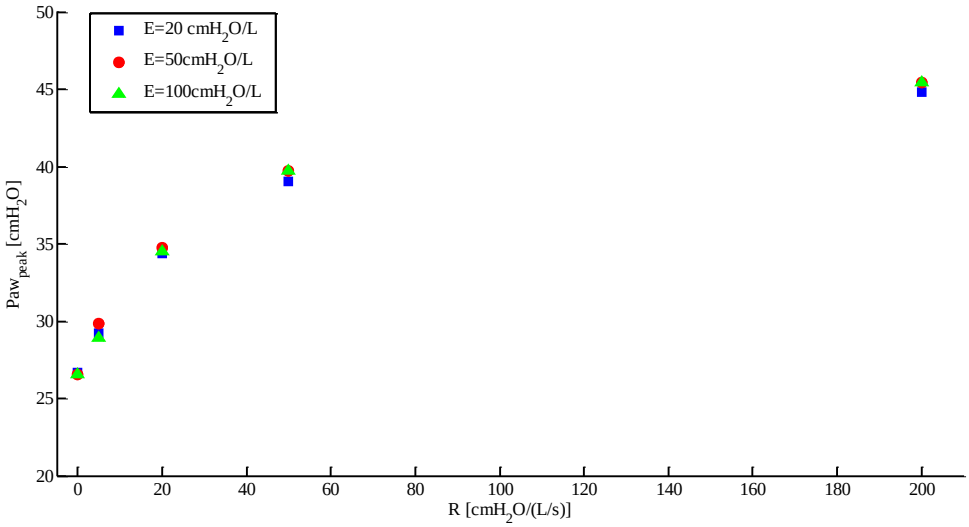

Figure 2.16 Peak airway pressure (Paw_{peak}) values corresponding to the 15 different combinations of resistive and elastic lung loads.

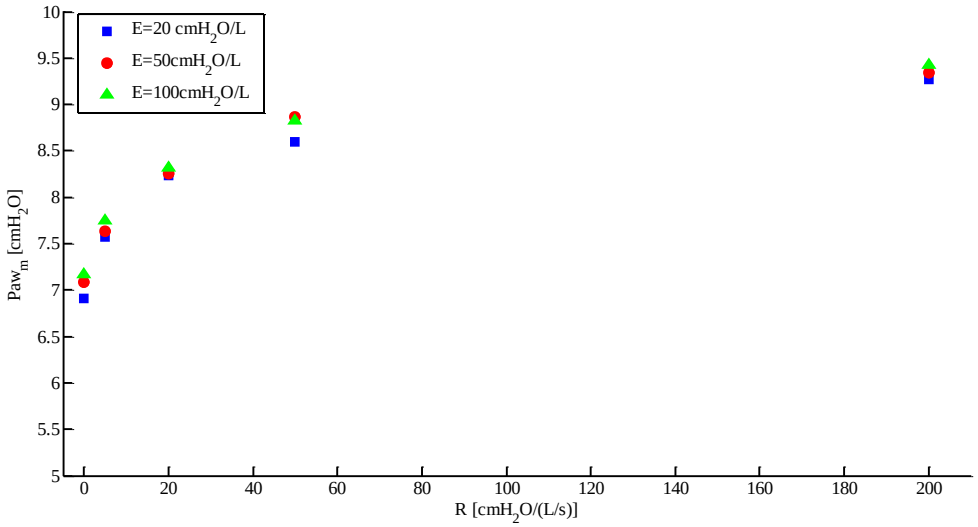

Figure 2.17. Mean airway pressure (Paw_m) values corresponding to the 15 different combinations of resistive and elastic lung loads.

Delivered tidal volume diminished with increasing of resistance and elastance loads (Figure 2.18), and showed higher dependence on E then on R. The highest R and E loads presented lowest tidal volume values.

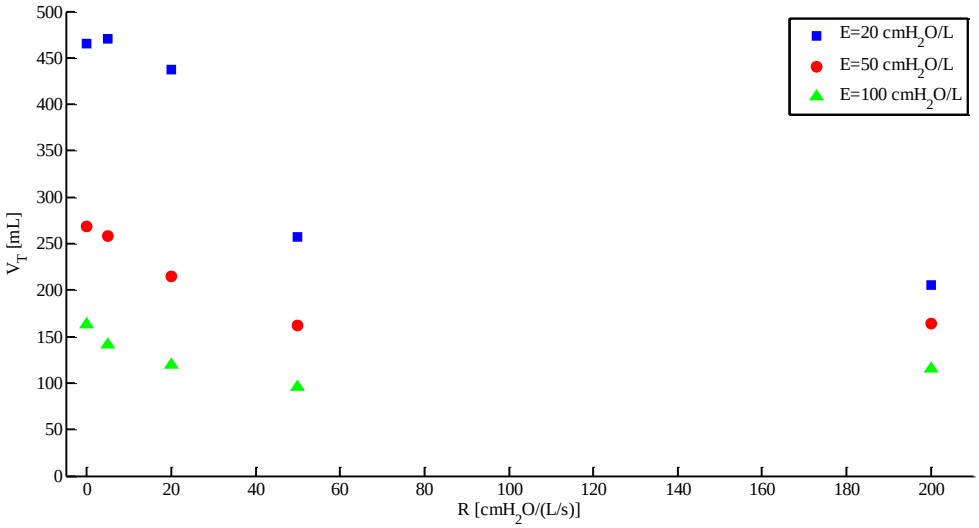

Figure 2.18. Tidal volume (V_T) corresponding to the 15 different combinations of resistive (R) and elastic (E) lung loads.

Peak and mean airway pressures showed low correlation with tidal volume (Figure 2.19). Similar tidal volume values corresponded to wide range of Paw_m and Paw_{peak}. Moreover, in the Figure 2.19 it can be seen that in a narrow range of Paw_m and Paw_{peak}, V_T varies largely. These large volume variations mainly depend on changes in resistive and elastic mechanical loads. These facts indicate the intrinsic limits of Paw_m and Paw_{peak} monitoring in face of volume delivery and lung impedance changes during HFPV.

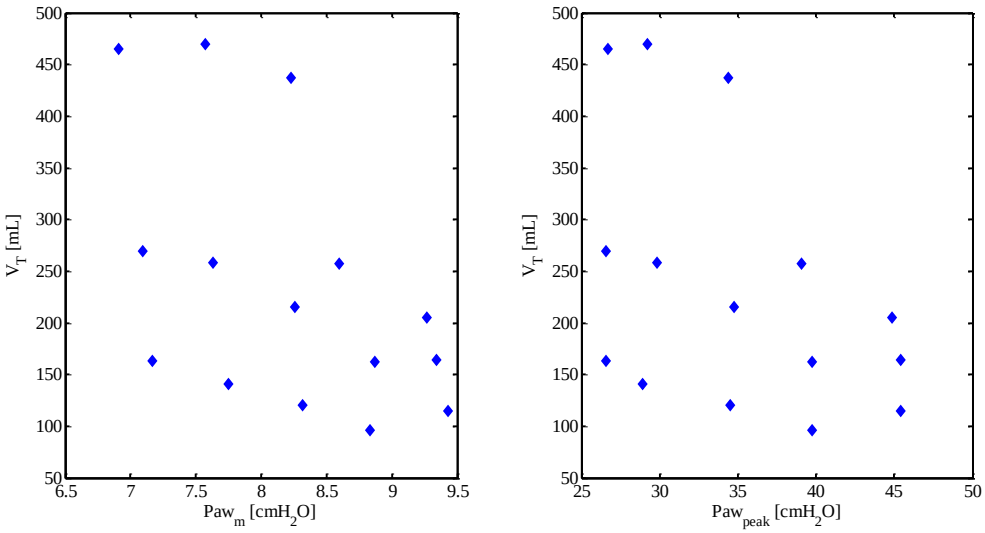

Figure 2.19. Tidal Volume (V_T) plotted versus Paw_m (left panel) and Paw_{peak} (right panel) in 15 different R and E experimental conditions.

Tidal volume during a HFPV is provided as the difference between delivered pulsatile input and output volumes, thus some amount of gas is washed out of the lungs throughout inspiration washing carbon dioxide out of it and moving oxygen in. This could be very important in case of short diffusive ventilation time. From the clinical point of view it is also important to evaluate the effects of respiratory system impedance on washout volume during HFPV in terms of tidal volume and lung washout parameters: cumulative input-volume (V_{in}), cumulative output-volume (V_{out}), total cumulative volume V_{tot} and plateau period $T_{plateau}$ corresponding to the mathematical integration of positive and negative flow during inspiration, total volume delivered by ventilator during inspiration and duration of plateau phase, respectively (Figure 2.13). The elastic or resistive loading modulates HFPV delivery a way that washout volume increases when time allowed for diffusive ventilation decreases and vice versa [29]:

- High turnover gas in the lung with V_T/V_{tot} from to 8.7 to 42.5 %. This ratio increases with R, while decreases with E
- V_T does not change significantly in lower resistances (R=0-20 cmH2O/L/s), while either V_{tot}, V_{in} and V_{out} decreases progressively as R increases
- $T_{plateau}/I$ increases and V_T/V_{tot} as alsoV_T decreases with increasing of E

2.3 HFPV clinical applications

The earliest use of HFPV occurred in the treatment of closed head injury [30] and patients with acute respiratory distress syndrome (ARDS) caused by burns and smoke inhalation [31] [32]. HFPV was successfully used for treatment of newborns with hyaline membrane disease and/or ARDS [33-35]. HFPV was also employed in patients with neuromuscular disease [36] and in patients with acute respiratory failure following chest trauma [37]. Over the years, HFPV has proven highly effective in severe hypoxemic non responders to conventional mechanical ventilation [38]. The efficacy of HFPV has been demonstrated also in removing bronchial secretions under diverse conditions [39].

This non-conventional ventilatory modality was found effective in physiotherapy of cystic fibrosis patents, during a pilot study which compared the effects of HFPV with those of conventional chest physiotherapy [40].

The outcome studies are limited because HFPV is being more used in clinical situations when other conventional ventilator modes have not achieved the targeted oxygenation and ventilation goals [27]. The study which involved 24 patients with acute respiratory failure showed that during the HFPV treatment the best combined effect on clearance of CO_2 and improvement of hypoxia is reached at percussion frequency of 500 cycles/min [41]. Comparing conventional ventilation and HFPV in seven patients with severe respiratory distress at equal airway peak pressure and FiO_2 lung gas exchange in terms of partial pressure of oxygen in the blood (PaO_2) improved significantly [42]. HFPV has been also recently inserted among the ventilatory strategies to use in severe hypoxemic respiratory failure [43].

HFPV was also employed during surgery [44] [45]. HFPV enabled adequate gas exchange during the surgical bronchial repair in a patient with one lung [44]. During thoracotomy, the nondependent lung was ventilated with HFPV to avoid hypoxemia in 22 patients and results were compared to other patients which 22 received continuous positive airway pressure (CPAP). HFPV improved oxygenation in one-lung ventilation during pulmonary resection and postoperatively, it decreased the length of stay and increased the mobilization and removal of endobronchial secretions in comparison with CPAP [45].

Most recently, Lucangelo et al. reported that early short-term application of HFPV improved gas exchange in 35 hypoxemic patients who did not respond to 12h conventional

treatment (Figure 2.20) [46]. HFPV applied for 12h at the same mean airway pressure as conventional ventilation significantly increased gas exchange in patients with different pulmonary diseases. The improvement stayed unchanged also under subsequent conventional ventilation 12h after end of HFPV treatment. During the first four hours of HFPV treatment the mean PaO_2/FiO_2 slope was 10.2 h^{-1}.

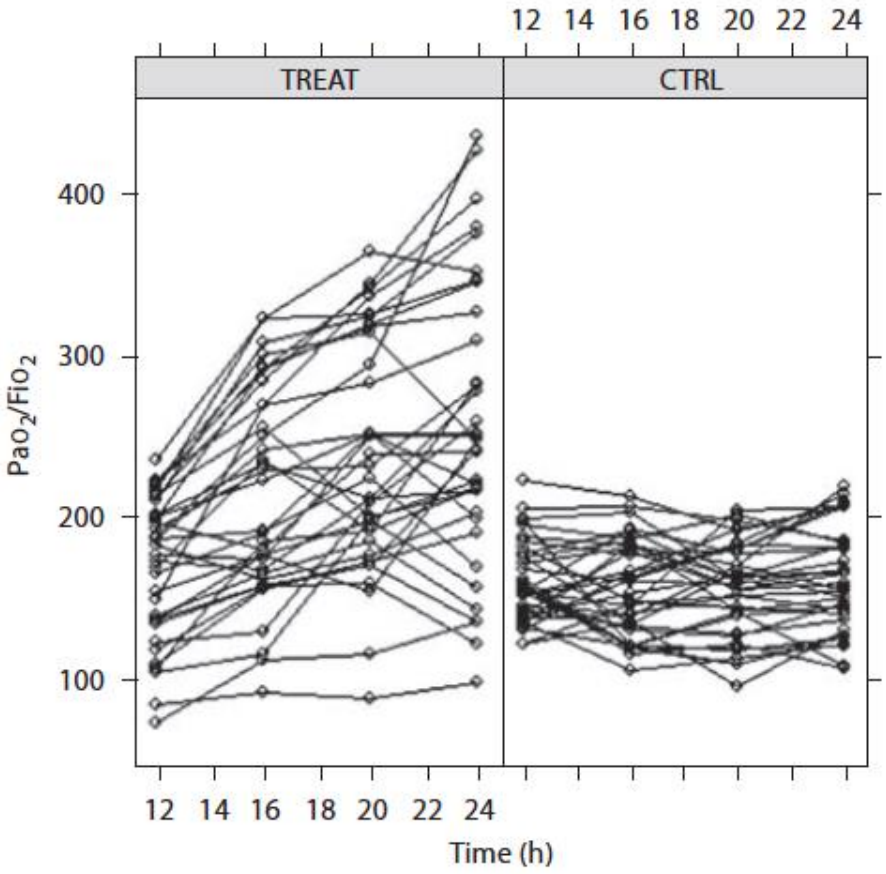

Figure 2.20 PaO_2/FiO_2 oxygenation rate over time in hypoxemic patients. After 12h (baseline) conventional treatment patients were switched to HFPV (right panel) or left under conventional ventilation (left panel). PaO_2/FiO_2 improved significantly in HFPV group, while the control conventional ventilation group remained unaltered [46].

Similar results are obtained by Rizkalla et al. in pediatric patients with acute respiratory failure. In a heterogeneous population of pediatric acute respiratory failure failing conventional ventilation, HFPV efficiently improved gas exchange setting the treatment at the same Paw_{mean} as during conventional ventilation [47].

HFPV has proven highly effective in patients with widely differing pathological conditions and especially in non-responders to conventional mechanical ventilation [37]

[46] [47]. However in these cases HFPV setup was based only on Paw_{mean} and gas exchange analysis without considering real delivered tidal volume, respiratory resistance and compliance and tracheal tube pressure drop parameters. Paw_{mean} is weakly correlated with V_T and respiratory resistance and compliance modify HFPV delivery, thus for tool for measuring and estimation of this parameters is required for a personalized HFPV ventilator setup in order to improve the treatment in the safe way.

Chapter 3 – In vitro estimation of respiratory parameters during HFPV

HFPV monitoring system currently is based exclusively on airway pressure measurement. The airway pressure tracings, peak and mean airway pressures, together with gas exchange analysis, at the present time are the only parameters that guide the physician during the HFPV treatment [46]. These parameters provide only partial information about HFPV treatment setup and its clinical effectiveness. In patients under diverse mechanical ventilation techniques the information on gas exchange alone may not suffice [46]. HFPV is not an intuitive ventilatory modality and the absence of valuable information during the treatment, as delivered tidal volume, respiratory system resistance and compliance, produces disaffection among the physicians [48]. Thus, knowing these parameters is necessary for a personalized HFPV setup in order to improve beneficial aspects of this non-conventional ventilatory strategy. To overcome aforementioned limitation the measurement of pressure, flow and volume respiratory signals together with tools for estimation of resistance and compliance parameters during HFPV are needed.

Pressure Paw(t) and flow $\dot{V}(t)$ may be measured using appropriate pressure and flow transducers, placing them between phasitron and endotracheal tube. Volume and volume acceleration can be calculated by numerical integration and derivation of acquired flow signal, respectively. On the contrary, respiratory mechanics parameters are not directly measurable.

3.1 Respiratory signal measurement during HFPV

High frequency percussive ventilation is characterized by high frequency pulsatile oscillations of pressure and flow respiratory signals. Monitoring devices widely used in conventional mechanical ventilation, which is characterized by low frequency respiratory signals, are not designed for monitoring of respiratory parameters undergoing this high frequency ventilatory modality. Slow response time of transducer and low sampling

frequency present the limit of these devices. In fact, Riscica et al. demonstrated that such devices in case of HFPV are generating errors in pressure flow and especially volume measurement, so they are not adequate in these ventilatory conditions [49]. Therefore, for a correct measurement of respiratory parameters undergoing HFPV a wide bandwidth measurement system is required using new generation high sensitivity and low response time.

The range of pressure measurements is defined by the absolute pressures reached during HFPV ventilation in the patients upper respiratory tract that have order of magnitude of some tens of cmH_2O. In this work pressures were measured by ASCX01DN unipolar pressure transducers (Honeywell, USA), which measures pressure in the range of 0-70 cmH_2O and has a response time of 0.1 ms. (Figure 3.1)

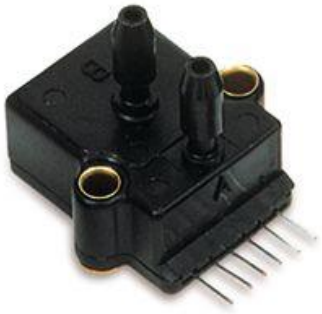

Figure 3.1 The ASCX01DN differential and gauge pressure transducer.

The flow signal $\dot{V}$ was measured by Fleisch pneumotachograph (Figure 3.2), which converts flow in a differential pressure, successively measured by high sensibility differential pressure transducer. The typical flow values generated by HFPV are lower than 2 L/s. Fleisch pneumotachograph Type 2 (Lausanne, Switzerland), characterized by maximum advisable flow of 2.5 L/s and dead space of 35mL, was used.

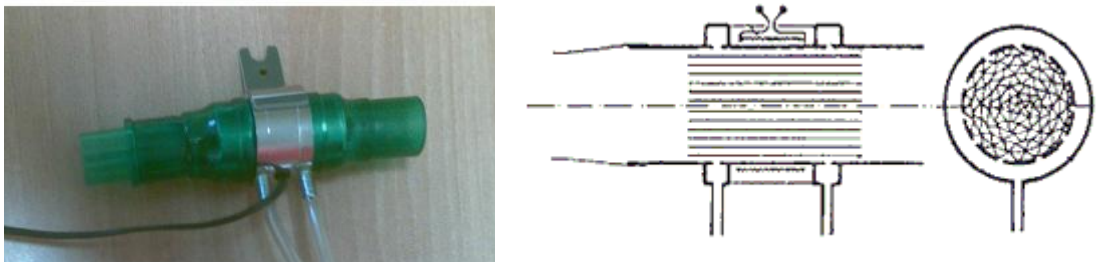

Figure 3.2 Fleisch pneumotachograph (left) and its cross sections (right)

The flow values up to 2 L/s correspond to differential pressures up to 0.66 cmH_2O in output of Fleisch type 2 pneumotachograph. High sensitivity, amplified differential low pressure (±0.63 cmH_2O) and fast response (0.5 ms) transducer 0.25INCH–D-4V (ALL SENSORS, USA) was used to measure differential pressure present across the pneumotachograph.

Figure 3.3 Low differential pressure transducer 0.25INCH–D-4V

0.25INCH–D-4V transducer provides a ratiometric 4-volt output, with reduced output off set errors owing to change in temperature, stability to warm-up, stability to long time period, and position sensitivity. The sensor uses a silicon, micromachined, stress concentration enhanced structure to provide a very linear output to measured pressure. These calibrated and temperature compensated sensors give an accurate and stable output over a wide temperature range.

The transducers were interfaced with a suitable conditioning boards designed and produced during this work at Biomedical Instrumentation and Signal Processing Laboratory at University of Trieste. The respiratory signals were filtered with a second order Butterworth low pass filters and sampled at 2kHz by using either PCI-6023E or NI-USB6009 (National Instruments, Austin, USA) data acquisition board with 12 and 14 bit resolution, respectively. Volume (V) was calculated by numerical integration [50]. Volume acceleration ($\ddot{V}$) was calculated by numerical differentiation of the air flow using low-noise Lanczos differentiator described by the following equation:

$$\ddot{V}(n) = \frac{f_s}{28}\left[\dot{V}(n+1) - \dot{V}(n-1) + 2\cdot(\dot{V}(n+2) - \dot{V}(n-2)) + 3\cdot(\dot{V}(n+3) - \dot{V}(n-3))\right]$$

where f_s is the sampling frequency and n the sample index.

The reliability of respiratory signal measurement, using described devices, was assessed in vitro. The volume measurement error lower than 3%.

3.2 In vitro estimation of viscoelastic parameters during HFPV

Assessment of respiratory mechanics viscoelastic parameters can play a central role in the management of acute respiratory failure (ARF) patients undergoing artificial ventilation [2] [8]. ARF is characterized by a rapid deterioration in pulmonary gas exchange that may be due either to alterations in the mechanical properties of the respiratory system leading to ventilation–perfusion mismatching or shunt, or to neuromuscular insufficiency causing alveolar hypoventilation [8]. Valuation of respiratory function and mechanics is very important in order to [8]:

- understand the pathophysiology of the disease underlying ARF;
- assess the status and progress of the disease;
- provide guidelines for therapeutic measures (positive end-expiratory pressure, bronchodilators, fluids);
- improve patient–ventilator interaction;
- prevent ventilator-related complications;
- plan the discontinuation of mechanical ventilation.

The rapid airway occlusion technique is regularly used for evaluation of respiratory mechanics parameters in patient undergoing conventional ventilation [51] [52]. Technique is based on brief occlusion, during constant flow inflation, applied at the end of expiration end expiratory occlusion, EEO) or at the end of the inspiration (end inspiratory occlusion, EIO). EEO provides only a measure of auto-PEEP (i.e. intrinsic positive end-expiratory pressure $PEEP_i$), while a EIO provides measurement of most respiratory mechanics parameters (R, C, PEEP). In the latter the occlusion is applied right before the end of the inspiration and results in an immediate airway pressure drop from a peak preassure (P_{peak}) to a lower value (P_1) followed by slow decay reaching the plateau value (P_{plat}) in a few seconds [53] (Figure 3.4).

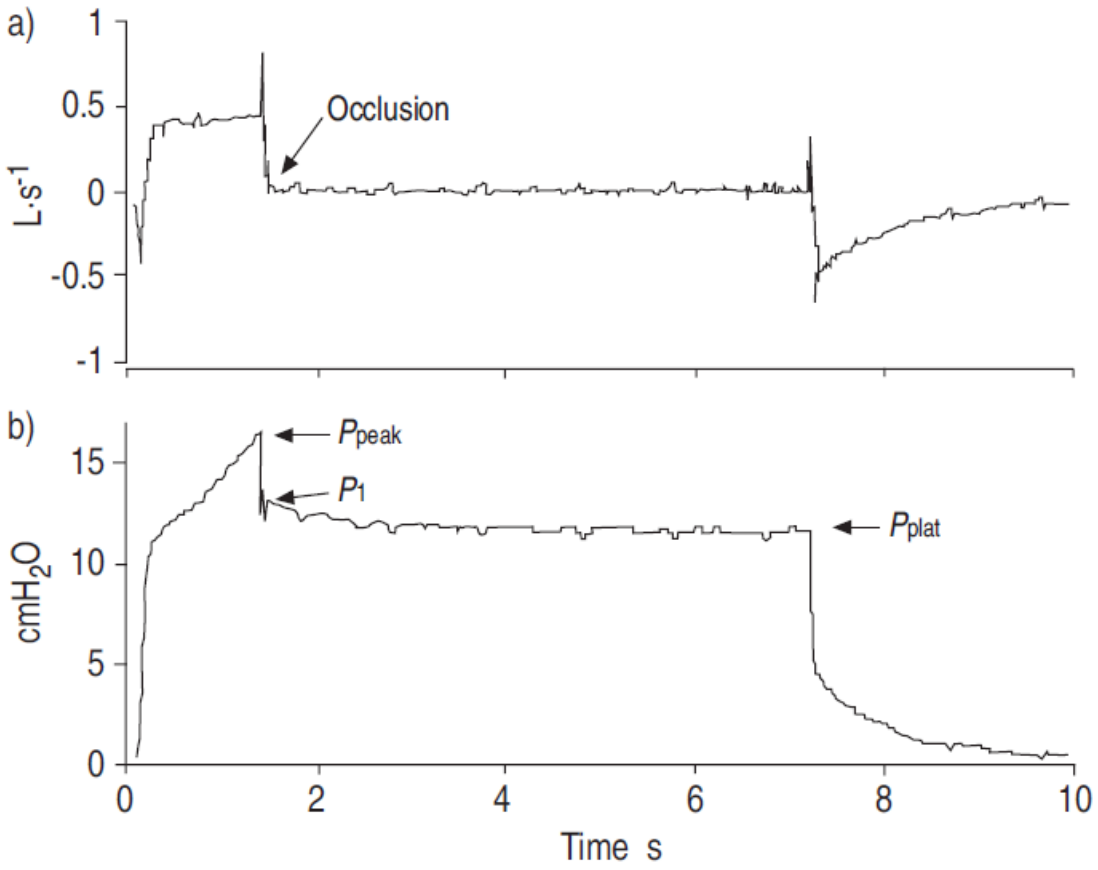

Figure 3.4 Pressure (a) and flow (b) tracings during end inflation occlusion procedure [53].

The pressure fall from P_{peak} to P_{plat} is due to the total resistance R_{tot} which can be calculated as:

$$R_{tot} = \frac{P_{peak} - P_{plat}}{\dot{V}}$$

where $\dot{V}$ is a constant flow value.

The static elastance E_{st} can be also calculated from these maneuvers:

$$E_{st} = \frac{P_{plat} - PEEP_i}{V_T}$$

where V_T is tidal volume value immediately preceding the occlusion.

However, the occlusion technique for estimation of respiratory mechanic parameters requires either ventilators adequately equipped (i.e Paw, $\dot{V}$, V measurement and occlusion valve) or additional equipment (i.e. pneumotachograph, pressure transducer, occlusion valve) inserted in line to the ventilator circuit. The occlusion method interferes

with the ventilator settings and ventilation pattern. Moreover, the occlusion method requires a constant flow, resulting inapplicable during HFPV, characterized by high frequency pulsatile flow.

An alternative method for assessment of respiratory mechanics is the parametric identification of respiratory system model starting from pressure and flow respiratory signals measurements. This method provides estimation of dynamic resistance, elastance and PEEP. The model usually used for this application in conventional ventilation is the first-order model of respiratory mechanics. The dynamics of breathing for clinical purposes can be satisfactory represented by a single-compartment model consisting of a single resistance and compliance [6] [7].

This method applied using the least square fitting with the first order model keeping resistance and compliance constant over the whole breathing cycle presented acceptable results undergoing conventional ventilation [54]. This technique, currently limited to patients without any respiratory activity, during controlled mechanical ventilation present a simple and robust tool for routine clinical use in the intensive care unit [8].

In case of high frequency ventilation the respiratory mechanics is more properly described by Dorkin high frequency model, which approximates the respiratory mechanics function at high frequencies taking into account inertance [13]:

$$Paw(t) = E \cdot V + R \cdot \dot{V}(t) + I \cdot \ddot{V}(t) + P_0$$

where, at every time t, Paw(t) represents the pressure applied to the respiratory system, V(t) is the pulmonary volume, $\dot{V}(t)$ is the airflow and $\ddot{V}(t)$ represents the volume acceleration; P_0 represents the pressure offset (i.e. PEEP). The resistance R, elastance E and inertance I parameters describe respectively the viscous, elastic and inertial mechanical properties of respiratory system. This three element model is suitable for everyday clinical practice because of its simplicity, immediate physiological interpretation of its parameters and its sensitivity to changes in lung mechanics.

In a previous study of our group [48], respiratory parameters during HFPV were estimated in vitro, at different percussive frequencies only at a working pressure (P_{work}) of 30cmH_2O. In order to assess this method in different ventilatory settings before application in patients undergoing HFPV in this work the previous research was to extend in the new study [55], estimating respiratory parameters by parametric identification, also to different

P_{work} that are commonly applied in clinical practice. Using the aforementioned linear model in 81 different experimental set-up combinations of working pressures, percussive frequencies, resistive and elastic lung loads, we verified the goodness of the model and of the identification method. The parameters were estimated by least squares method starting from measured pressure and flow signals, considering inspiratory phase exclusively in order to simulate the effective clinical condition.

3.2.1 Material and methods

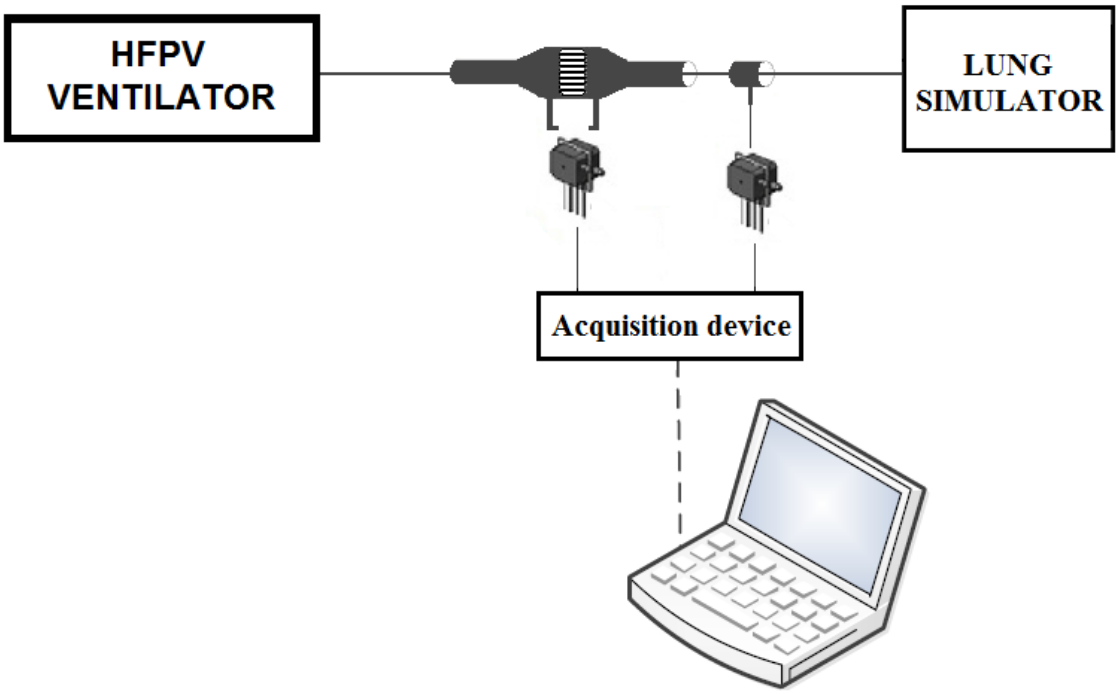

Figure 3.5 Schematic diagram of experimental set-up.

The experimental setup used in this study is shown in Figure 3.5. High Frequency Percussive Ventilation of the lung simulator was provided by a volumetric diffusive respirator (VDR-4®; Percussionaire Corporation, USA) through the Phasitron®. A ventilator circuit was connected via a dedicated connector to the pressure and flow sensors; the distal part of the latter was linked to the described physical model of respiratory system. A physical model of respiratory system was provided by a single-compartment lung simulator (ACCU LUNG, Fluke Biomedical, USA) with 1L capacity (Figure 3.6). The lung model consist of an elastomer bellow between two plates, different springs

stretched between the top and bottom plate to simulate different compliance and resistors with different orifice diameters used to create varying levels of airway resistance. The accuracy of the fixed resistance was 20% up to 2 L/s, and the accuracy of the fixed compliance was 10% up to 500 mL of tidal volume, while the inertance can be considered negligible.

Figure 3.6 ACCU Test-Lung

Lung simulator loads were chosen to represent normal subjects, obstructive and restrictive patients, and ventilator settings were chosen to represent usual clinical application range. In our measurements the lung simulator was set according to the combinations of resistive loads R of 5 and 20 $cmH_2O/(L/s)$ and elastic loads E of 20, 50 and 100 cmH2O/L (corresponding to compliance values of 50, 20 and 10 $cmH_2O\ L^{-1}$, respectively).

The VDR-4® ventilator was set to pulse inspiratory/expiratory (i/e) duration ratio of 1:1, and the overall inspiratory and expiratory duration (I/E) ratio of 1:1. The tele-inspiratory work pressure P_{work} was set to 20, 30 and 40 cmH_2O, while the percussive frequency *f* was set to 300, 500 and 700 cycles/min.

Measurements of respiratory signals were performed for the 81 possible combinations of resistive and elastic loads, percussive frequencies, and work pressures during three successive respiratory cycles. The measurement of flow signal $\dot{V}(t)$ was performed using Fleisch pneumotachograph (Type 2, Switzerland) connected to a differential pressure transducer (0.25 INCH-D-4V, All Sensors, USA). The pressure signal Paw(t) was measured using a differential pressure transducer (ASCX01DN, Honeywell, USA). Data were acquired at a sampling frequency of 2000Hz with 12 bit resolution (PCI-

6023E, National Instruments, USA). Volume V(t) and volume acceleration $\ddot{V}(t)$ were calculated respectively by numerical integration and differentiation of flow.

The least squares regression was employed to estimate the model coefficients during inspiratory phase of each respiratory cycle. The estimation of the parameter vector θ was calculated:

$$\theta = \left(A^T \times A\right)^{-1} \times A^T \times B$$

with

$$\theta = \begin{bmatrix} E \\ R \\ I \\ P_0 \end{bmatrix}$$

$$A = \begin{bmatrix} V_1 & \dot{V}_1 & \ddot{V}_1 & 1 \\ V_2 & \dot{V}_2 & \ddot{V}_2 & 1 \\ \vdots & \vdots & \vdots & \vdots \\ V_{N-1} & \dot{V}_{N-1} & \ddot{V}_{N-1} & 1 \\ V_N & \dot{V}_N & \ddot{V}_N & 1 \end{bmatrix}$$

$$B = \begin{bmatrix} P_1 \\ P_2 \\ \vdots \\ P_{N-1} \\ P_N \end{bmatrix}$$

The adequacy of the model used to describe the measured system was evaluated by means of the normalized residual root mean square error:

$$\text{rmse}\% = \sqrt{\frac{\sum_{k=0}^{N-1}\left[P_{awm}(kT) - P_{awest}(kT)\right]^2}{N}} \frac{100}{P_{awpeak}}$$

where P_{awm} represents the measured airway pressure, P_{awest} the estimated airway pressure, T the sampling period, N the number of samples and P_{awpeak} the measured peak pressure.

3.2.2 Results

Figure 3.7 shows the estimated resistance values (R_{est}) versus P_{work}, obtained for different set-up combinations of lung elastances and percussive frequencies.

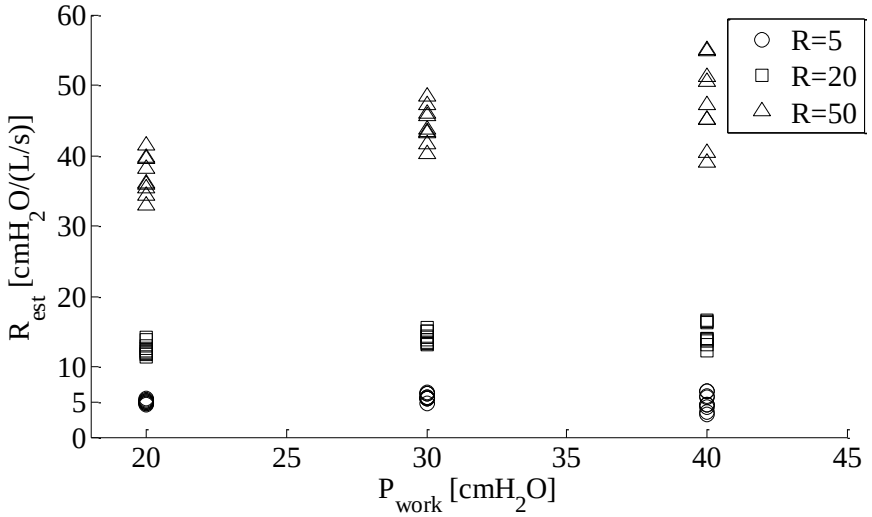

Figure 3.7 Estimated resistance values R_{est} of R values [$cmH_2O/(L/s)$] set on the lung simulator in function of P_{work}. Each point represents the result of the parametric estimation in one of the 81 different experimental setting combinations (P_{work}, f_P, R, E)

Underestimated values were found for a lung simulator R of 20 $cmH_2O/(L/s)$ while a good approximation was present for R = 5 $cmH_2O/(L/s)$. In both cases R_{est} did not show dependency on P_{work}. For R=50 $cmH_2O/(L/s)$, R_{est} increased as P_{work} increased, presenting a large variability due to the different elastances and percussive frequencies examined. Estimated elastance values E_{est} in function of P_{work} are shown in Figure 3.8. The estimated values resulted slightly higher than lung simulator nominal ones for E=20 cmH_2O/L and E=50cmH_2O/L, while for E=100 cmH_2O/L overestimated values were present. No dependency on P_{work} was detected. The E_{est} varied for different lung resistances and percussive frequencies, even if without a clear relationship, especially in case of E=100 cmH_2O/L.

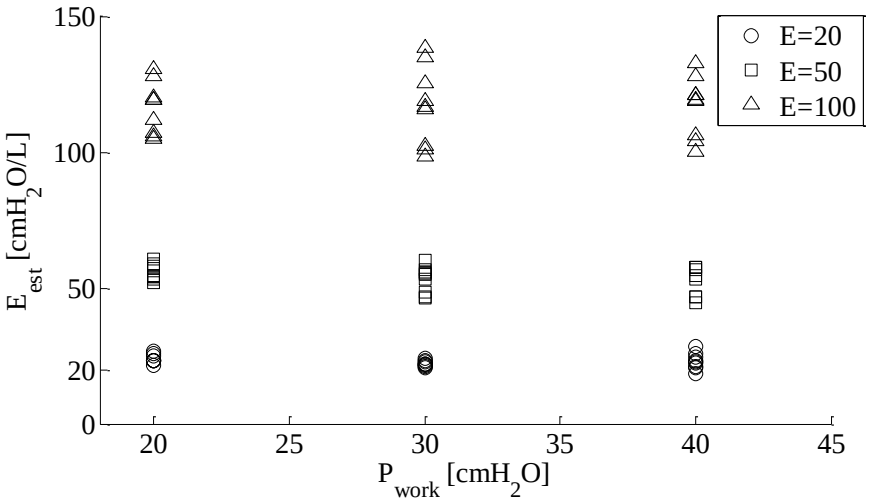

Figure 3.8 Estimated elastance values E_{est} of E values [cmH_2O/L] set on the lung simulator in function of P_{work}. Each point represents the result of parametric estimation in one of the 81 different experimental setup combinations (P_{work}, f_P, R, E).

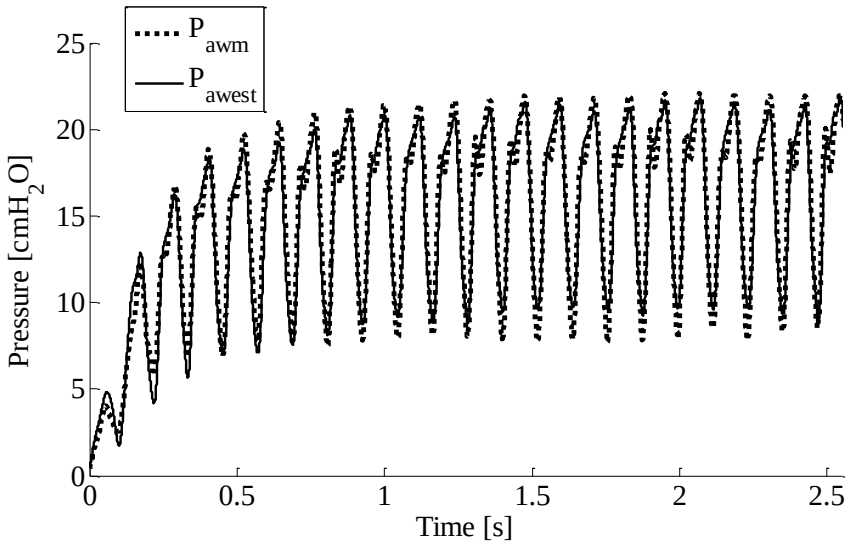

Figure 3.9 Example of the measured pressure P_{awm} curve and the relative comparison with the estimated P_{awest} curve for R=5cmH_2O/(L/s), E=100cmH_2O/L, f =500cycles/min and P_{work}=20cmH_2O

The estimated inertance values were very low and were considered negligible.

Figure 3.9 shows an example of the measured P_{awm} and the relative comparison with the estimated P_{awest}. Comparing estimated and measured pressures, low rmse% values (4.95$\pm$1.51)% were found among the 81 considered combinations.

3.2.3 Discussion

This in vitro study study aimed to estimate respiratory mechanics parameters during HFPV under different working pressures, percussive frequencies and imposed resistive and elastic lung loads. For such purpose we estimated parameters of the Dorkin linear model by least squares method, from inspiratory pressure and flow signals. The estimated R and E parameters generally showed low dependency on P_{work}. On the other hand, these estimated parameters showed an increasing dependence on *f* and E for higher imposed R values and on *f* and R for higher imposed E values. The values obtained with the parameter estimation procedure were generally near to the nominal ones assessed on the lung simulator. However, the estimated resistance presented underestimation for higher values of simulated R (i.e. R = 20 and 50 $cmH_2O/(L/s)$). This could be due to the fact that the resistance of lung simulator partially depends on the flow, as reported in the manufacturer's specifications. The airway resistance simulated by orifice exhibits nonlinear characteristics, in regards to pressure change as a function of flow.

On the contrary, elastance parameters obtained by parametric identification were slightly higher than the value set on lung simulator, especially for E=100 cmH_2O/L. In the latter case the differences respect to the set values did not present a clear relationship with f_P and R, but only a large spread.

Even though some estimated values of R and E did not match the setup ones, it is important to underline the fact that the low rmse% values confirm the adequacy of the model to describe over time the measured system. This fact leads to the assumption that the differences may be mainly due to an imperfect match between nominal and effective values of the lung simulator undergoing high frequency pulsatile flow.

The estimated inertia coefficients were negligible, probably because of the absence of endotracheal tube in the ventilatory circuit. In fact, the presence of endotracheal tube the inertance effect would be more significant [56].

The performed in vitro study under different ventilatory conditions encouraged the further clinically assessment of this method in patients undergoing HFPV.

Chapter 4 – Estimation of pressure drop across endotracheal tubes during HFPV

4.1 *In vitro* estimation of pressure drop across endotracheal tubes during HFPV

Endotracheal tube (ETT) is a catheter routinely used in clinical practice to connect mechanical ventilator to the airway of a patient undergoing artificial respiration (Figure 4.1). The distal end of the endotracheal tube is placed into the trachea through the mouth or nose, while the proximal end of the tube is connected to the output of breathing machine via a dedicated connector. ETT provides an open and unobstructed airway so that air and oxygen from mechanical ventilator can be provided to the lungs.

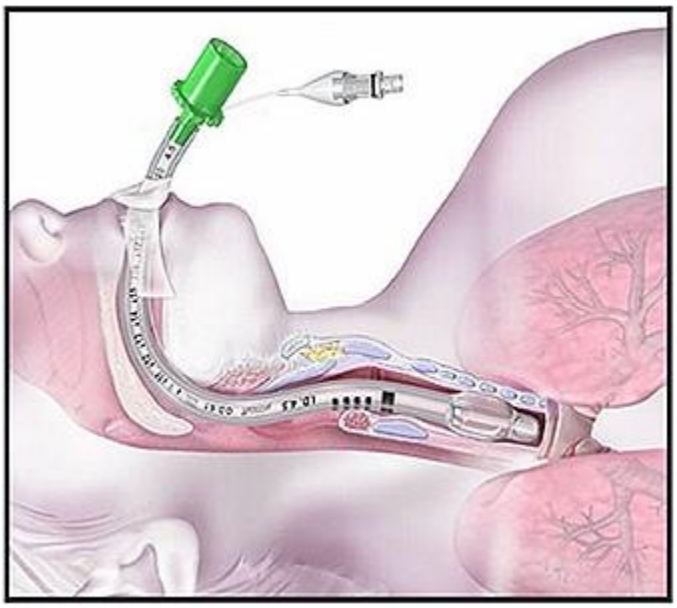

Figure 4.1 Endotracheal tube

The tubes are usually made from polyvinyl chloride. The inflated cuff on the proximal end of ETT forms a seal against the tracheal wall. This seal allows positive pressure ventilation preventing gases from leaking past the cuff and prevents also matter

such as regurgitated gastric contents going into the trachea. The EET size (i.e. tube inner diameter) is chosen based on the patient's body size, with grater sizes used for adults and adolescents and the smaller sizes used for pediatric and neonatal patients.

The presence of ETT during mechanical ventilation contributes an additional mechanical load to the respiratory system impedance, causing different pressure values at the proximal and the distal end of the ETT (Figure 4.2) [57] [58]. The airway pressure measured (Paw) by ventilator represents the sum of the endotracheal tube pressure drop (ΔP_{ETT}) and the tracheal pressure (Ptr) dissipated to inflate lung.

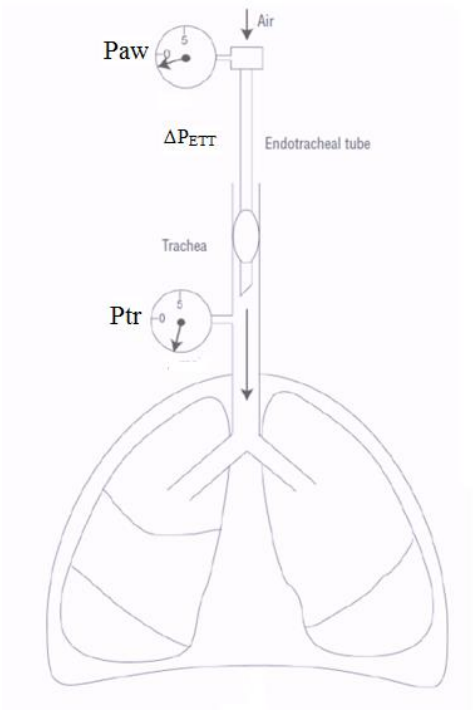

Figure 4.2 Pressure drop across endotracheal tube

From the clinical point of view it is of paramount importance to take into account the real amount of pressure used to overcome the tube impedance to avoid acute lung injury and an erroneous estimate of the volume delivered to the patient [59]. While the pressure at the ventilator end of the EET can be measured easily, measuring the tracheal pressure of a patient is more difficult and, in every day clinical practice, such a measure cannot be done invasively. For this reason, HFPV requires a model for accurately estimating endotracheal tube pressure drop value based solely on non-invasive flow measurements.

The ETT pressure-flow relationship, for various kinds of endotracheal tubes, was widely studied in conventional ventilation [59-67]. Several approaches for estimation of endotracheal tube pressure drop based on flow dependent model and flow measurement have been developed. Under certain conditions, e.g., laminar low flow, the pressure-flow relationship characterizing endotracheal tubes may be considered linear [60] [61], and the relationship between ΔP_{ETT} and flow $\dot{V}$ yields tube resistance R_{tube}.

$$\Delta P_{ETT}(t) = R_{tube} \cdot \dot{V}(t)$$

However, in most cases a non-linear pressure-flow relationship has been found. In such cases this relationship has been generally described as:

$$\Delta P_{ETT}(t) = K_1 \cdot \dot{V}(t) + K_2 \cdot \dot{V}^2(t)$$

or

$$\Delta P_{ETT}(t) = a \cdot \dot{V}^b(t)$$

where, at any time (t), $\dot{V}(t)$ represents flow, K_1 and K_2 are the Rohrer's constants [62], and a and b are constants that define the power function relating $\Delta P_{ETT}(t)$ and $\dot{V}(t)$ [59] [63-65]. Moreover, instead of the previous flow–dependent Rohrer's or power equations, the Blasius' formula for circular tubes has also been used to estimate in vitro adult and neonatal ΔP_{TT} [66] [67]:

$$\Delta P_{ETT}(t) = K_b \cdot \dot{V}^{1.75}(t)$$

where the K_b coefficient depends on tube geometry and physical gas properties [66] [67].

During high frequency ventilation (HFV) the aforementioned approaches do not properly describe the pressure-flow relationship in endotracheal tubes possibly owing to turbulence and the presence of mechanical inertance (I) pertaining to the tubes. Indeed, under high-frequency oscillatory ventilation (HFOV) inertance was taken into consideration [68]. The pressure drop due to inertial effects is directly proportional to volume acceleration ($\ddot{V}$).

HFPV is characterized by high frequency pulsatile flow during inspiration.

Although HFPV has been increasingly used in the clinical practice, the mechanical behaviour of endotracheal tubes under this type of ventilation has not been described yet.

Thus, in order to characterize in vitro pressure drop across the endotracheal tube during HFPV, the modelling of ETT pressure drop-flow relationship under different working pressures, percussive frequencies, and added resistive and elastic loads was performed in this work [69].

4.1.1 Material and methods

In order to perform *in vitro* study the experimental laboratory bench setup was built (Figure 4.3). A physical model of respiratory system was provided by a single-compartment lung simulator (ACCU LUNG, Fluke Biomedical, Everett, WA, USA). In this study the lung simulator was set according to all the combinations of resistive loads (R), namely, 5 and 20 $cmH_2O\ L^{-1}\ s$ and elastic loads (E): 20, 50, and 100 $cmH_2O\ L^{-1}$.

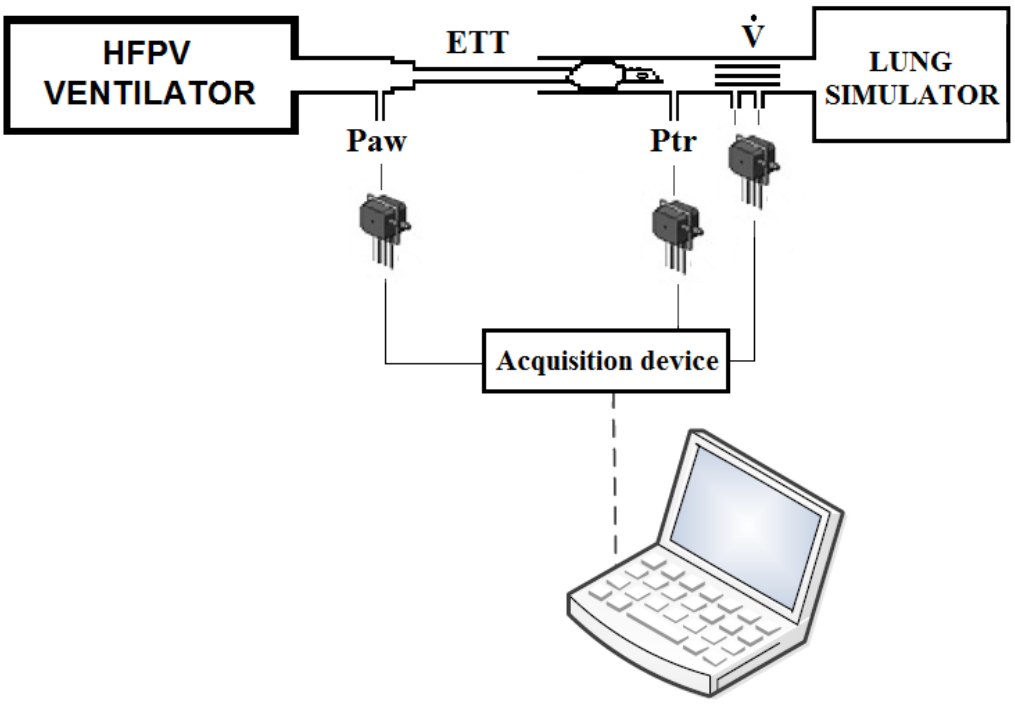

Figure 4.3 Experimental set-up. Paw and Ptr pressures measured before and after the endotracheal tube (ETT), respectively. V̇ is flow measured by Fleisch pneumotachograph.

The lung simulator was connected to a Fleisch pneumotachograph (Type 2, Lausanne, Switzerland) linked to a differential pressure transducer (0.25 INCH-D-4V, All

Sensors, Morgan Hill, CA, USA) for the measurement of airflow. Its other extremity was attached to a tube with a sideport for the measurement of tracheal pressure (Ptr) by means of a differential pressure transducer (ASCX01DN, Honeywell, Morristown, NJ, USA). Endotracheal tube sizes 6.5, 7.5 and 8 (Rusch, Germany) were indwelled into the artificial trachea. Their cuffs were inflated to avoid leaks. These tubes sizes were chosen because they are the most frequently used in adolescent and adult patients. Another differential pressure transducer followed (ASCX01DN, Honeywell, Morristown, NJ, USA) for the measurement of airway pressure (Paw). Finally, a high-frequency percussive ventilator (VDR-4, Percussionaire Corporation, Sandpoint, ID, USA) was linked to the circuit.

The VDR-4 ventilator was set to deliver a pulse inspiratory/expiratory (i/e) duration ratio of 1:1, and inspiratory and expiratory duration (I/E) ratio of 1:1. The tele-inspiratory work pressure (P_{Work}), i.e., peak inspiratory pressure measured by the VDR-4® ventilator, was progressively increased in 5 cmH_2O steps from 20 to 45 cmH_2O, resulting in different airflow rates. The percussive frequency was set to 300, 500 and 700 cycles/min. Measurements were performed for all 108 possible combinations of loads, frequencies, and work pressures for each endotracheal tube size. Each measurement setting included three respiratory cycles. The signals were sampled at 2 kHz by a 12-bit acquisition board (PCI-6023E, National Instruments, Austin, TX, USA) and fed into a low-pass second order Butterworth filter (cut-off frequency 35 Hz).

Volume acceleration ($\ddot{V}$) was calculated by numerical differentiation of the air flow using low-noise Lanczos differentiator described by the following equation:

$$\ddot{V}(n) = \frac{f_s}{28}\left[\dot{V}(n+1) - \dot{V}(n-1) + 2\cdot(\dot{V}(n+2) - \dot{V}(n-2)) + 3\cdot(\dot{V}(n+3) - \dot{V}(n-3))\right]$$

where f_s is sampling frequency and n is sample index.

ΔP_{ETT} was calculated by subtracting Ptr from Paw during the inspiratory phase exclusively.

ΔP_{ETT} was characterized during the inspiratory phase of the breathing cycle by parametric identification of coefficients pertaining to the three proposed models, defined according to the following equations:

Model 1: $\Delta P_{ETT}(t) = R_{tube} \cdot \dot{V}(t) + I\,\ddot{V}(t)$

Model 2: $\Delta P_{ETT}(t) = K_1 \cdot \dot{V}(t) + K_2 \cdot \dot{V}^2(t) + I\,\ddot{V}(t)$

Model 3: $\Delta P_{ETT}(t) = K_b \cdot \dot{V}^{1.75}(t) + I\,\ddot{V}(t)$

Model 1 is characterized by linear resistive [$R_{tube}\cdot\dot{V}(t)$] and inertial [$I\cdot\ddot{V}(t)$] terms. Model 2 takes into consideration Rohrer's approach [$K_1\cdot\dot{V}(t) + K_2\cdot V^2(t)$] and inertance [$I\cdot\ddot{V}(t)$]. In Model 3 the pressure drop caused by friction is represented by the non-linear Blasius component [$K_b\cdot\dot{V}^{1.75}(t)$] and the inertial term [$I\cdot\ddot{V}(t)$]. In this study we assumed that coefficients include both distributed and concentrated pressure drops. The latter takes into account the connectors and the effect of abrupt changes in cross sectional area [70] [71]. The least squares method was used to estimate the coefficients pertaining to the different models. The estimation of the parameter vectors $\hat{\theta}_1$, $\hat{\theta}_2$ and $\hat{\theta}_3$ for the three Models was defined as:

$$\hat{\theta}_i = \left(A_i^T \times A_i\right)^{-1} \times A_i^T \times B \qquad i=1,2,3$$

with:

$\hat{\theta}_1 = [\mathrm{R_{tube}}\ \mathrm{I}]^T$

$\hat{\theta}_2 = [\mathrm{K_1}\ \mathrm{K_2}\ \mathrm{I}]^T$

$\hat{\theta}_3 = [\mathrm{K_B}\ \mathrm{I}]^T$

$$A_1 = \begin{bmatrix} \dot{\mathrm{V}}(1) & \ddot{\mathrm{V}}(1) \\ \dot{\mathrm{V}}(2) & \ddot{\mathrm{V}}(2) \\ \vdots & \vdots \\ \dot{\mathrm{V}}(\mathrm{N}) & \ddot{\mathrm{V}}(\mathrm{N}) \end{bmatrix}$$

$$A_2 = \begin{bmatrix} \dot{\mathrm{V}}(1) & \dot{\mathrm{V}}(1)\cdot\left|\dot{\mathrm{V}}(1)\right| & \ddot{\mathrm{V}}(1) \\ \dot{\mathrm{V}}(2) & \dot{\mathrm{V}}(2)\cdot\left|\dot{\mathrm{V}}(2)\right| & \ddot{\mathrm{V}}(2) \\ \vdots & \vdots & \vdots \\ \dot{\mathrm{V}}(\mathrm{N}) & \dot{\mathrm{V}}(\mathrm{N})\cdot\left|\dot{\mathrm{V}}(\mathrm{N})\right| & \ddot{\mathrm{V}}(\mathrm{N}) \end{bmatrix}$$

$$A_3 = \begin{bmatrix} \dot{V}(1) \cdot |\dot{V}(1)|^{0.75} & \ddot{V}(0) \\ \dot{V}(2) \cdot |\dot{V}(2)|^{0.75} & \ddot{V}(1) \\ \vdots & \vdots \\ \dot{V}(N) \cdot |\dot{V}(N)|^{0.75} & \ddot{V}(N) \end{bmatrix}$$

$$B = [\Delta P_{ETT}(1) \quad \Delta P_{ETT}(2) \quad \dots \quad \Delta P_{ETT}(N)]^T$$

The matrix elements $\dot{V}(n)$, $\ddot{V}(n)$, $\Delta P_{ETT}(n)$, where n = 1,2, … N is the sample index , N is the number of acquired samples for each experimental setting and tube.

As indicator of the adequacy of the model used to describe the measured system, the residual root mean square error (RMSE) was calculated:

$$RMSE = \sqrt{\frac{\sum_{k=0}^{N-1}[\Delta P_{TTm}(kT) - \Delta P_{TTe}(kT)]^2}{N}}$$

where ΔP_{ETTm} and ΔP_{ETTe} represent the measured and estimated ΔP_{ETT}, respectively, N is the number of samples, and T represents the sampling period.

Endotracheal tubes display an inertial fluid dynamic component proportional to the volume acceleration ($\ddot{V}$), particularly evident during high frequency ventilation, which also consumes energy in terms of pressure drop. Inertance (I) was estimated for each endotracheal tube according to:

$$I = \rho L A^{-1}$$

where ρ is the gas density, L the tube length and A the cross-sectional area [72].

The RMSE and inertance pertaining to the three models were compared. The normal distribution of the data and the homogeneity of the variances were assured by the Kolmogorov-Smirnov (with Lilliefors' correction) and Levene median tests, respectively. One-way ANOVA was then applied and since statistically significant values were found, Bonferroni's post hoc test was used to assess differences among the three models. $\alpha = 5\%$. Statistical analysis was performed using Statistica 6.1 software (StatSoft, Vigonza, Italy).

4.1.2 Results

Three measurements were done in each condition (108 for each model). The reproducibility of the estimated parameters was assessed as the median and range of the corresponding coefficients of variation, as listed in Table 4.1. Model 2 presented the broadest range of variability, whereas model 3 displayed the narrowest range. Inertance data were similar in the three models.

Constants	Tube 8		Tube 7.5		Tube 6.5	
			Model 1			
R_{tube} ($cmH_2O\ L^{-1}\ s$)	0.0065	(0.0003-0.0662)	0.0055	(0.00001-0.046)	0.0034	(0.0002-0.0560)
I ($cmH_2O\ L^{-1}\ s^2$)	0.0106	(0.0001-0.2016)	0.0055	(0.0003-0.217)	0.0105	(0.00045-0.215)
			Model 2			
K_1 ($cmH_2O\ L^{-1}\ s$)	0.0827	(0.0058-6.8510)	0.1004	(0.0002-11.62)	0.0871	(0.0023-10.0)
K_2 ($cmH_2O\ L^{-2}\ s^2$)	0.0445	(0.0048-0.8230)	0.0263	(0.0002-4.456)	0.0229	(0.0001-5.110)
I ($cmH_2O\ L^{-1}\ s^2$)	0.0105	(0.00001-0.2011)	0.0055	(0.0006-0.2157)	0.0106	(0.0003-0.214)
			Model 3			
K_b ($cmH_2O\ L^{-1.75}\ s^{1.75}$)	0.0065	(0.0004-0.0300)	0.006	(0.0001-0.060)	0.0034	(0.0001-0.0588)
I ($cmH_2O\ L^{-1}\ s^2$)	0.0105	(0.00001-0.2012)	0.0055	(0.0006-0.2160)	0.0106	(0.0003-0.214)

Table 4.1 Reproducibility of the estimated parameters. Values are expressed as median and (range) of coefficients of variation of the measurements of three consecutive breaths for each model considering the possible 108 settings in each one. R_{tube}, resistance. I, inertance. K_1 and K_2, are Rohrer's constants. K_b, Blasius' constant [69] .

RMSE was measured in all 108 possible combinations of loads, frequencies, work pressures for each ETT sizes. In all instances model 1 presented RMSE values significantly higher than those in models 2 and 3 (Table 4.2), and no significant difference was detected between models 2 and 3. Correlation coefficients between gathered curves and fitted data are very similar among the three methods.

Inertances (I) were similar in the three models [0.081 ± 0.005, 0.096 ± 0.0006 and 0.095 ± 0.0007 $cmH_2O\ L^{-1}\ s^2$ (mean ± SD) for tubes 8, 7.5 and 6.5, respectively], but significantly different among tube sizes ($P < 0.002$). Furthermore they were very close to I calculated based on fluid dynamics, i.e., 0.081, 0.097 and 0.111 $cmH_2O\ L^{-1}\ s^2$ for tubes 8, 7.5 and 6.5, respectively.

Figure 4.4 shows the mean and standard deviations of the estimated parameters pertaining to the three proposed models plotted against P_{Work} obtained for all 108 possible combinations of loads and frequencies. The results obtained for the three endotracheal tubes are depicted. $R_{tube,}$ K_1 and K_2 values depended on P_{Work}, which was not the case for

the K_b value. Furthermore, $R_{tube,}$ K_1 and K_2 values presented higher variability than the K_b parameter.

Model	Tube 8	Tube 7.5	Tube 6.5
	RMSE (cmH_2O)		
1	1.097±0.38	1.661±0.57	1.720±0.57
2	0.915±0.29	1.330±0.35	1.330±0.30
	P = 0.00011	P < 0.00001	P < 0.00001
3	0.933±0.28	1.400±0.38	1.038±0.32
	P = 0.00062	P = 0.00007	P < 0.00001
	Correlation coefficient		
1	0.964 (0.895 - 0.994)	0.958 (0.886 - 0.990)	0.970 (0.911 - 0.991)
2	0.974 (0.906 - 0.995)	0.969 (0.893 - 0.993)	0.980 (0.916 - 0.994)
3	0.973 (0.906 - 0.995)	0.970 (0.895 - 0.993)	0.981 (0.914 - 0.995)

Table 4.2 Root mean square errors and correlation coefficients between experimental and fitted curves. Mean ± SD of 108 different experimental conditions (three measurements per condition) of root mean square errors (RMSE) and median (range) of correlation coefficients. Model 1 assumes a linear relationship between pressure and flow; model 2 introduces a flow-dependent quadratic equation; and model 3 incorporates the term $\dot{V}^{1.75}$. *P* values describe difference between models 2 and 3 versus model 1. No significant difference was detected between models 2 and 3 [69].

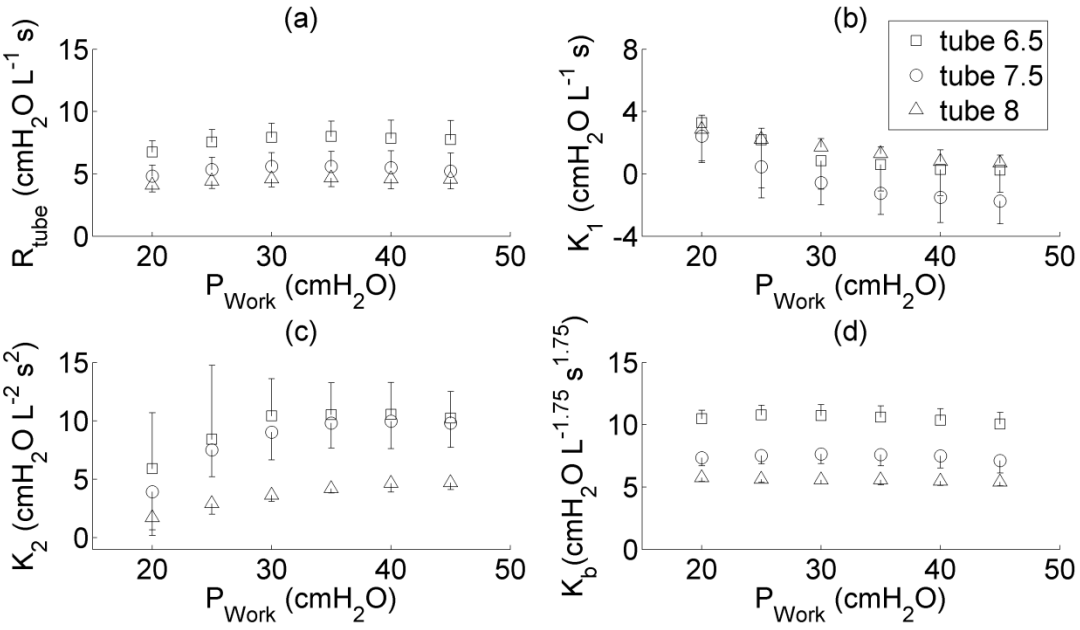

Figure 4.4 Estimated model constants plotted against working pressure (P_{Work}). (a) linear model (#1), R_{tube}, Newtonian flow resistance. (b and c) model #2, K_1 and K_2, Rohrer's coefficients. (d) Blasius' constant, K_b (model #3). Each data point is the average of 18 estimated model constants encompassing two and three resistive and elastic loads, respectively, and 3 percussive frequencies. Bars, + or – SD. Open squares, circles and triangles represent tubes 6.5, 7.5, and 8.0, respectively [69].

In Figure 4.5 pulsatile flow, Paw, Ptr and ΔP_{ETT} (= Paw - Ptr) tracings during one inspiration (R = 5 $cmH_2O\ L^{-1}\ s$; E = 50 $cmH_2O\ L^{-1}$; percussive frequency = 300 cycles/min; P_{Work} = 25 cmH_2O and tube size = 8) are shown. ΔP_{ETT} is represented as measured and also calculated with models 1, 2 and 3. To facilitate identification of the four ΔP_{ETT} curves one mini-burst (identified in the third tracing from top to bottom was expanded and depicted as a fourth tracing). It can be seen that models 2 and 3 closely fitted the experimentally registered ΔP_{ETT} curve.

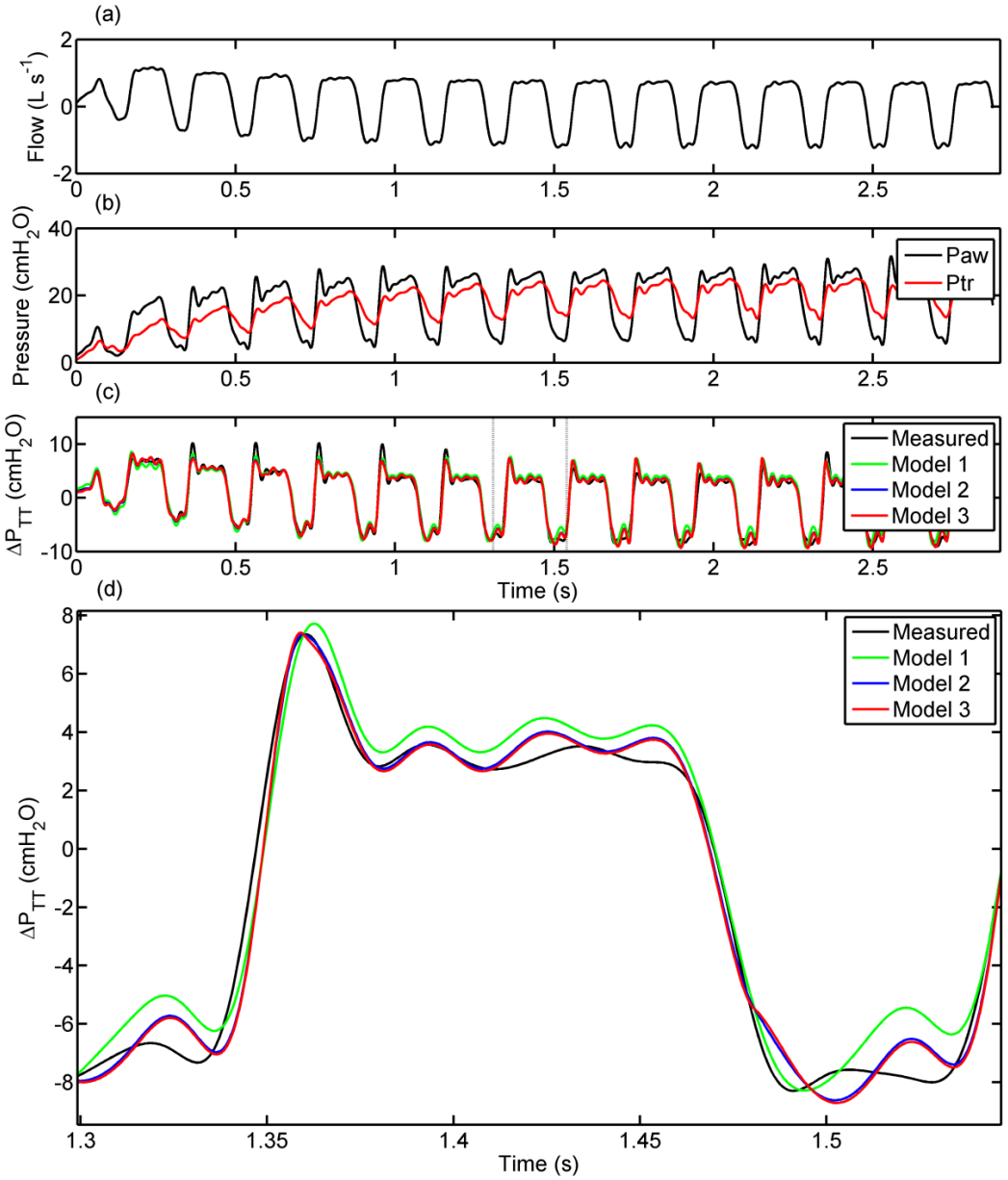

Figure 4.5 Flow and pressures tracings during one inspiration under high-frequency percussive ventilation. Panel (a) shows pulsatile flow; panel (b) displays Paw (black) and Ptr (red); in panel (c) ΔP_{TT} is represented as the measured curve (black) and also calculated with models 1 (green), 2 (blue) and 3 (red); panel (d) shows one ΔP_{TT} mini-burst identified in panel (d) [69].

Medians and ranges of the 108 measured pressure drops across each tube (ΔP_{ETT}) during the inspiratory phase of the mini-bursts were also calculated: 9.28 (4.95-12.93), 9.48 (5.05-13.47), and 10.04 (5.62-16.97) cmH_2O for tubes 8, 7.5 and 6.5, respectively.

4.1.3 Discussion

This study aimed at identifying the most adequate model and respective calculated parameters for estimating the pressure drop across endotracheal tubes during high frequency percussive ventilation under different working pressures, percussive frequencies, and resistive and elastic loads. For such purpose three models were evaluated: a linear (1) and two non-linear models (2 and 3), all of them taking into account inertance and both distributed and concentrated pressure losses. So far the modeling of pressure losses across endotracheal tubes in the face of HFPV has not been reported.

From the clinical point of view the real time estimation of endotracheal tube contribution to pressure losses within the breathing system is of paramount importance. Frequently the physician can only assess the pressure delivered by the ventilator, usually measured before the tubing ensemble (endotracheal tube included) linking the ventilator to the patient. This pressure does not represent that actually delivered to the patient. If the latter pressure is too high, barotraumas may ensue [73]. Thus, a tool that can provide information about the endotracheal tube flow-dependent resistance during HFPV and that could also be implemented in future monitoring systems is wanted.

Three simple common models relating ΔP_{ETT} and flow were tested. Model 1 assumes a linear relationship between pressure and flow; model 2 introduces a flow-dependent quadratic equation; and model 3 incorporates the term $\dot{V}^{1.75}$. Inertance is included in all three models since the ventilatory mode is based on high-frequency pulsatile flow. Using two and three diverse resistive and elastic loads, respectively, three percussive pressures, and six working pressures, 108 different combinations were generated, and three breathing cycles were measured in each one of them. The smallest variability among the measurements of the estimated parameters was presented by model 3, while model 2 depicted the broadest range of results (Table 4.1).

To the experimental pressure and flow curves the three aforementioned models were fitted using the least square method. The similarity between the correlation

coefficients (Table 4.2) would suggest that the three models adequately fitted the experimental data. However, considering that RMSE is a measure of the differences between values estimated by a model and the values actually observed in an experiment, we used it to evaluate the goodness of our fittings. Table 4.2 shows that Model 1 presented significantly higher RMSE than Models 2 and 3, and that the latter did not differ between them. Thus, the former is not as accurate as the latter, possibly due to turbulence, a term not included in Model 1, as previously reported [66] [67] [72]. Furthermore, Models 2 and 3 seem to present the same predictive power. Following the parsimony principle we have to consider Model 3 more convenient than Model 2 [74]. Model 2 is frequently used in respiratory physiology to describe pressure-flow relationships. Blasius' formula was used to determine the effect of mucus deposition on the effective diameter of endotracheal tubes in patients [67], and to calculate in vitro the pressure drop along pediatric endotracheal tubes under constant flow [66]. The latter study reports that a linear model can adequately describe flow-pressure relationship under laminar flow, but when turbulence ensues, Blasius' formula represents a better descriptor of the system [66]. On the other hand, in a pediatric study with high-frequency oscillation, Blasius' and Rohrer's formulas resulted inaccurate to calculate pressure drop across endotracheal tubes based on measured flows [68]. Hence, our study fitted experimentally generated pressure and flow signals with a linear and two non-linear models and estimated R_{tube} K_1, K_2, K_b and I.

The estimated coefficients are plotted against P_{Work} (Figure 4.4). The wider the tube the smaller is the SD in all instances and the smaller are the estimated coefficients, except for K_1. The large variability of estimated Rohrer's coefficients has also been previously reported [68]. Additionally, K_b does not depend on P_{Work}, in opposition to the other coefficients. Finally, K_b presents the smallest SD. Indeed, the overall means±SDs were 5.57±0.34, 7.46±0.84; and 10.51±0.87 $cmH_2O\ L^{-1.75}\ s^{1.75}$ for tubes 8.0, 7.5 and 6.5, respectively. The corresponding coefficients of variation were 0.061, 0.11, 0.08. The median values did not differ appreciably from the means. It should be stressed that each point represents data collected with two resistive and three and elastic loads, and three pulsatile frequencies, i.e., each point is a lumped value. Taken together these results strongly suggest that estimated K_b is the most robust resistance-related coefficient calculated in our study.

Other models [65] under conventional mechanical ventilation take into

consideration the asymmetry between inspiratory and expiratory phases, expressed by their exponents K2. In HFPV each inspiration comprises many mini-bursts, which in our case presented frequencies amounting to 300, 500 and 700 cycles/min. Each mini-burst represents one mini-inspiration and a mini-expiration [15] [29]. In their study [65] the results are expressed considering inspiration and expiration separately. In our case, we have inspiratory and expiratory phases in each mini-burst plus the whole cycle inspiration and expiration, which would result in a series of values possibly difficult to be handled and understood in clinical practice. Furthermore, the aforementioned models do not take into consideration inertance, which represents an important mechanical component in high-frequency ventilation, as seen in Figure 4.6.

Because inertial forces are negligible during tidal breathing they are usually disregarded in curve fitting [6]. However inertance may became important during fast breathing, which is the case in HFPV. For this reason we included an inertial term in our models, as also reported in other studies [48] [68] [72] [75] [76]. In Figure 4.6 the measured ΔP_{ETT} was split into its inertance-dependent ($\Delta P_{ETT}I$) and resistive-dependent ($\Delta P_{ETT}R$) components. The former plays a major role during rapid changes in ΔP_{ETT}, whereas the latter responds for the slower variations in ΔP_{ETT}, corresponding to the phases where gas accelerations are high and small, respectively. Once again there is no single value for the contributions of either I or R to $\Delta P_{ETT.}$ This finding applies to all settings.

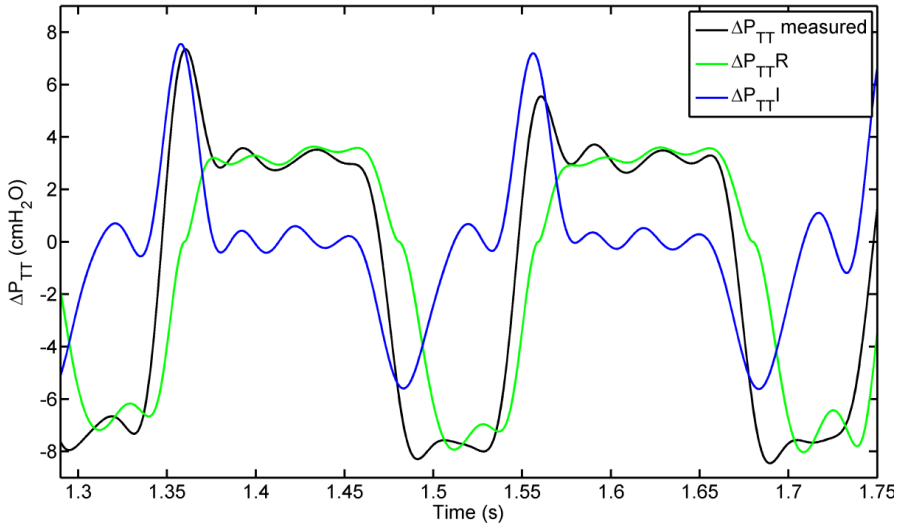

Figure 4.6 The measured ΔP_{TT} (black line) and its inertance-dependent (blue line $\Delta P_{TT}I$) and resistive-dependent (green line $\Delta P_{TT}R$) components are shown for two complete mini-bursts (R = 5 $cmH_2O\ L^{-1}\ s$; E = 50 $cmH_2O\ L^{-1}$; percussive frequency = 300 cycles/min; P_{Work} = 25 cmH_2O and tube size = 8).

In the present study the estimated inertances did not vary among the models, thus rendering inertia not responsible for the differences in fitting the models to the experimental data using the same tube. However, possibly due to geometric factors [72] [75] [76], inertance varied in the present work according to tube size.

Considering that for each tube size only Model 3 is characterized by two constant coefficients (resistance- and inertia-dependent), it may be very useful for the clinician: using two constants and the flow value he/she may be able to estimate the average pressure lost owing to the endotracheal tube as:

$$\Delta P_{TT}(t) = 5.57\ \dot{V}^{1.75}(t) + 0.081\ \ddot{V}(t) \quad \text{(tube 8)}$$

$$\Delta P_{TT}(t) = 7.46\ \dot{V}^{1.75}(t) + 0.096\ \ddot{V}(t) \quad \text{(tube 7.5)}$$

$$\Delta P_{TT}(t) = 10.51\ \dot{V}^{1.75}(t) + 0.095\ \ddot{V}(t) \quad \text{(tube 6.5)}$$

This study present some limitations: (a) results were gathered under HFPV; (b) resistive and elastic loads, pulsatile frequency were constrained within specific ranges; (c) clinical limitations may also arise: curvature of the tube, its partial blockage due to mucus and/or condensed water vapour, and connectors. In conclusion, the method provided by this work allows the rapid calculation of the pressure drop across endotracheal tubes in high-frequency percussive ventilation.

4.2 *In vitro* estimation of pediatric endotracheal tube pressure drop

Endotracheal tubes are also regularly used in pediatric patients undergoing HFPV. In these cases the estimation of pressure drop becomes even more important because of frailty of pediatric patients and because of greater pressure drop between the proximal and the distal end of the pediatric ETT, because of smaller inner diameter. Consequently the previous study was extended to the tube regularly used in pediatric cases [77]. The experimental setup and acquisition device (Figure 4.3) used in the previous study, were also used to collect pressure and flow data for the examined pediatric ETT (size 5.5, Rusch, Germany, ID = 5.5 mm, length = 29.5 cm). The respiratory signals were acquired in 108

different experimental conditions combining different P_{work}, *f*, R and E. Work pressure (P_{work}) was varied from 20 to 45 cmH_2O with increasing steps of 5 cmH_2O. The percussive frequency (*f*) was set to 300, 500 and 700 cycles/min. The lung simulator was set according to the combinations of resistive loads (R) 5 and 20 $cmH_2O/L/s$ and elastic loads (E) 20, 50, and 100 cmH_2O /L.

4.2.1 Results

The estimated inertance (I) was identical in all three models 0.126±0.009 $cmH_2O/L/s^2$ and did not present particular dependence on working conditions.

Figure 4.7 shows the mean and standard deviations of the parameters of the three evaluated models versus P_{work}, obtained for different combinations of lung elastances and percussive frequencies.

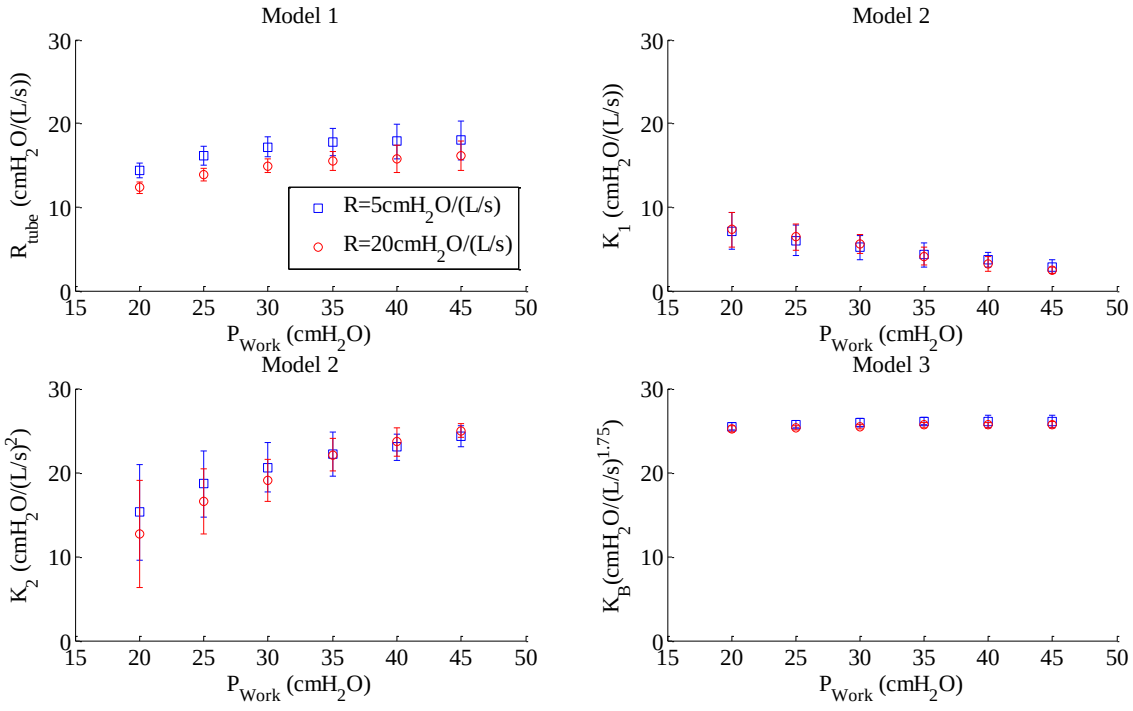

Figure 4.7. Mean±1SD of the parameters of the three proposed models versus P_{work} [77].

The values of R_{tube} were higher at lower lung resistance R; K_2 parameter also showed a similar behavior up to 30 cmH_2O of P_{work}. On the other hand, K_1 and K_B parameters did not show a significant dependency on lung resistance. However, in the Model 1, R_{tube} slightly increased as the P_{work} increased from 20 to 35 cmH_2O. In the Model

2 K_1 decreased and K_2 increased as P_{work} increased. Finally, in the Model 3, K_B was independent from P_{work} at all the considered experimental setup conditions. The parameters of Model 1 and Model 2 (especially K_2) presented variability (SD shown in Figure 2) due to the different lung elastances and percussive frequencies, even if without a clear relationship.

Figure 4.8 shows the mean values (±1SD) of the RMSE errors of the ΔP_{ETT} estimation in the three Models in function of P_{work}. Model 1 presented higher values of RMSE for lower value of lung resistance, while in Model 2 and Model 3 these differences were reduced. RMSE errors of Model 1 were directly proportional to P_{work}, while in Model 2 and Model 3 the errors increased from P_{work} of 20 to 35 cmH_2O and decreased at a P_{work} of 45 cmH_2O. In all three models RMSE errors varied with percussive frequency and lung elastance but without a definite relationship with these variables. The linear Model 1 presented RMSE values significantly higher (from 18% at 20 cmH_2O up to 98% at 45 cmH_2O) than those obtained from Rohrer's Model 2 and Blasius' Model 3. In order to evaluate the slight differences between Models 2 and 3, we plotted the RMSE errors of Model 2 versus the RMSE errors of Model 3 (Figure 4.9) using all the 108 setup combinations. The Model 2 proved to be slightly better that Model 3 at every setup combination.

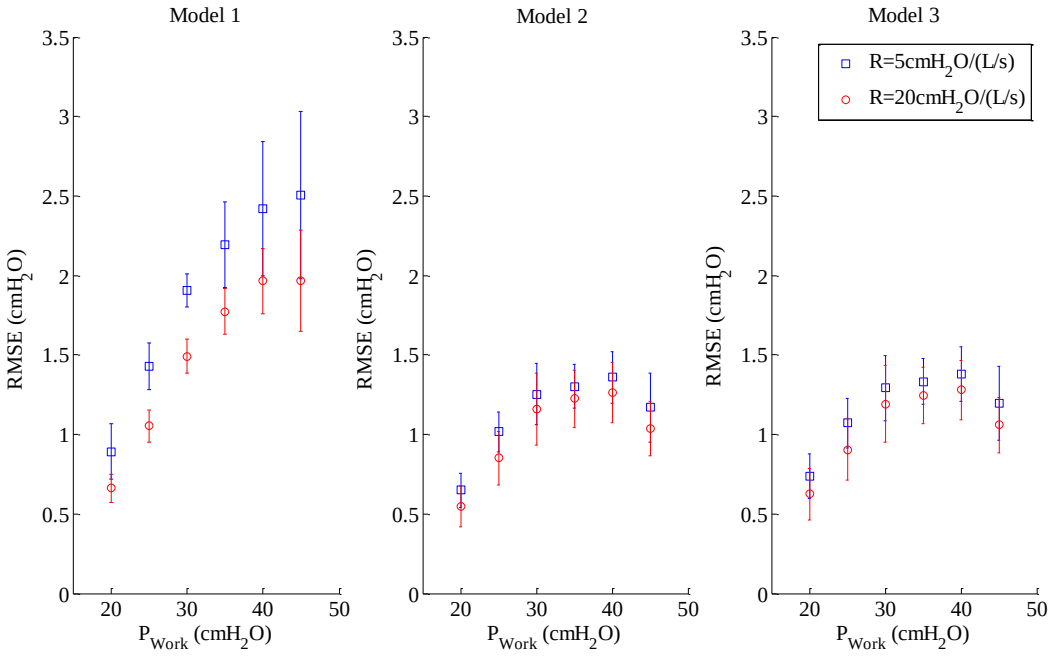

Figure 4.8 Mean ±1SD RMSE errors of the ΔP_{ETT} estimation in the three Models in function of P_{work} [77].

4.2.2 Discussion

This study aimed at identifying the most adequate model and parameters for estimating the pressure drop of pediatric endotracheal tube ΔP_{ETT} during HFPV under different working pressures, percussive frequencies and resistive and elastic lung loads. As in a previous adult ETT study we considered the linear Model 1 and the non-linear Models 2 and 3, all of them taking into account inertance and both distributed and concentrated pressure losses. The estimated inertance values were identical in all the models (0.126 ± 0.009 $cmH_2O/L/s^2$) and slightly smaller than theoretical value (0.152 $cmH_2O/L/s^2$) for the examined ETT.

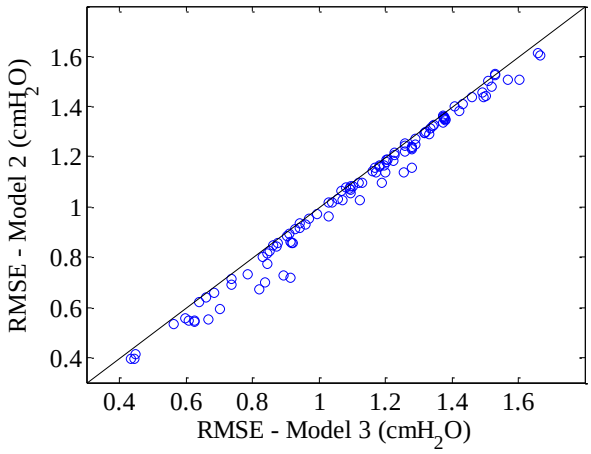

Figure 4.9 RMSE errors of Model 2 versus the RMSE errors of Model 3 [77].

The linear Model 1 presented RMSE values significantly higher than those obtained from the two non-linear Models, especially at the highest working pressures. This is probably due to the fact that Model 1 does not consider the presence of turbulent flow, that introduces non linearity in pressure-flow relationship. This phenomenon particularly occurs in presence of high values of pulsatile flow; thus we considered the linear model unable to describe properly ΔP_{ETT} during HFPV.

In Model 2 coefficients K_1 and K_2 showed strong dependency on P_{work} and in addition they presented a meaningful variability related to different lung elastances and percussive frequencies. The large variability of Rohrer's coefficients was also present in the case of pediatric HFOV, as reported in [68]. On the other hand, results showed that the Blasius' Model 3 coefficient K_B was widely independent from the setup conditions as well as from the P_{work}, differently from the parameters of the other models, even if it presented a

very slightly higher estimation error than Model 2. Thus this model seems to be the best approximation of the non-linear behavior of the considered pediatric ETT. The results of this study were broadly similar to those obtained in previous adult ETT study [69]. Blasius coefficient was significantly higher than those estimated for adult and adolescent tubes, due to the smaller inner diameter. This simple Blasius model may be implemented as a clinical tool for the estimation of ΔP_{ETT} and consequently for the evaluation of tracheal pressure signal during pediatric HFPV.

4.3 *In vitro* estimation of tracheal pressure by Genetic programing

Endotracheal pressure drop was also modeled in terms of tracheal pressure (Ptr) estimation using automatic generation of models by Genetic programing (GP) [78]. GP is a method for automatically generating solutions, in the form of computer programs and formulas, inspired by biological evolution. In this subchapter, is described synthesis of such tracheal pressure model by means of GP. This study was conducted in collaboration with Machine Learning Lab. of Department of Engineering and Architecture of University of Trieste. The results obtained by GP-generated models were compared to the results obtained by fluid dynamics based models used in previous study [69].

GP has been used in a wide range of applications as, electricity price prediction [79] and text mining [80]. In GP, a population of computer programs is generated at random starting from a predefined set of building blocks. Each of these programs constitutes a candidate solution for the problem and is called an individual. The process is based on a predefined fitness function for the problem to be solved. This function quantifies the performance of any given candidate solution for that problem. Usually, the fitness of an individual is computed on a set of solved instances of the problem (the learning corpus) by comparing—in terms of some predefined performance index— the solutions provided by the individual against the known correct solutions.

A GP execution consists in an evolutionary search structured as follows: (i) compute the fitness of each individual; (ii) construct new individuals by applying certain genetic operators (such as “crossover” and “mutation”) to the individuals with highest

fitness; (iii) construct a new population composed of individuals with highest fitness and new individuals as created at the previous step. These steps constitute a generation. This process is iterated until either a solution with perfect fitness is found or some termination criterion is satisfied, e.g., a predefined maximum number of generations have evolved. Usually, the population size is kept constant across all generations.

In many scenarios of practical interest, each GP individual represents a formula rather than a more general computer program. The formula is represented as an abstract syntax tree, where a branch node is an element taken from a predefined functions set and a leaf node is an element taken from a predefined terminal set (terminal set and function set constitute the building blocks mentioned above). The function set may contain mathematical functions like the arithmetic operators whereas the terminal set usually contains constants and variables.

In this work GP models were generated by executing the evolutionary search and applying the genetic operators crossover and mutation, starting from initialized formulas using predefined functions (+, -, ·, ÷, exp and power) and terminal (Paw, $\dot{V}$, $\ddot{V}$, P_{work}, *f*, constants) set. As a result of the evolutionary search, minimizing both mean square error (MSE) and the individual size (i.e. the number of nodes in order to enforce parsimony principle) a series of five models for each tube was produced. These models can be represented as nonlinear function of the above mentioned functions and variables:

$$Ptr = f(\mathrm{Paw}, \dot{V}, \ddot{V}, P_{work}, f, \alpha)$$

where α is the set of random constants uniformly distributed in [0.01 10].

GP searches were performed using a tool developed by Machine Learning Lab of University of Trieste [79] [80]. In this study were used dataset consisting of in vitro measured respiratory signals pressure and flow signals for tubes sizes 6.5 and 7.5, acquired in a previous study [69].

The mean square errors obtained by GP-based models are reported in Table 4.3. The GP-generated models presented good predicting performance in all the repetitions, with the only exception of the fourth repetition for tube size 7.5 (Table 4.3). The GP models generally presented lower error values (corresponding to a better estimation of the tracheal pressure) than those of fluid dynamics models but are considerably more complex

(more than 100 elements) than fluid dynamics models. Considering the median and range values of the inspiratory pressure drop (i.e. 10.04 (5.62–16.97) cmH_2O for tube 6.5 and 9.48 (5.05–13.47) cmH_2O for tube 7.5 [69]) from the clinical point of view both approaches adequately fit the experimental data. The difference between fitting errors obtained implementing two approaches is not clinically relevant.

	MSE [cmH_2O^2]	
Repetitions	Tube size 6.5	Tube size 7.5
1	1.01	0.9
2	0.78	1.06
3	0.76	1.03
4	0.82	3.21
5	0.84	1.03
Mean	0.84	1.44

Table 4.3 MSE obtained by GP generated models averaging on all the combinations of different working pressures, percussive frequencies and added mechanical resistive and elastic loads [78].

The computational complexity and the non-direct interpretability of the parameters of models generated by genetic programing make their application very difficult in everyday clinical practice. Moreover, the partitioning between resistive and inertance components is not allowed. On the other hand, for each tube size the Blasius model is characterized by only two constant coefficients (resistance dependent and inertia dependent). Therefore, the contribution of resistive and inertance components is easily interpretable in this model. Thus, by using of Blasius coefficients and the flow value the pressure drop and consequently the tracheal pressure can be calculated rapidly.

The physician can use this information to avoid potential iatrogenic lung damage due to not adequate pressure and volume delivery. In this way lung hyper and hypo-inflation is prevented and the HFPV ventilator setup can be tailored to the real patient requirement.

Chapter 5 - Respiratory parameters measurements in patients undergoing HFPV

The pressure measurements and gas exchange analysis are currently the only variables that guide the physician during the HFPV ventilator setup. Evaluation of respiratory system resistance and compliance parameters in patients undergoing mechanical ventilation is used for lung dysfunctions detection, ventilation setup and treatment effect evaluation. The estimation of across endotracheal tube pressure drop may be very useful to the clinician to avoid over-treatment and associated lung injury or under-treatment (e.g. alveolar de-recruitment). Avoiding the baro and volu-trauma is the cornerstone of the protective ventilatory strategy, which requires also a measurement of the tidal volume delivered to the patient. At the same time from a clinical point of view alveolar de-recruitment must be avoided, so recruitment maneuvers are frequently necessary to keep the lung open. Presently, it is not possible to evaluate the delivered tidal volume, respiratory resistance and compliance parameters, endotracheal pressure drop and the alveolar recruitment effect in patients undergoing HFPV treatment.

In previous chapters, the *in vitro* methods developed for estimation of respiratory system viscoelastic parameters and endotracheal pressure drop were described. In this Chapter the results concerning the application of these methods in some cases of patients undergoing HFPV are described. By using new bedside respiratory signals measurements, personalized ventilator setup was realized, in order to tailor HFPV treatment to the specific patient's needs.

5.1 Material and Methods

The *in vivo* study was conducted in patients receiving HFPV for failure of conventional ventilation at General Intensive Care Unit (ICU) of Cattinara Hospital, University of Trieste. Ten patients (eight male) aged between 60 and 83 years were prospectively studied. The group encompassed patients presenting chest trauma (n = 2), sepsis (n = 3), bacterial pneumonia (n = 4), neurogenic pulmonary edema (n = 1).This study was performed during a standardized HFPV clinical protocol without interfering with patients care and under the supervision of a physician not involved in the study. The information obtained by the data acquisition and the consequent ventilator setup variations were applied in agreement with the physician. The study posed no added risk to the patient and did not interfere with usual patient care.

5.1.1 Bedside acquisition system and respiratory parameters estimation

Respiratory signals in patients undergoing HFPV were acquired and processed with a device suitably designed and developed, in this work, for bedside use (Figure 5.1). The pressure signal Paw was acquired through pressure sensor (ASCX01DN, Honeywell, USA), while the flow signal ($\dot{V}$) was acquired using Fleisch pneumotachograph (Type 2, Lausanne, Switzerland) linked to a differential pressure transducer (0.25 INCH-D-4V, All Sensors, USA). Conditioning boards in addition to transducers mount a DC/DC converter for power supply of sensors and a second-order Butterworth low-pass filters (cut-off frequency of 300 Hz). The pressure and flow signals were sampled at 2 kHz by a 14 bit acquisition board (NI USB-6009, National Instruments, Austin, TX, USA) connected to a PC notebook. The volume (V) and volume acceleration ($\ddot{V}$) were calculated by numerical integration and differentiation of flow, respectively.

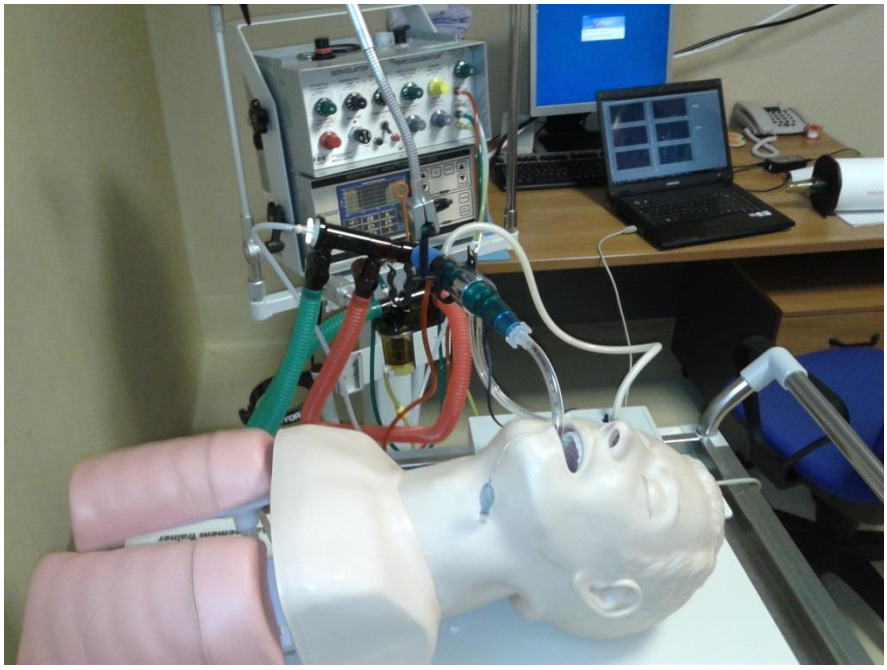

Figure 5.1 Bedside acquisition device (in this figure applied on anatomical simulator in respect to a patient privacy).

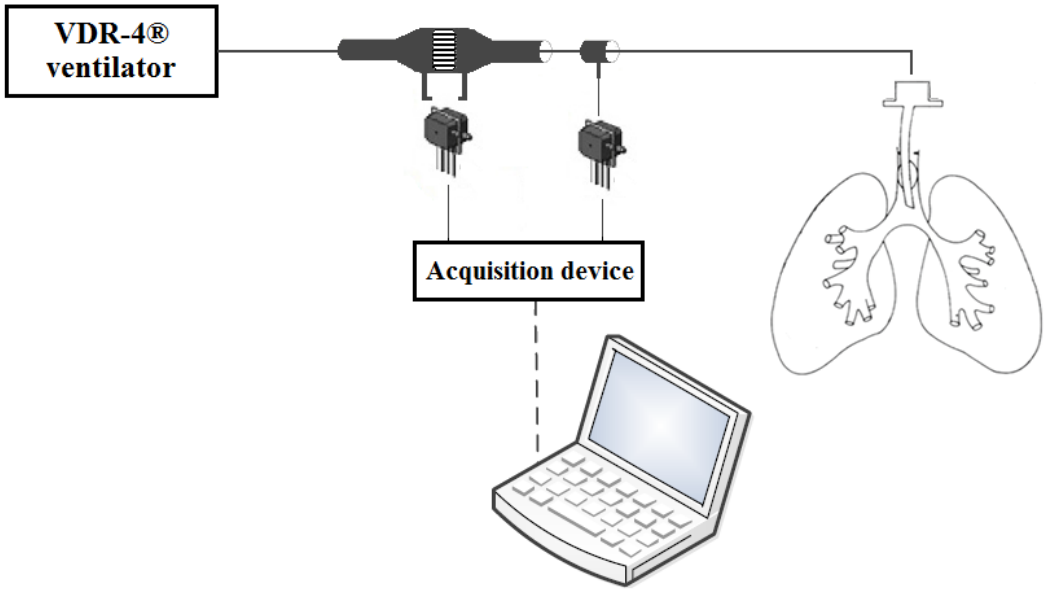

Figure 5.2 Schematic diagram of respiratory circuit and acquisition system

The schematic diagram of respiratory circuit and acquisition system is shown in Figure 5.2. The VDR-4® ventilator was connected to endotracheal tube of intubated patient through a Fleisch pneumotachograph and a sideport for pressure measurement. The acquisition device was supplied by isolated power supply, so there was no risk of electrical injury. The apparatus was heated for five minutes before and during use, in order to prevent water vapor condensation in the duct system.

The respiratory mechanics function was estimated by the approximated Dorkin high frequency model, defined by following equation of motion [13]:

$$Paw(t) = R \cdot \dot{V}(t) + \frac{1}{C} \cdot V(t) + I \cdot \ddot{V}(t) + P_0$$

where Paw(t) represents the pressure applied to the respiratory system, V(t) is the volume, $\dot{V}(t)$ is the airflow, $\ddot{V}(t)$ is the volume acceleration and P_0 represents the pressure offset. The resistance R, compliance C and inertance I parameters represent respectively the viscous, elastic and inertial mechanical properties of the respiratory system described in previous chapters.

The estimation of the respiratory system resistance and compliance was performed by applying least squares regression approach on above mentioned model by using in vivo acquired respiratory signals.

$$\theta = \left(A^T \times A\right)^{-1} \times A^T \times B$$

with

$$\theta = \begin{bmatrix} \frac{1}{C} \\ R \\ I \\ P_0 \end{bmatrix}$$

$$A = \begin{bmatrix} V_1 & \dot{V}_1 & \ddot{V}_1 & 1 \\ V_2 & \dot{V}_2 & \ddot{V}_2 & 1 \\ \vdots & \vdots & \vdots & \vdots \\ V_{N-1} & \dot{V}_{N-1} & \ddot{V}_{N-1} & 1 \\ V_N & \dot{V}_N & \ddot{V}_N & 1 \end{bmatrix}$$

$$B = \begin{bmatrix} Paw_1 \\ Paw_2 \\ \vdots \\ Paw_{N-1} \\ Paw_N \end{bmatrix}$$

The adequacy of the model used to describe respiratory system in patients undergoing HFPV was evaluated by means of residual root mean square error RMSE% (representing the difference between measured and estimated Paw) expressed as a percentage of the measured peak pressure Paw_{peak}

$$RMSE\% = \sqrt{\frac{\sum_{k=0}^{N-1}\left[Paw_{meas}(kT) - Paw_{est}(kT)\right]^2}{N}} \frac{100}{Paw_{peak}}$$

where Paw_{meas} represents the measured airway pressure, Paw_{est} the estimated airway pressure, T the sampling period, N the number of samples and Paw_{peak} the measured peak pressure.

The endotracheal pressure drop (ΔP_{ETT}) was calculated applying Blasius model on measured flow signal:

$$\Delta P_{ETT}(t) = K_B \cdot \dot{V}(t)^{1.75} + I_T \cdot \ddot{V}(t)$$

where K_B e I_T are the resistance and inertance coefficients, respectively. The K_B and I_T used in this study were those previously obtained in previous study reported in Chapter 4.

5.1.2 Conventional ventilation protocol

During the first 12 h after admission to the ICU the patients underwent conventional mechanical ventilation (CV). All patients were initially ventilated in volume controlled mode with tidal volume (V_T) set in accordance to protective ventilatory strategy, i.e. $V_T \leq 8$ mL/Kg predicted body weight (PBW) . The predicted body weight was calculated using the following equations suggested by "The Acute Respiratory Distress Syndrome Network" [81]

$$PBW = 50 + 0.91 \cdot (h - 152.4) \text{ for males}$$

$$PBW = 45.5 + 0.91 \cdot (h - 152.4) \text{ for females}$$

where h is height in centimeterts.

During CV the positive end-expiratory pressure (PEEP) and inspired oxygen fraction (FiO_2) were selected to obtain arterial oxygen saturation (SaO_2) of 90% or more. After 12 hours of CV arterial blood gas was analyzed and the patients that present ratio between pressure oxygen level and inspired oxygen fraction (PaO_2/FiO_2) of 200 or less or greater than 200 but with an increase below 20% in relation to the admission value were shifted to HFPV, as non-responders to CV.

5.1.3 High frequency percussive ventilation protocol

HFPV was set up similarly to CV by using the same inspiratory-expiratory time ratio (I:E), mean airway pressure (Paw_{mean}) and PEEP. The percussive frequency of pulsatile flow was set to 500 cycles/min, and the pulse inspiratory and expiratory ratio (i:e) was fixed to 1. After a short stabilization period of 10 minutes, the measurement of respiratory parameters pressure, flow and volume was performed and the R, C and ΔP_{ETT} parameters were estimated.

The measured tidal volume was compared to the one measured during CV, at the same Paw_{mean}. In case the tidal volume was above the protective limit (i.e. V_T>8 mL/Kg PBW), the flow was reduced on the VDR-4®. When the safety tidal volume was reached the measurement was repeated.

A *mini recruitment maneuver* was then applied in the form of peak airway pressure increment by the calculated ΔP_{ETT} value. A new measurement of respiratory parameters was performed in order to assess the variations in respiratory system and verify if the tidal volume is within the safety limits.

During the following 12 hours the patient was ventilated maintaining these ventilator settings and every 4 hours blood samples were collected for gas analysis and the PaO_2/FiO_2 ratio was calculated. At the end of 12 hours of HFPV treatment the patients returned to CV.

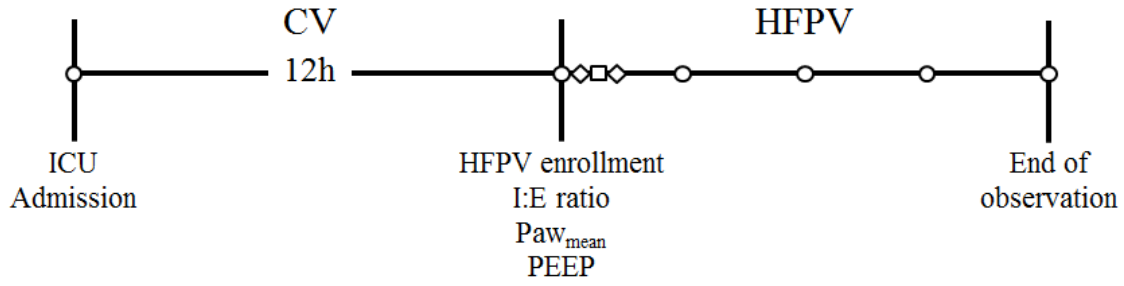

Figure 5.3 Experimental timeline. HFPV was substituted for CV in patients who did not respond to conventional treatment after 12 hours. HFPV was set up similarly to CV by using the same inspiratory-expiratory time ratio (I:E), mean airway pressure (Paw_{mean}) and PEEP. ◊- measurement of respiratory parameters; □ - ΔP_{TT} pressure increment; ○- PaO_2/FiO_2 arterial blood gas analysis

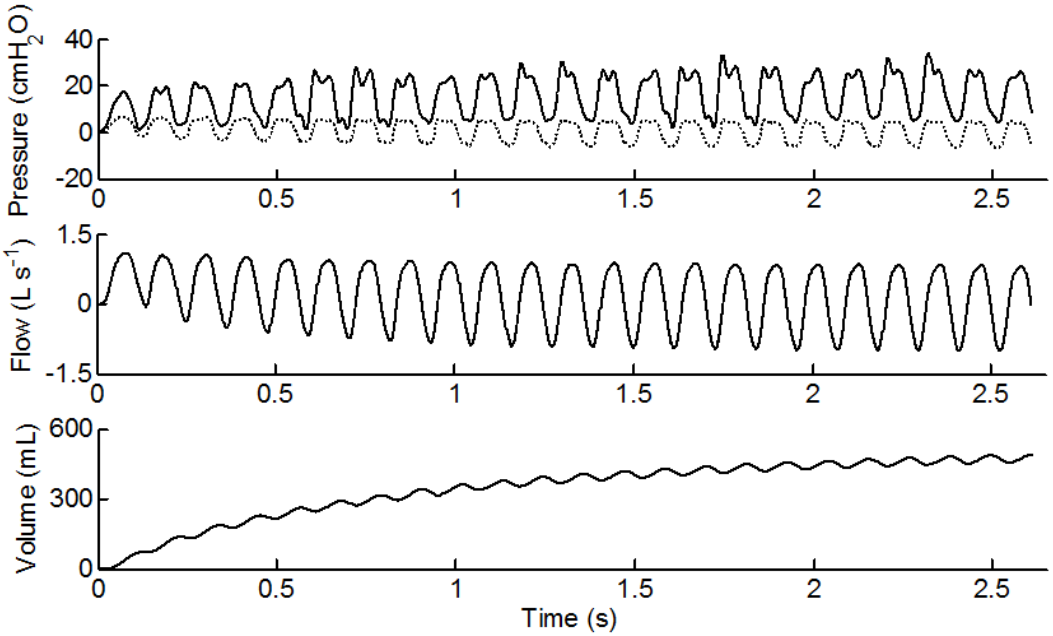

Figure 5.4 From top to bottom: Pressure (airway pressure Paw – full line, calculated ΔP_{ETT} - dotted line), Flow and Volume during an inspiratory phase of a single respiratory cycle

5.2 Results

In Figure 5.4 are shown the tracings of airway pressure, flow and volume measured in a patient undergoing HFPV. In the top panel calculated ΔP_{ETT} is also depicted. The comparison between tidal volumes measured during the transition from CV to HFPV at the same at the same Paw_{mean} is reported in table 5.1.

Patient	Paw_{mean} (cmH_2O)	V_T CV (mL)	V_T HFPV (mL)	V_T/Kg PBW CV (mL/Kg PBW)	V_T/Kg PBW HFPV (mL/Kg PBW)
1	10	440	530	7.33	8.83*
2	14	500	520	6.25	6.50
3	15	610	630	7.18	7.41
4	12	450	620	6.43	8.86*
5	12	400	390	5.97	5.82
6	11	500	840	5.56	9.33*
7	17	520	480	6.50	6.00
8	10	380	415	6.13	6.69
9	9	510	490	6.14	5.90
10	15	500	420	6.41	5.38

Table 5.1 Comparison of tidal volume delivery between CV and HFPV at the same Paw_{mean}.* - patients that exceeded the upper safety volume limit. Results partially presented in [82].

During the transition from CV to HFPV in 30% of examined patients was detected that V_T exceeded the upper safety limit of 8 mL/Kg PBW as shown in table 5.1. In two cases the upper limit was 10% exceeded (8.83 and 8.86 mL/Kg PBW), while in third case the increment was more important, reaching 9.33 mL/Kg PBW. In all three cases V_T was immediately decreased to safety range by acting on HFPV setup.

Once achieved the safety volume range, the ΔP_{ETT} was estimated, and the pressure increment perturbation was applied. In Figure 5.4 the measured airway pressure curve is compared to corresponding curve estimated with Dorkin model. Comparing estimated and measured airway pressures low RMSE% (5.55+1.74)% values were found in all patients. Moreover, as can be seen in Figure 5.4 the proposed method well estimates also PEEP value. The measured tidal volume, and the estimated resistance and compliance values before (V_T, R, C) and after (V_T', R', C') the application of ΔP_{ETT} increment are reported in Table 5.2.

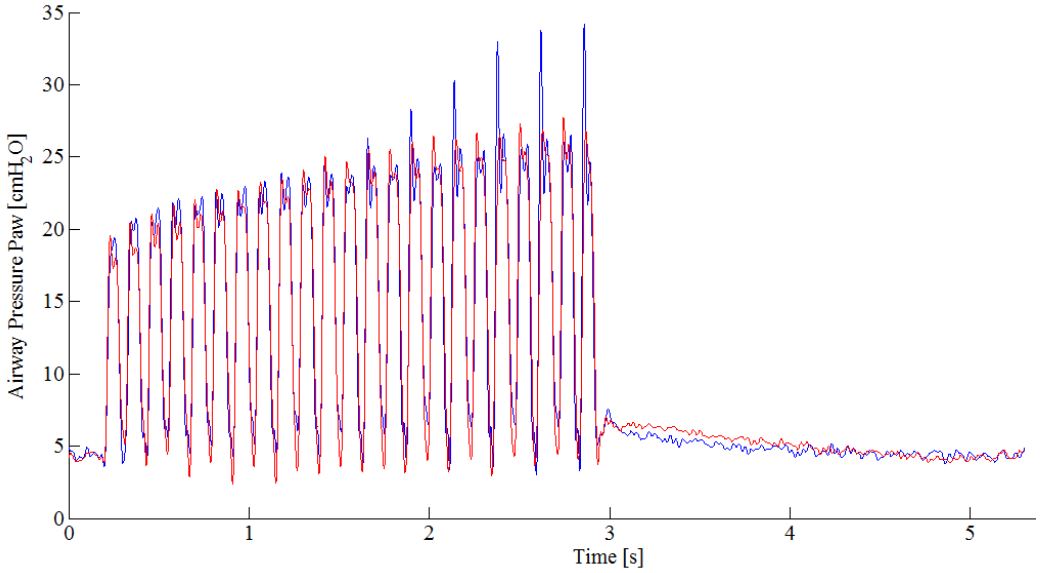

Figure 5.4 Comparison between of the measured pressure curve (blue line) and the relative estimated curve with Dorkin model (red line).

Patient	R ($cmH_2O\ L^{-1}\ s$)	C (mL/cmH_2O)	V_T/Kg PBW (mL/Kg PBW)	ΔP_{TT} (cmH_2O)	R' ($cmH_2O\ L^{-1}\ s$)	C' (mL/cmH2O)	V'_T/Kg PBW (mL/Kg PBW)	ΔC (%)
1	12	25	6.5	6	11.5	31	7.9	24
2	18.2	40.3	6.5	4	17.8	41.8	7.5	3.7
3	15.6	44.2	7.4	5	14.9	49	8	10.9
4	18	55.8	7.1	4	18	52.6	7.7	-5.3
5	13	31	5.8	5	14	33	6.1	6.5
6	18	39	6.6	5	16.5	44	7.6	12.8
7	17	47.4	6	6	18.3	53.6	6.7	13.1
8	10.7	27	6.7	4	12	29	7.2	7.4
9	8.8	27.6	5.9	6	9.2	37	7.8	34.1
10	11	50.2	5.4	6	11.5	61.3	6.6	22.1

Table 5.2 Comparison between the respiratory parameters before and after the application of ΔP_{TT} increment C - C' and V_T -V_T' differed significantly p = 0,016 and p = 0,005 respectively. ΔC (%) represents compliance variation. Results partially presented in [83].

After the application of the mini recruitment maneuver, the respiratory system compliance and delivered tidal volume varied significantly (p = 0,016 and 0,005 respectively), while the variation of the respiratory airway resistance was negligible. In all cases except one the pressure increment resulted in significant tidal volume increase, i.e. ΔC% was positive (from 3.7% to 34.1%) suggesting a potential alveolar recruitment. Compliance increment greater than 10%, which was retained clinically significant, was detected in six patients. Therefore, the six patients can be identified as recruitment cases.

On the other side, in only one patient the pressure increment resulted in compliance decrease suggesting a potential alveolar over-distention. An intermediate behavior characterized by the compliance increment lower than 10% occurred in three patients. In these cases the perturbation maneuver did not affected compliance. At the same time in all patients, the tidal volume values remained within the safety limits (Table 5.2).

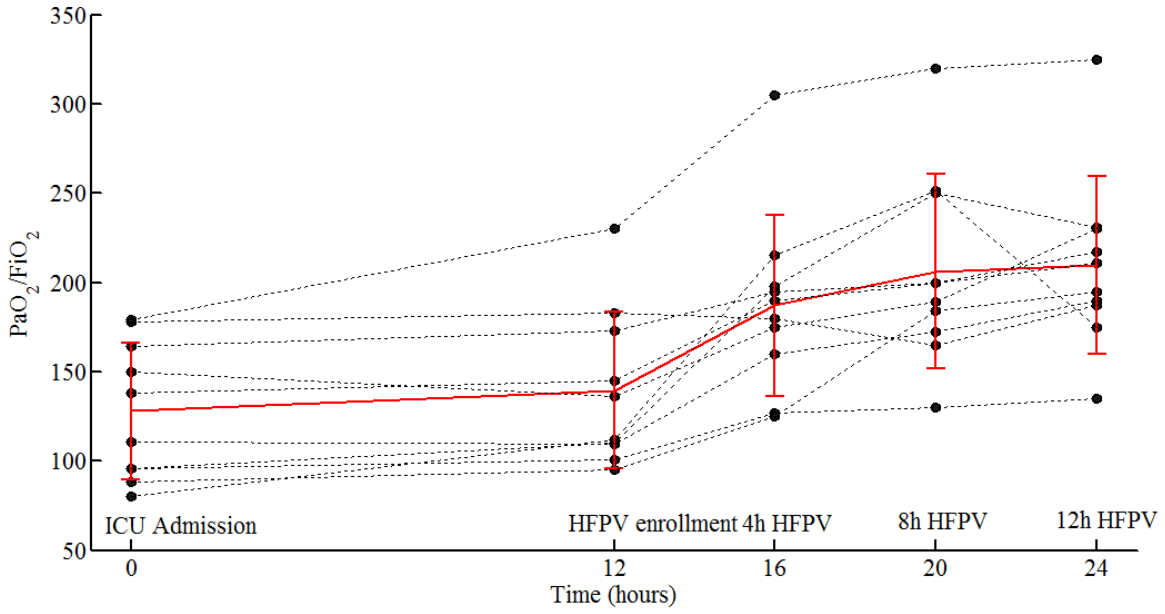

Figure 5.5 PaO_2/FiO_2 values in the ten patients at the ICU admission (initial observation), HFPV enrollment (after 12 hours), four, eight and twelve hours of HFPV treatment, respectively. The exact PaO_2/FiO_2 values are represented by circles, connected with dotted lines for each patient. Full line represents the mean and 1SD values among patients. Results partially presented in [83]

In Figure 5.5 PaO_2/FiO_2 values before and during the HFPV treatment are reported. The gas exchange did not differ from initial observation to HFPV enrollment. After the first four hours of HFPV, PaO_2/FiO_2 increased significantly (mean slope = 12.1 h^{-1}). On the whole the mean slope of the 12 hours HFPV treatment was 5.8 h^{-1}, compared to 1 h^{-1} obtained during previous 12 hours of conventional treatment.

5.3 Discussion

This *in vivo* study aimed to personalize HFPV treatment using non-invasive measurements and parameter estimation. The study was performed in ten non-responder patients after 12 hours of conventional ventilation. HFPV initially was setup at the same mean airway pressure of volume controlled CV.

The delivered tidal volume at the same mean airway pressure differed between volume controlled CV and HFPV (Table 5.1). For this reason Paw_{mean} cannot be considered a reliable parameter for the monitoring of tidal volume changes during transition from CV to HFPV. These results confirm intrinsic limits of Paw_{mean} monitoring already reported in a previous in-vitro study [29]. Moreover, in three cases the delivered tidal volume exceeded significantly the upper safety limit of 8 mL/Kg PBW, violating the protective ventilatory strategy. This indicates that the volume measurement is mandatory during HFPV setup.

The estimated R and C values identified different lung conditions giving the information about viscoelastic properties when the patients complied with protective ventilatory strategy. The low RMSE% values obtained during parameter identification confirm the adequacy of the high frequency Dorkin model to describe over time the respiratory mechanics in patients undergoing HFPV.

After the assessment of appropriate tidal volume, a pressure increment (ΔP_{ETT}) was performed. This mini recruitment maneuver perturbation produced in six patients (2 chest trauma, 3 sepsis and 1 pneumonia) a significant increment (≥10%) of compliance without compromising the patient's safety $V_T' \leq 8$ mL/Kg PBW (Table 5.2). This behavior is characteristic of alveolar recruitment and it can be described as a shift from low inflation zone to linear zone in the pressure–volume curve (Figure 5.6).

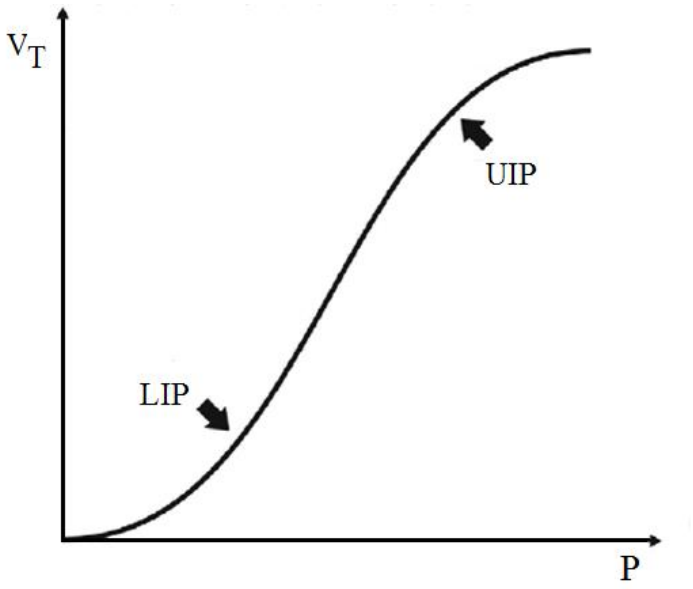

Figure 5.6 Characteristic inspiratory limb of a P-V curve. LIP and UIP represent lower and upper inflation point respectively. Three segments of P-V curve are defined by these points: Low inflation zone below the LIP, linear zone between LIP and UIP and over-distention zone above UIP

The elastic lung properties can suddenly change when alveolar recruitment or de-recruitment occurs. From a clinical point of view alveolar de-recruitment must be avoided in order to keep the lung open. In the five of six recruitment cases the etiology of the acute hypoxemia is not related to direct lung injury.

On the other hand, in one patient with stiff lungs due to bilateral pneumonia the pressure increment produced an increase in V_T and at the same time, a decrease in compliance, resulting in an undesired over-distention. Finally the other three patients (2 pneumonia and 1 neurogenic pulmonary edema) presented an intermediate respiratory mechanics behavior corresponding to linear part of P-V curve (Figure 5.6). In this case a volume increment resulted in poor compliance variation as expected in subjects suffering hypoxemia due to primitive lung lesions. On the contrary, the resistance did not change significantly after perturbation in all patients. In fact the airway resistance mainly depends on the presence of secretions and their mobilization is a known, but not immediate, feature of HFPV [84].

The aforementioned variations of respiratory mechanics should be pathophysiologically understood by considering the pressure volume relationship during

mechanical ventilation. The pressure-volume curve (P-V) of the respiratory system is not linear; it usually assumes a characteristic sigmoidal shape, with a central linear part where C is higher and two inflection points respectively located at the beginning (LIP) and at the end of the curve (UIP) (Figure 5.6) [85] [86]. These points represent the pressures at which recruitment and de-recruitment begin and end. At the beginning the P-V curve is flat and reflects very low compliance. For inspiratory pressures below the inspiratory LIP, the increase in lung volume is mainly due to aeration of normally poorly aerated areas, while when the airway pressure increases above the LIP recruitment starts [86]. The following linear segment is characterized by a steeper slope due to Gaussian distribution of recruitment pressures [87] and represents the maximum compliance. The UIP indicates the end of the massive recruitment and beginning of alveolar over-distension segment in which compliance decreases. It is important to detect the beginning of this segment in order to avoid over-distension. Thus the tidal volume ventilation is desirable in the central zone of the P-V tracing, between the two inflexion points [86], in order to maximize alveolar recruitment and to minimize ventilatory induced lung injury. These considerations confirm the clinical relevance of the pressure and volume monitoring as also the clinical relevance of the viscoelastic respiratory system parameters estimation.

Blood gas analyses were recorded before and during the HFPV treatment and the PaO_2/FiO_2 ratio did not differ from initial observation to HFPV enrollment, as expected in non-responder patients. During the first four hours of the HFPV treatment, after the mini recruitment maneuver, the mean slope of PaO_2/FiO_2 was 12.1 $h^{-1,}$ compared to 10.2 h^{-1} obtained in the previous HFPV study based only on Paw_{mean} setup [46] without ΔP_{ETT} compensation. This increment is clinically relevant particularly because obtained in accordance within the limits defined by protective ventilatory strategy. However, these preliminary results should be confirmed in future study.

The *in vivo* study results suggest that is of paramount importance to evaluate V_T, R and C during HFPV to avoid under and over-treatment. The clinical studies demonstrated that HFPV as a pressure controlled logic ventilation promotes alveolar recruitment [46] [88]. The alveolar recruitment becomes particularly evident after at least 12 hours of continuous HFPV treatment [46].The possibility to early optimize the pressure volume relationship in safe way represents an important result, and can improve the positive effect

of high frequency ventilation, minimizing iatrogenic lung damage. However, it is important to underline that the tidal volume delivery should be chosen considering also the heterogeneity of underlying lung injury typically present in these patients. Thus, it is very important that V_T be tailored, based on compliance value, in patients with acute lung injury and acute respiratory distress syndrome. Deans et al point out that although some patients, such as those with poor compliance and high airway pressures, would benefit from very low tidal volume, others with less severe lung injury may require larger volumes to maintain ventilation and avoid alveolar collapse during conventional mechanical ventilation [89]. Furthermore, it was reported that the effect of changing tidal volume on mortality is dependent on initial pulmonary compliance [89]. Patients with higher compliances did poorly if V_T was lowered, while the patients with relatively lower compliances did well if V_T was lowered. These findings agree with the idea that HFPV ventilator setup should be tailored on the main respiratory parameters taking into account the disease severity [90] [91].

Conclusions

High frequency percussive ventilation demonstrated over the years its high effectiveness in the treatment of critical hypoxemic patients. However, the HFPV ventilator setup is presently chosen basing only on pressure measurements and gas exchange information. From a clinical point of view it is important to evaluate respiratory system viscoelastic parameters during the ventilator setup in order to avoid under or over-treatment.

This thesis offers a new approach for HFPV ventilator setup in accordance with protective ventilatory strategy and optimization of alveolar recruitment using estimation of the respiratory mechanics parameters and endotracheal pressure drop. Respiratory system resistance and compliance were estimated, firstly in vitro and successively in patients undergoing HFPV, applying least squares regression on Dorkin high frequency model, starting from measured respiratory signals. Moreover, the Blasius model was identified as the most adequate to estimate pressure drop across the endotracheal tube during HFPV. Beside measurement device was developed in order to measure respiratory parameters in patients undergoing HFPV.

The possibility to tailor HFPV ventilator setup, using respiratory signals measurement and estimation of resistance, compliance and pressure drop across endotracheal tube, provided by this thesis, open a new prospective to this particular ventilatory strategy, improving its beneficial effects and minimizing ventilator-induced lung damage.

Bibliography

1. Weibel ER, “Morphometry of the human lung” Berlin: SpringerVerlag. 1963
2. Tobin MJ, Van de Graaff WB. “Monitoring of lung mechanics and work of breathing” In: Tobin MJ, ed. “Principles and Practice of Mechanical Ventilation” McGraw-Hill, New York, 1994, pp. 967–1003
3. Grinnan, DC, Truwit JD. “Clinical review: respiratory mechanics in spontaneous and assisted ventilation” Critical Care. 2005; 9(5):472
4. Johnson AT. “Biomechanics and Exercise Physiology” New York, Wiley. 1991
5. Avanzolini G, Barbini P, Costantino ML, Pedotti A, Rossi A. “Bioingegneria del sistema respiratorio” Bologna: Pàtron Editore. 2001
6. Rodarte JR, Rehder K. “Dynamics of respiration” In Macklem PT, Mead J, “Handbook of Physiology. The Respiratory System. Mechanics of Breathing” Bethesda: The American Physiological Society, 1986:131–44
7. Bates JHT, Rossi A, Milic-Emili J. “Analysis of the behaviour of the respiratory system with constant inspiratory flow” J Appl Physiol. 1985; 58:1840–1848
8. Polese G, Serra A, Rossi A. “Respiratory mechanics in the intensive care unit” In “European respiratory monograph” 2005; 31:195
9. Otis AR, McKerrow CB, Bartlett RA, Mead J, Mcllroy MB, Selverstone NJ, Radford EP Jr. “Mechanical factors in distribution of pulmonary ventilation” J. AppI. Physiol. 1956; 8:427-443
10. Mead J. “Contribution of compliance of airways to frequency dependent behavior of lungs” J. AppI. Physiol. 1969; 26: 670-673
11. Mount LE. “The ventilation flow resistance and compliance of rat lungs” J. Physiol. Lond. 1955; 127:157-167
12. Bates JHT, Brown KA, Kochi T. “Respiratory mechanics in the normal dog determined by expiratory flow interruption” J. Appl. Physiol. 1989; 67: 2276-2285
13. Dorkin HL, Lutchen KR, Jackson AC. “Human respiratory input impedance from 4 to 200 Hz: physiological and modeling considerations” J Appl Physiol. 1988; 64:823-31

14. Krishnan JA, Brower RG. “High-frequency ventilation for acute lung injury and ARDS” Chest. 2000; 118(3): 795–807
15. Lucangelo U, Antonaglia V, Zin WA, Fontanesi L, Peratoner A, Bird FM, Gullo A. “Effects of mechanical load on flow, volume and pressure delivered by high-frequency percussive ventilation” Respir Physiol Neurobiol. 2004; 142(1):81-91
16. Oberg PA, Sjostrand U. “Studies of blood-pressure regulation” Acta Physiol. Scand. 1969; 75.3: 287-300
17. Chang H.K. “Mechanisms of gas transport during ventilation by high frequency oscillations” J. Appl. Physiol. , 1984; 56:553– 563
18. Drazen JM, Kamm RD, Slutsky AS. “High-frequency ventilation” Physiol. Rev. 1984; 64:505–543.
19. Slutsky AS. “Mechanisms affecting gas transport during high frequency oscillations” Crit. Care Med. 1984; 12:713–717
20. Froese AB, Bryan AC, “High frequency ventilation” Am. Rev. Respir. Dis. 1987; 135, 1363–1374
21. Fort P, Farmer C, Westerman J, Johannigman J, Beninati W, Dolan ., Derdak S “High-frequency oscillatory ventilation for adult respiratory distress syndrome--a pilot study” Critical care medicine. 1997; 25 (6): 937-947
22. Lucangelo U, Fontanesi L, Antonaglia V, Pellis T, Berlot G, Liquori G, Bird FM, Gullo A. “High Frequency Percussive Ventilation (HFPV) Principles and techinique” Minerva Anestesiol, 2003; 69:841-51
23. Salim A, Martin M. “High-frequency percussive ventilation” Critical care medicine 2005; 33:241-245
24. Lucangelo U, Gramaticopolo S; Fontanesi L. “High-frequency percussive ventilation” In: “Respiratory System and Artificial Ventilation” Springer: Milan 2008; p. 237-244.
25. Product information. Percussionaire Corporation. Sandopoint, ID, USA,1997
26. Branson RD. “High frequency ventilators” in Branson et al, “Respiratory care equipment”, Philadelphia: Lippincott; 1995: 446-58
27. Kunugiyama SK, Schulman CS. “High-frequency percussive ventilation using the VDR-4 ventilator: an effective strategy for patients with refractory hypoxemia” AACN advanced critical care, 2012, 23.4: 370-380

28. The VDR®-4 manual of understanding. Percussionaire Corporation, 2009.
29. Lucangelo U., Antonaglia V, Zin W A, Berlot G, Fontanesi L, Peratoner A, Gullo A "Mechanical loads modulate tidal volume and lung washout during high-frequency percussive ventilation" Respiratory physiology & neurobiology. 2006; 150.1: 44-51
30. Hurst JM, Branson RD, De Haven CB. "The role of high-frequency ventilation in posttraumatic respiratory insufficiency" J Trauma 1987; 27:236 –242
31. Lentz CW, Peterson HD. "Smoke inhalation is a multilevel insult to the pulmonary system" Curr Opin Pulm Med 1997; 3:221–226
32. Reper P, Dankaert R, Van Hille F, Van Laeke P, Duinslaeger L, Vanderkelen A. "The usefulness of combined high-frequency percussive ventilation during acute respiratory failure after smoke inhalation" Burns 1998; 24:34–38
33. Campbell PJ, Chilton HW, Garvey PA, Gupta JM. "Volumetric diffuse respirator use in neonatal respiratory failure" J. Paediatr. Child Health. 1991; 27, 31–33
34. Velmahos GC, Chan LS, Tatevossian R, Cornwell EE, Dougherty WR, Escudero J, Demetriades D "High-frequency percussive ventilation improves oxygenation in patients with ARDS" 1999; Chest 116:440–446
35. Spapen H, et al. "High-frequency percussive ventilation in severe acute respiratory distress syndrome: A single center experience" Journal of anaesthesiology, clinical pharmacology. 2014, 30.1: 65
36. Soudon P. Mechanical ventilation by tracheostomy in neuromuscular disease: experience and evaluation. Eur Respir Rev 1993; 3:300-4
37. Hurst JM, Branson RD, DeHaven CB. The role of high-frequency ventilation in post-traumatic respiratory insufficiency. J Trauma 1987; 27:236-42
38. Paulsen SM, Killyon GW, Barillo DJ. "High frequency percussive ventilation as a salvage modality in adult respiratory distress syndrome: a preliminary study" Am Surg 2002; 68:852–856
39. K. Deakins and R. L. Chatburn, "A comparison of intrapulmonary percussive ventilation and conventional chest physiotherapy for the treatment of atelectasis in the pediatric patient," Respiratory care. , 2002; vol. 47, no. 10, pp. 1162–1167

40. Natale JE, Pfeifle J, Homnick DN. “Comparison of intrapulmonary percussive ventilation and chest physiotherapy. A pilot study in patients with cystic fibrosis. Chest” 1994; 105:1789-93
41. Lucangelo U. “High Frequency Percussive Ventilation” in Gullo, “Anaesthesia pain, intensive care and emergency medicine” APICE, Proceedings of the 15th postgraduate course in critical care medicine. Berlin: Springer – Verlag; 2001: 163-71
42. Gallagher JT, Boysen PG, Davidson DD, Miller JR, Leven SB. High frequency percussive ventilation compared with mechanical ventilation. Crit Care Med 1989; 17:364-6
43. Esan A, Hess DR, Raoof S, George L, Sessler CN. Severe hypoxemic respiratory failure: part 1--ventilatory strategies. Chest 2010; 137:1203-16
44. Lucangelo U, Zin WA, Antonaglia V, Gramaticopolo S, Maffessanti M, Liguori G, Cortale M, Gullo A. High-frequency percussive ventilation during surgical bronchial repair in a patient with one lung. Br J Anaesth 2006; 96:533-6
45. Lucangelo U, Antonaglia V, Zin WA, Confalonieri M, Borelli M, Columban M, Cassio S, Batticci I, Ferluga M, Cortale M, Berlot G. High-frequency percussive ventilation improves perioperatively clinical evolution in pulmonary resection. Crit Care Med 2009; 37:1663-9
46. Lucangelo U, Zin WA, Fontanesi L, Antonaglia V, Peratoner A, Ferluga M, Marras E, Borelli M, Ciccolini M, Berlot G. “Early short-term application of high-frequency percussive ventilation improves gas exchange in hypoxemic patients” Respiration 2012; 84:369-76
47. Rizkalla NA, Dominick CL, Fitzgerald JC, Thomas NJ, Yehy N. “High-frequency percussive ventilation improves oxygenation and ventilation in pediatric patients with acute respiratory failure” 2014; Journal of critical care, 29(2): 314-e1.
48. Riscica F, Lucangelo U, Ferluga M, Accardo A. “In vitro measurements of respiratory mechanics during HFPV using a mechanical lung model” Physiological measurement. 2011; 32(6): 637-48
49. Riscica F, Lucangelo U, Accardo A. “Development of an innovative instrument for the online characterization of high frequency percussive ventilators” Proceedings of

the World Congress on Medical Physics and Biomedical Engineering, September 7-12, 2009, Munich, Germany. Berlin: Springer; 2009:480-3.

50. Shaw A, Gregory NL, Davis PD, Patel K. “Flow-volume integrator for respiratory studies” Med Biol Eng. 1976; 14(6):695-6
51. Rossi A, Gottfried SB, Higgs BD, Zocchi L, Grassino A, Milic-Emili J. “Respiratory mechanics in mechanically ventilated patients with respiratory failure” J Appl Physiol. 1985; 58(6):1849-58
52. Bernasconi M, Ploysongsang Y, Gottfried SB, Milic-Emili J, Rossi A. “Respiratory compliance and resistance in mechanically ventilated patients with acute respiratory failure” Intensive Care Med. 1988; 14(5):547-53
53. Nucci G, Mergoni M, Polese G, Cobelli C, Rossi A. On-line monitoring of respiratory mechanics. In: Brusasco V, Macklem PT, Pedotti A, eds. Mechanics of Breathing. Milan, Springer-Verlag, 2002: 327–336.
54. Volta CA, Marangoni E, Alvisi V, et al. Respiratory mechanics by least squares fitting in mechanically ventilated patients: application on flow-limited COPD patients. Intensive Care Med 2002; 28: 48–52
55. Ajcevic M, Accardo A, Fornasa E, Lucangelo U. “Estimation of Respiratory Mechanics Parameters during HFPV” In XIII Mediterranean Conference on Medical and Biological Engineering and Computing. 2014; pp. 591-594 Springer International Publishing.
56. Accardo A, Ajcevic M, Lucangelo U. “Flow Resistance Estimation of Endotracheal Tube during High Frequency Percussive Ventilation: Preliminary Results” In: World Congress on Medical Physics and Biomedical Engineering May 26-31, 2012, Beijing, China. Springer Berlin Heidelberg, 2013. p. 20-23.
57. Bersten AD, Rutten AJ, Veding AE, Skowronski GA. “Additional work of breathing imposed by endotracheal tubes, breathing circuits, and intensive care ventilators” Crit Care Med. 1987; 17:671–7
58. Bolder PM, Healy TEJ, Bolder AR, Beatty PCW, Kay B. “The extra work of breathing through adult endotracheal tubes” Anesth Analg. 1986; 65:853–9
59. Rocco PRM, Zin WA. “Modelling the mechanical effects of tracheal tubes in normal subjects” Eur Respir J. 1995; 8:121–6

60. Conti G, De Blasi R A, Lappa A, Ferretti A, Antonelli M, Bufi M, Gasparetto A. “Evaluation of respiratory system resistance in mechanically ventilated patients: the role of the endotracheal tube” Intensive Care Med. 1994; 20:421–4
61. Zin WA, Pengelly LD, Milic-Emili J. “Active impedance of respiratory system in anesthetized cats” J Appl Physiol. 1982; 53:149–57
62. Rohrer F. “Der Stroemungswiderstand in den menschlichen atemwegen und der Einfluss der unregelmaessigen verzweigung des bronchialsystems auf den atmungsverlauf in verschiedenen lungenbezirken” Pfluegers Arch Gesamte Physiol. Menschen Tiere. 1915; 162:225–59
63. Rossi A, Gottfried S B, Higgs B D, Zocchi L, Grassino A, Milic-Emili J. “Respiratory mechanics in mechanically ventilated patients with respiratory failure” J Appl Physiol. 1985; 58:1849–58
64. Lorino AM, Beydon L, Mariette C, Dahan E, Lorino H. “A new correction technique for measuring respiratory impedance through endotracheal tube” Eur Respir J. 1996; 9:1079–86
65. Guttmann J, Eberhard L, Fabry B, Bertschmann W, Wolff G. “Continuous calculation of intratracheal pressure in tracheally intubated patients” Anesthesiology. 1993; 79:503–13
66. Jarreau PH, Louis B, Dassieu G, Desfrere L, Blanchard PW, Moriette G, Isabey D, Harf A. “Estimation of inspiratory pressure drop in neonatal and pediatric endotracheal tubes” J Appl Physiol. 1999; 87:36–46
67. Lofaso F, Louis B, Brochard L, Harf A, Isabey D. “Use of the Blasius resistance formula to estimate the effective diameter of endotracheal tubes” Am Rev Respir Dis. 1992; 146:974–9
68. Shumann S, Krappitz M, Moeller K, Hentschel R, Braun G, Guttmann J. “Pressure loss caused by pediatric endotracheal tubes during high frequency oscillation ventilation” Respir Physiol Neurobiol. 2008; 162:132–7
69. Ajčević M, Lucangelo U, Ferluga M, Zin WA, Accardo A. “In vitro estimation of pressure drop across tracheal tubes during high-frequency percussive ventilation” Physiological measurement. 2014; 35(2):177- 88.
70. Chang HK, Mortola JP. “Fluid dynamic factors in tracheal pressure measurement” J Appl Physiol. 1981; 51:218–25

71. Loring SH, Elliot EA, Drazen JM. “Kinetic energy loss and convective acceleration in respiratory resistance measurements” Lung. 1979; 156:33–42
72. Sullivan M, Paliotta J, Saklad M. “Endotracheal tube as a factor in measurement of respiratory mechanics” J Appl Physiol. 1976; 41:590–2
73. Gammon RB, Shin MS, Buchalter SE. “Pulmonary barotrauma in mechanical ventilation. Patterns and risk factors” Chest. 1992; 102:568–72
74. Khattree R, Naik DN. “Computational Methods in Biomedical Research” Boca Raton: Chapman and Hall. 2008
75. Guttmann J, Kessler V, Mols G, Hentschel R, Haberthuer C, Geiger K. “Continuous calculation of intratracheal pressure in the presence of pediatric endotracheal tubes” Crit Care Med. 2000; 28:1018–26
76. Peslin R, Fredberg JJ. “Oscillation mechanics of the respiratory system” in Macklem PT, J Mead J, “Handbook of Physiology. The Respiratory System. Mechanics of Breathing”, Bethesda: The American Physiological Society, 1986:145–78
77. Ajcevic M, Accardo A, Fornasa E, Lucangelo U. “Estimation of pressure drop in pediatric endotracheal tubes during HFPV” In: Signal Processing Conference (EUSIPCO), 2013 Proceedings of the 21st European. IEEE, 2013. p. 1-5.
78. Ajcevic M, De Lorenzo A, Accardo A, Bartoli A, Medvet E. “A novel estimation methodology for tracheal pressure in mechanical ventilation control” In: Image and Signal Processing and Analysis (ISPA), 2013 8th International Symposium on. IEEE, 2013. p. 695-699.
79. A. Bartoli, G. Davanzo, A. De Lorenzo, and E. Medvet, “Gp based electricity price forecasting,” in Genetic Programming, ser. Lecture Notes in Computer Science, S. Silva, J. Foster, M. Nicolau, P. Machado, and M. Giacobini, Eds. Springer Berlin Heidelberg, 2011, vol. 6621, pp. 37–48.
80. A. Bartoli, G. Davanzo, A. De Lorenzo, M. Mauri, E. Medvet, and E. Sorio, “Automatic generation of regular expressions from examples with genetic programming,” in Proceedings of the fourteenth international conference on Genetic and evolutionary computation conference companion. ACM, 2012, pp. 1477–1478.

81. De Campos T, et al. “Ventilation with lower tidal volumes as compared with traditional tidal volumes for acute lung injury and the acute respiratory distress syndrome. The Acute Respiratory Distress Syndrome Network.” N Engl J Med. 2000; 342(18):1301-8
82. Ajčević M, Lucangelo U, Accardo A. “In Vivo Measurements of Respiratory Parameters during HFPV” In: 6th European Conference of the International Federation for Medical and Biological Engineering. Springer International Publishing, 2015. p. 472-475
83. Ajčević, M; Lucangelo U, Accardo A. “Tailoring of HFPV Treatment by Respiratory Parameters Measurement” In: 16th Nordic-Baltic Conference on Biomedical Engineering. Springer International Publishing, 2015. p. 9-12
84. Hall JJ, Hunt JL, Arnoldo BD, Purdue GF (2007) Use of high-frequency percussive ventilation in inhalation injuries. J Burn Care Res 28:396–400
85. Albaiceta GM, Blanch L, Lucangelo U. “Static pressure-volume curves of the respiratory system: were they just a passing fad?” Curr Opin Crit Care. 2008; 14(1):80-6
86. Correger E, Murias G, Chacon E, Estruga A, Sales B, Lopez-Aguilar J, Montanya J, Lucangelo U, Garcia-Esquirol O, Villagra A, Villar J, Kacmarek RM, Burgueño MJ, Blanch L. “Interpretation of ventilator curves in patients with acute respiratory failure” Med Intensiva. 2012; 36(4):294-306.
87. Pelosi P, Goldner M, McKibben A et al (2001) Recruitment and derecruitment during acute respiratory failure: an experimental study. American journal of respiratory and critical care medicine 164(1):122-130
88. Kunugiyama SK, Schulman CS. “High-frequency percussive ventilation using the VDR-4 ventilator: an effective strategy for patients with refractory hypoxemia” AACN Adv Crit Care. 2012; 23(4):370-80.
89. Deans KJ, Minneci PC, Cui X, Banks SM, Natanson C, Eichacker PQ. “Mechanical ventilation in ARDS: One size does not fit all*” Critical care medicine. 2005; 33(5):1141-1143.
90. Marini JJ, Gattinoni L. “Ventilatory management of acute respiratory distress syndrome: A consensus of two” Crit Care Med. 2004; 1:250–255

91. Ricard JD. “Are we really reducing tidal volume—And should we?” Am J Respir Crit Care Med. 2003; 10:1297–1298